Faculty of Science and Engineering
Department of Chemical Engineering

Hydrodynamics of Industrial Scale FCCU Stripper

Ganesh K Veluswamy

This thesis is presented for the Degree of
Doctor of Philosophy
of
Curtin University of Technology

September 2010

Declaration

To the best of my knowledge and belief this thesis contains no material previously published by any other person except where due acknowledgment has been made.

This thesis contains no material which has been accepted for award of any other degree or diploma in any university.

Signature: 

Date: 15/02/2011

BIOGRAPHY OF THE AUTHOR

Ganesh K Veluswamy has studied the principles of chemical engineering for past 10 years which includes a degree in chemical engineering and current enrolment as PhD student at Curtin University of Technology. He has extensively worked in the area of chemical engineering design, multiphase applications, numerical modelling and process engineering principles for the past three and half years, he has spent as a researcher at Curtin University of Technology. His research interest lies into multiphase modelling studies, especially gas-solid systems and Computational Fluid Dynamics. In the course of the PhD research his work has been presented at international conferences. His research work is ready to be communicated to international journals which include:

List of Publications

1) Veluswamy, G.K., Upadhyay, R., Utikar, R.P., Pareek, V., Roy, S., Tade, M., Glenny, M.E., 2010. Hydrodynamics of Fluid Catalytic Cracking Stripper. Submitted to Industrial Engineering Chemistry Research (IECR).

2) Veluswamy, G.K., Utikar, R.P., Pareek, V., Tade, M., Glenny, M.E., 2011. CFD simulation of industrial scale FCC strippers: Comparison of steam inlet configurations. To be communicated.

3) Veluswamy, G.K., Utikar, R.P., Pareek, V., Tade, M., Glenny, M.E., 2011. A comparative study of the internal configuration of fluid catalytic cracking strippers. To be communicated.

4) Veluswamy, G.K., Upadhyay, R., Utikar, R.P., Pareek, V., Roy, S., Tade, M., Glenny, M.E., 2011. Hydrodynamic study of fluid catalytic cracker unit (FCCU) stripper-CFD Studies. To be communicated.

International Conferences

1) Veluswamy, G.K., Upadhyay, R., Utikar, R.P., Pareek, V., Roy, S., Tade, M., 2010. -May-30. Hydrodynamic study of Fluid catalytic cracker unit strippers. Presented at-International Conference for Multiphase Flow ICMF-2010-Florida, USA.

2) Veluswamy, G.K., Utikar, R.P., Pareek, V., Tade, M., 2010-June-16. Comparative study of effect of internal configuration on FCC Strippers hydrodynamics. Presented at-International Symposia for Chemical Reactor Engineering ISCRE-21, 2010, Philadelphia, USA.

ABSTRACT

Stripper is an important component of a fluid catalytic cracking (FCC) unit. It strips and recovers the adsorbed/deposited light hydrocarbons on the catalyst particle surface using steam in a counter current flow process. Suboptimal performance of an FCC stripper can severely affect the operation of the whole FCC process. The common flow problems encountered in an FCC stripper unit include channelling, bridging and maldistribution. The internal of FCC stripper and inlet design configurations also play an important role in determining the hydrodynamics of the stripper unit. Therefore, there have been both academic and industrial efforts on improving the understanding of the hydrodynamics of this complex counter current system. However, nearly all of the experimental studies have been either carried out for a pilot scale unit, and modelling studies have been limited to 2D simulations. The present research focuses on the hydrodynamics of an industrial-scale FCC stripper unit using a combined approach of extensive experiments and 3D computational fluid dynamics (CFD) modelling. Hence, γ-ray densitometry and time of flight experiments were conducted for a scaled down small stripper. 3D CFD simulations were conducted and the model predictions were validated against the experimental results. The 3D CFD model was extended to industrial scale FCC stripper to study effect of different steam inlet configurations and internals design on the hydrodynamics of FCC stripper.

In the experimental part of the research, a small scale stripper with 140 mm diameter and 440 mm height fitted with disc and donut baffles was designed and commissioned. The experiments were performed using air-glass particle system. Particle holdup and time of flight were determined using γ-ray densitometry and time of flight experimental techniques for different operating conditions. The particle flow rates varied from 0.025 kg/s to 0.042 kg/s and the superficial air velocity varied from 0.74 m/s to 1.1 m/s. It was noticed that the shape and position of baffles made the flow to flow in a zigzag manner. Dead zones were noticed under the baffle regions indicating unused areas in the stripper. The measured solid holdup radial profiles were of asymmetric nature underlying the fact and importance for 3D studies. The solid holdup decreased with increase in air superficial velocity and radial segregation of solid phase was noticed for low superficial air velocity. However, the change in solid flow rates did not have any effect of solid holdup. The average particle time of flight, increased with increase in the superficial air velocity, and at the same time, it was found to decrease with increase in the solid flow rate. In summary, the experimental study has not only

provided new insights on FCC stripper but also provided a large data base which can be used to benchmark the CFD models.

In order to validate CFD models using the above experimental data, a small scale stripper with same dimensions and identical operating conditions as used experiments was modelled using 3D CFD. An Eulerian-Eulerian approach was used to simulate the gas-solid flow in the stripper column. The CFD simulations also predicted asymmetric solid holdup profiles re-emphasizing the importance of 3D simulations. The CFD model predictions matched well with the experimental data for the solid holdup from experiments. The CFD model also clearly predicted the recirculation's and dead zones as noticed in the experimental analysis. Local defluidization zones were also noticed near the donut baffle wall regions. The particles axial velocity was low near the baffle walls, indicating that the particle slide down on the baffle walls.

After validating CFD models using the experimental-scale FCC stripper, 3D CFD simulations were conducted on an industrial-scale FCC stripper having disc and donut baffles. Firstly, the effect of steam inlet configuration on the stripper hydrodynamics was analysed for an operating condition of 45 kg/m^{2}s catalyst flux and 0.25 m/s steam superficial velocity. Both a single steam inlet and a full ring steam inlet configurations were studied. Along with the effect of steam inlet configuration, the effect of lack of symmetry in the catalyst outlet was also investigated. The simulations showed that the stripper fitted with a single steam inlet exhibited segregation and maldistribution of catalyst phase in all sections of the stripper, and there was significant channelling of the steam phase. The lack of symmetry in catalyst outlet was one of the possible reasons for these shortcomings. Large variations in the steam radial and axial velocities were also noticed for the stripper with single pipe steam inlet. This then led to segregation and low residence time and, eventually resulted in poor stripping operation. On the other hand, the stripper fitted with full ring steam inlet showed minimal channeling and segregation. The uniform steam injection pattern helped in attaining better distribution of phases. It was also clear that the baffles play a vital role in bringing the phases in contact with each other by enabling recirculation or backmixing.

Finally, 3D CFD simulations were conducted on an industrial-scale stripper fitted with structured internal packing and full ring steam inlet for the operating conditions of 45 kg/m^{2}s catalyst flux and 0.25 m/s steam superficial velocity. The simulation results were compared with the model predictions for the industrial-scale stripper having disc and donut baffles. The

simulations showed that the stripper with structured packing internals provided a significantly more uniform distribution of the phases, and eliminated dead zones. By removing dead zones, the stripper with structured packing internals utilized up to ~95% of the vessel area for the stripping operation. In doing so, the steam consumption rate for the same amount of hydrocarbon stripping was decreased. The structured packing internals also reduced back mixing of the phases, therefore providing a uniform distribution and contact of the phases. For the same operating conditions, more uniform catalyst velocity and catalyst volume fraction were noticed for the stripper fitted with structure packing, when compared with the stripper with baffles. Also, higher solid holdup profiles were noticed in all sections of the stripper fitted with packing internals.

In summary, this study was provided an in-depth understanding on the effect of inlet and internals on the hydrodynamics of multiphase flow in FCC stripper. Of the two different types of internals considered, the stripper fitted with structured packing's was more efficient option both with respect to plant operability and reliability as well energy savings.

ACKNOWLEDGMENTS

There are many people whom I owe acknowledgement and who have helped me in several ways during my doctorate degree. First of all, I am highly indebted to Professor Vishnu Pareek my supervisor. I express my deepest gratitude to him for giving me an opportunity to work in his group. He has been a constant source of inspiration and motivation. Working with him has changed my way of looking towards chemical engineering problems. He gave me a lot of freedom, while he has always there to help me see things in perspective. I express my sincere gratitude to my co-supervisor Professor Moses Tade for his timely support and advice. I am thankful to both of them for sharing ideas on many varied issues such as report writing, time managements, presentation techniques etc. which helped me to develop my personal skills as well. I would also like to thank chairman of the doctoral commission, Professor Ming H. Ang, for evaluating my work and granting permission to complete my experimental studies in India. Also I take this opportunity to thank our industrial partner/Supervisor Mr. Michael Glenny for his valuable inputs on the FCC stripping operation. Despite his busy schedule, he was always there to discuss and compare the results with industrial data.

My very special thanks to Dr Ranjeet P. Utikar, who was like my other co-supervisor. Without his knowledge, perceptiveness and approach to crack problems, I would never have finished this work in time. My sincere thanks to Professor Shantanu Roy from Indian Institute of Technology, Delhi (IITD), India, for granting me permission to perform experiments at their labs. The experimental part of my thesis was impossible to do without their help. Several people have helped in making my work and life at IITD an enjoyable experience. In particular my special thanks to Rajesh Upadhyay and Prakash for their invaluable assistance during my stay.

I would also like to thank my colleagues, Divy, Emmannuel, Faye, Johan, Kailash, Milin, Owen, TJ who ensured a technically stimulating, creative and pleasant working environment and helped in technical and non-technical matters. The support given by technical and IT staff, notably Mr. Glennvill and Mrs. Alison Lynton is worth mentioning. Timely help from the secretarial staff, namely Ms.Jann Bolton and Ms. Naomi Mockford is highly appreciated.

Finally, I am thankful to my parents and family for their support during my tough times. I also acknowledge everyone who has assisted me directly or indirectly in the completion of this work. Their assistance invaluable and shall always be held in high regards.

TABLE OF CONTENTS

NOMENCLATURE

C_D	=	Drag coefficient
d	=	Solid diameter, m
d_m	=	Modified solid diameter, m
e	=	Coefficient of restitution
f	=	Drag function
F	=	Interphase momentum exchange term, $kg.m^{-1}.s^{-2}$
F_D	=	Diameter factor
g	=	Gravitational acceleration, $m.s^{-2}$
g_o	=	Radial distribution function
G_0	=	Solid flux, kg m^2 s
I	=	Intensity
I_0	=	Intensity in free space
K	=	Momentum exchange coefficient
l	=	Effective length, m
L	=	Length of measured Chord, m
P	=	Pressure, $kg.m^{-1}.s^{-2}$
R	=	Radial distance form centre of stripper, m
Re	=	Particle Reynolds number
T	=	Mean time of flight, s
t	=	Time of flight, s
$\vec{v}$	=	velocity vector, $m.s^{-1}$
$v_{r,s}$	=	Particle terminal velocity, ms^{-1}
u	=	velocity, $m.s^{-1}$

U_r = ratio of multi particle terminal velocity to single particle terminal velocity

U_0 = Superficial velocity, m s^{-1}

Greek letters

ε = phase volume fraction

ρ = density, $kg.m^{-3}$

$\bar{\tau}$ = occurrence of peak, s

τ = viscous stress tensor, $kg.m^{-1}.s^{-2}$

μ_s = solid shear viscosity, $kg.m^{-1}s^{-1}$

μ = mass attenuation coefficient

γ = gamma ray

ζ = solid bulk viscosity, $kg.m^{-1}s^{-1}$

σ = Variance of time of flight

Θ = granular temperature, $m^2.s^{-2}$

γ_θ = dissipation of granular energy, $kg.m^{-3}.s^{-1}$

ϕ = angle of internal friction

ϕ_{fs} = energy exchange between fluid and solid, $kg.m^{-1}.s^{-2}$

Subscripts

C = collisional

eff = effective

k = either phase

g = gas phase

m = metal

max = maximum

s = solid phase

q = either phase

T = operation of transpose

Acronyms

CARPT= computed automated radioactive particle tracking

CFD = computational fluid dynamics

FCC = fluid catalytic cracking

FRSI = full ring steam inlet

SPSI = Simple pipe steam inlet

RPT = Radioactive particle tracking

1. INTRODUCTION

In a Fluid Catalytic Cracking (FCC) unit, low value heavy hydrocarbons from an oil refinery crude distillation column are converted to more valuable gasoline, diesel oil, and light olefins. In the FCC, the heavy hydrocarbons are fed to riser where it comes in contact with the hot catalyst from the regenerator, which then leads to cracking reactions. The spent catalyst is then separated from the product and is regenerated in a regenerator before recirculating back into the riser. The spent catalyst coming out of the riser contains valuable hydrocarbon product along with coke adsorbed on the surface. The spent catalyst has to be stripped off using steam to recover the adsorbed/deposited hydrocarbons on its surface before it is sent to the regenerator. Incomplete stripping leads to loss of valuable hydrocarbon to the regenerator. The process of stripping of hydrocarbons from the catalyst surface occurs in a unit called steam stripper. Typically, FCC strippers have steam superficial velocity between 0.15 - 0.3 m /s and a catalyst mass flux of 30-75 kg /m^2s.

The steam stripper is an important component of an FCC, as incomplete stripping not only leads to the loss of valuable hydrocarbon to the regenerator; it also affects the stability of FCC by affecting the heat balance by increasing the regenerator dense bed temperature. A high regenerator dense bed temperature can lead to faster deactivation of the catalyst (McCarthy et al. 1997, McKeen and Pugsley, 2003a), hence affecting both the short term energy economics of the loop as well as long term catalyst inventory costs as shown in Figure 1.1.

Poor performance of stripper unit, leads to carry over of the unstripped hydrocarbons to the regenerator along with the catalyst. In the regenerator unit along with the coked catalyst particle, these unwanted excess hydrocarbons are combusted in the presence of oxygen, which is an overload on the regenerator. In turn this leads to very high dense bed temperature inside the regenerator. Also, this undesired combustion results in increase in emissions of undesired CO and CO_2 to the atmosphere. The consequence of high dense bed temperature in the regenerator also leads to an increase in the riser temperature. Undesired thermal cracking reactions of the feed mixture occur in the riser unit, due to the supply of hot catalyst particles from the regenerator unit. In turn, the thermal cracking reaction leads to faster deactivation and coking of catalyst particles. The catalyst particles loaded with more hydrocarbons are again passed to the stripper unit, further overburdening the stripper unit resulting in more

stripping steam consumption. Since FCC is a closed loop system, the poor performance of stripping unit, will have cyclic implications on the whole FCC process and can trigger a chain of activities which will not only decrease the efficiency of the stripper but will also increase the emission of greenhouse gases.

The common flow problems encountered in a stripper unit are channeling, bridging and maldistribution. Stripper internals, inlets and outlets design/configurations play a vital role in determining the hydrodynamics of the stripper unit. Therefore, to optimize the hydrodynamics of an FCC stripper, it is important to conduct complete 3D computational fluid dynamics (CFD) simulations of industrial-scale FCC strippers are needed. Therefore, the overall objective of this thesis was to conduct CFD simulations for small and industrial scale FCCU stripper and validating the predictions with experimental results and industrial observations with specific objectives as outlined below.

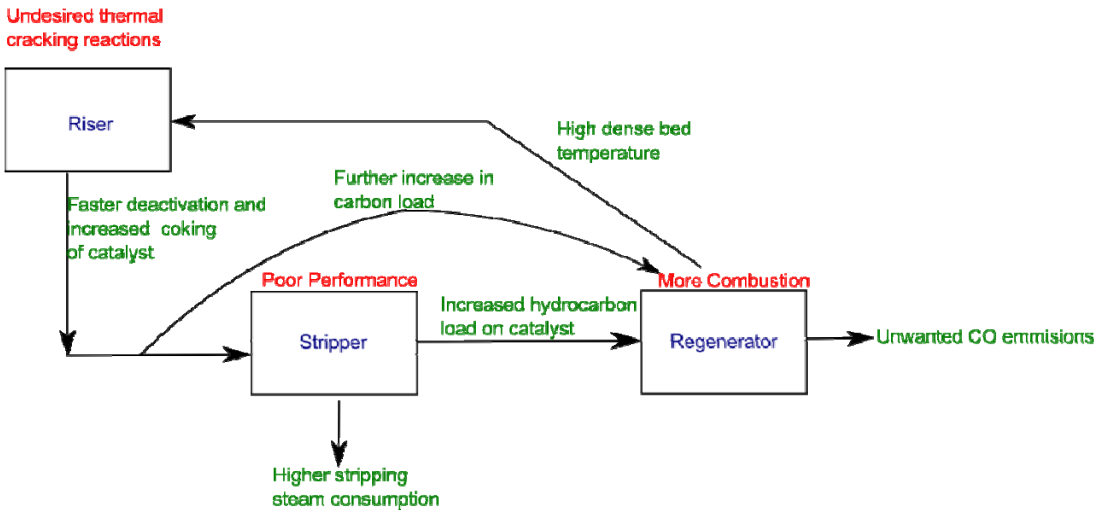

Figure 1.1: Schematic showing the importance of stripper performance.

1.1. Specific Objectives

The key objectives of the present work were:

- To develop an in-depth understanding on the hydrodynamics of counter-current dense bed stripping operation.
- To identify and understand the cause of various flow problems associated with FCC stripper.

- To understand the effect of different inlet and internal designs on the performance of the stripper unit.

The methodology adopted to carry out this work is described in the following section.

1.2. Integrated Experimental and Modelling Approach

The study was divided into two parts: experimental characterization and CFD simulations.

1) An experimental scale FCC stripper was designed and commissioned to conduct cold flow experiments. Line average solid holdup characteristics and mean particle time of flight were estimated at different operating conditions using γ-ray densitometry and RPT based time of flight experiments for gas-solid systems.
2) A CFD model was developed using the Eulerian-Eulerian approach, and was validated by comparing the predicted results with the experimental data.
3) The validated CFD model was then used to simulate industrial scale stripper system.
4) A detailed parametric study was done to understand the effect of different steam inlet configurations on the hydrodynamics of industrial scale FCC stripper. Both simple pipe steam inlet (SPSI) and a full ring steam inlet (FRSI) configurations were studied.
5) The effect of stripper internals on the hydrodynamics of an industrial scale FCC stripper was analysed by studying two different configurations, namely, disc and donut baffles and structured packing.

The outcome of this research resulted in important scientific and industrial contributions, which are discussed in the next section.

1.3. Scientific and Industrial Significance

This research project had substantial industrial significance, particularly with respect to fluid catalytic cracking operation. The outline of research work is depicted in Figure 1.2. Below is the summary of important scientific and industrial contributions that this research has accomplished:

1) The experimental work conducted in this research is first of its kind, in terms of applying γ–ray densitometry and time of flight experimental techniques for a complex geometry like FCC stripper.

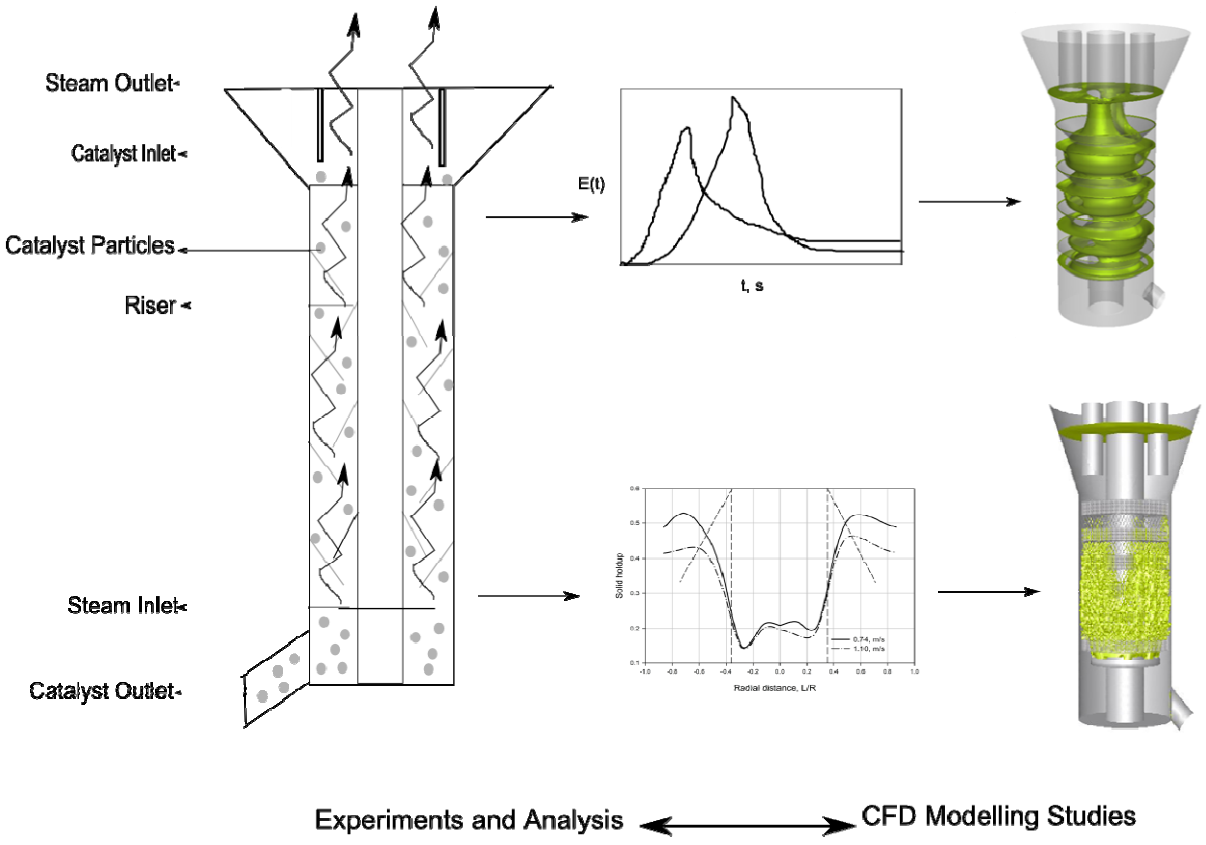

Figure 1.2: Schematic depicting research outline

2) The γ–ray densitometry experiments conducted on the small scale FCC stripper showed that the solid holdup profiles were asymmetric in nature. This observation was in contrast to the previous modelling studies, which were conducted in 2D domains.

3) E-curves of the time of flight experiments conducted using the radioactive particle (RPT) exhibited long tails for the stripper fitted with baffles, thus indicating the presence of dead zones in FCC stripper. This is an important finding for the operation of FCC units.

4) The detailed 3D CFD numerical experiments conducted for both small scale and industrial scale FCC stripper provided an improved more detailed understanding on the hydrodynamics of this complex counter current dense bed system.

5) The 3D CFD simulations also showed that the paths of the gas-solid flow in the FCC stripper are greatly influenced by the shape and presence of the internals. The disc and

donut baffle internals forced the phases to flow in a zigzag manner, while the structured packing allowed the phases to move freely in a plug flow manner. The understanding gained from this research will assist in designing new internals for the FCC strippers.

6) Based on the in-depth analysis of CFD simulations, new insights were gained on the mixing behaviour of the phases. Although the phases traverse in a counter current mode, the mixing is primarily achieved because of the internals. The disc and donut baffles allow the formation of local recirculation zones and mixing of phases. On the other hand, the interlocked plates in the structured packing elements force the phases to come in to contact with each other in each packing element. This study has for the first time provided a basis for new FCC stripper designs.

7) The cohesive nature of Geldart A FCC particles was accounted for by using a modified Wen-Yu drag model. The model predictions showed reasonable agreement with industrial data for solid distribution percentage when compared with Syamlal-O'Brien drag model.

6) The research undertaken in this project was in collaboration with a multinational industrial partner. The recommendations made from this work have helped the industrial partners to revamp its systems for optimum contacting of steam and catalyst. The operational and hardware changes have directly helped our industrial partner in optimizing their hydrocarbon recovery thus resulting in both economic and environmental benefits.

1.4. Thesis Structure

Figure 1.3 schematically shows the thesis structure of this research. The work was divided into a total of 7 chapters. The next chapter (Chapter 2) starts off by discussing the importance of FCC stripper unit, which is then followed by a detailed literature survey. Then chordal averaged solid holdup profiles and particle time of flight studies were studied using γ-ray densitometry and RPT based experiments for an experimental scale stripper in Chapter 3. In Chapter 4, the results from CFD simulations on an experimental-scale stripper have been discussed. The CFD models prediction and comparison with the experimental results have been analysed in detail for different operating conditions. Following this, an industrial scale FCC stripper has been simulated and discussed in

chapter 5. The study of hydrodynamics of an industrial FCC stripper is continued in Chapter 6, where the effect of different internal configurations on the stripper performance has been discussed. Finally, Chapter 7 provides a summary of conclusions and also discusses opportunities for future research in this area.

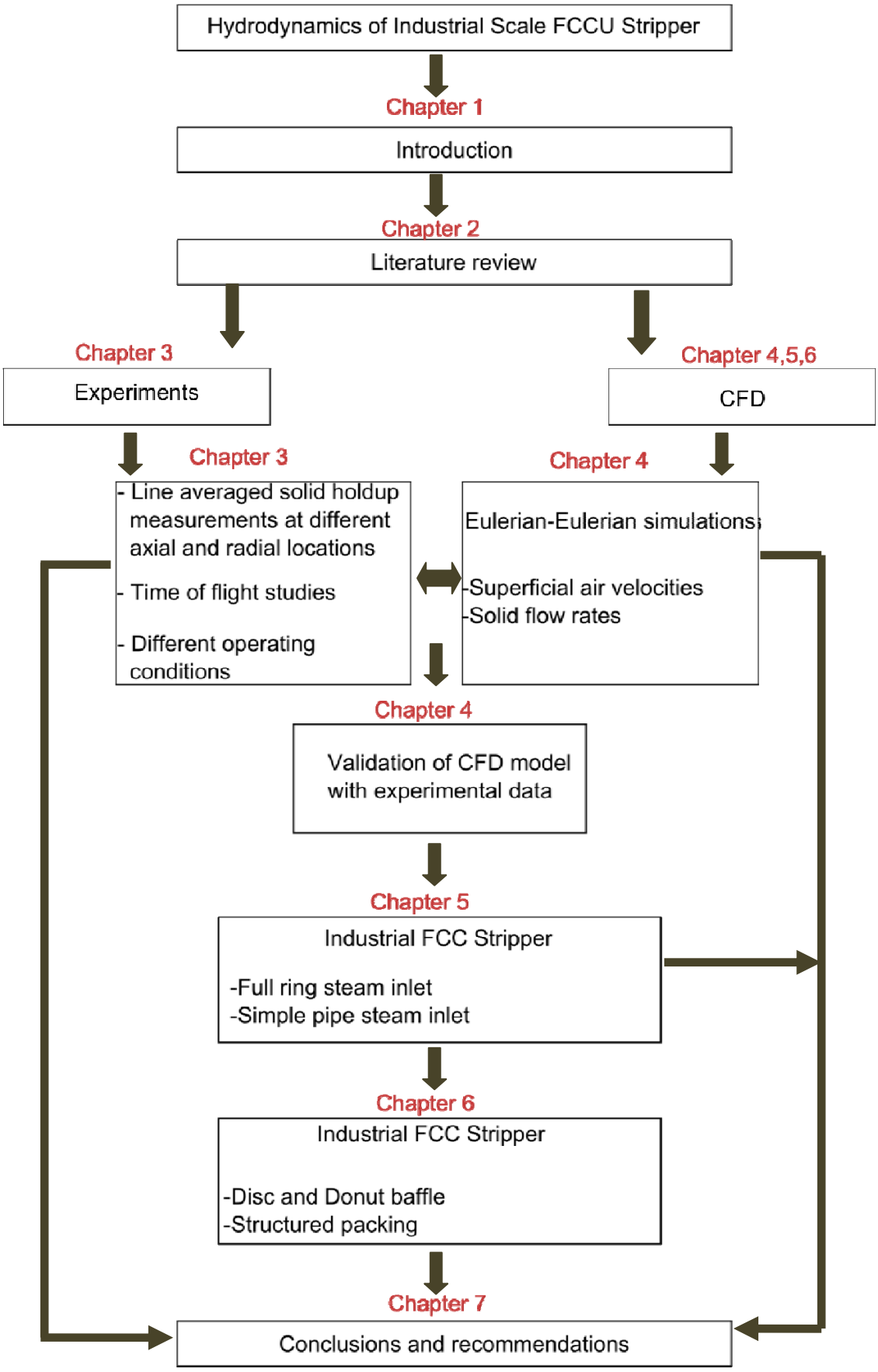

Figure 1.3: Thesis structure.

2. FLUID CATALYTIC CRACKING STRIPPER

The fluid catalytic cracking (FCC) unit is one of the most important unit operations of an oil refinery (Avidan et al. 1990). It converts low value heavy hydrocarbons to more valuable gasoline, diesel oil, and light olefins (Wang et al. 2004). The FCC unit consist of a riser, stripper and a regenerator (Arandes et al. 2000; Arbel et al. 1995). The schematic of a modern FCC unit is shown in Figure 2.1.

Preheated gas-oil mixture (300°C-500°C) is injected at the bottom of riser along with hot active catalyst feed from the regenerator. The feed vaporises and flows upward through the riser along with the catalyst. The gas-oil mixture is cracked to more useful light hydrocarbon products in the presence of catalyst in the riser unit. The light hydrocarbon products are passed to the distillation column for further fractionation. The cracking reaction is an endothermic reaction and leads to drop in temperature in the riser from bottom to top. To minimize, unnecessary thermal cracking, the riser is operated in short residence times (~2 seconds). In spite the short residence time, coking of catalyst occurs and leads to deactivation of catalyst. Also some valuable light hydrocarbons get deposited/adsorbed on the catalyst surface. The spent catalyst is separated in the cyclones from the products using a series of cyclone separators. The spent catalyst is stripped with steam in the stripper unit for the remove the hydrocarbons on its surface before being passed to regenerator unit for decoking. The regenerator is a hot, dense fluidised bed reactor with temperatures varying between 650°C-760°C, where catalyst is burnt in presence of air, to remove the carbon deposition on its surface. Combustion products and entrained catalyst particles are conveyed upwards, out of dense bed, into a dilute phase zone, where cyclones are used to separate the catalyst from the flue gas. The hot and nearly coke free catalyst is sent to the riser, thereby completing the cycle. The hot catalyst, therefore, provides heat for the endothermic reactions taking place in the riser.

About 45 % of worldwide gasoline-production comes from the FCC and its ancillary units. Since FCC is the dominant upgrading process in a refinery, it has a key role to play in the wake of increasing gasoline needs. Future FCC developments will not only be driven by profit but also by social and environmental constraints (eg. product quality). There is

increasing pressure on FCC processes to produce gasoline with reduced olefins and sulphur (Cheng et al. 1998). There is also immense pressure on the FCC to reduce emission of SO_X, NO_X and particulates. More importantly, these requirements should be achieved amid the challenges to process heavier feedstock (that contain more sulfur and heavy asphaltenes and aromatics).

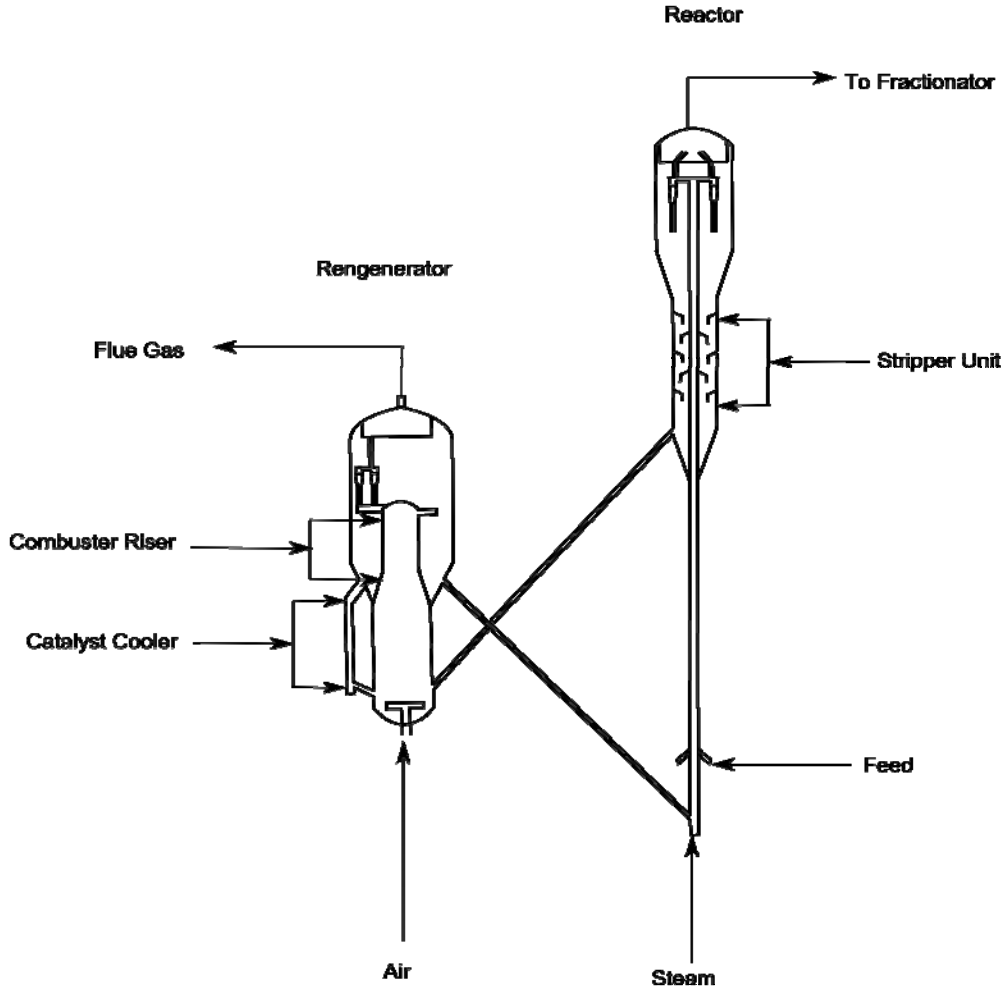

Figure 2.1: Schematic of a modern fluid catalytic cracking unit. (Wilson, 1997)

In order to maximize gasoline production and accommodate constantly varying feed conditions, several modifications have been proposed in the past for air and catalyst distribution in the regenerator unit. Some significant changes include; introduction of zeolite catalyst particles, switching to riser cracking, new nozzles for feed injection, efficient riser termination devices, and steam distribution design in strippers (Wrench and Glasgow, 1992; Murphy et al. 1992). However of all these modifications in the past, FCC stripper received little attention. Recently when it was realized that FCC strippers in many FCC units have

been pushed beyond the design limits (McKeen and Pugsley, 2003). Hence, it is important to understand the effect of different inlet and internal designs on FCC stripper performance. Also it is necessary to identify the cause of irregularities in the flow dynamics associated with FCC stripper. Therefore, it necessitates the research undertaken in this study to understand the key hydrodynamic features of FCCU stripping operation.

2.1. Hydrodynamics of FCC Stripper

As the catalyst particles move upward in the riser along with the mixture of hydrocarbon vapours, valuable hydrocarbons are deposited and adsorbed on the catalyst surface. It is very important to strip these precious hydrocarbons from the catalyst prior to sending it to the catalyst regenerator. The hydrocarbons are removed from the catalyst in a counter current flow of steam which is injected at the bottom of the stripper. The FCC stripper is an annular vessel that is designed to be concentric with and around the riser column. The resulting steam-hydrocarbon mixture flows up into the fractionators unit. An incomplete stripping would result in loss of valuable hydrocarbons with the catalyst particles to the regenerator section. The coke combustion reaction along with the combustion of these hydrocarbons in the regenerator unit can lead to higher temperatures in regenerator. This higher temperature will then have adverse effects on the FCC unit heat balance, which eventually will promote faster catalyst degradation and mechanical wear of components (McCarthy et al. 1997). High regenerator temperatures then compel to reduce the catalyst circulation rate and oil feed to the riser, eventually have a toll on the yield of FCC process (Miller et al. 2000). Therefore, the stripping operation is an important bottle neck in several FCC units (Rall and DeMudler, 2000).

The common flow problems encountered in the stripping operation are channeling, maldistribution and bridging (Senior et al. 1998), which can lead to inefficient or incomplete stripping. Flooding can be caused by high catalyst and high steam rates or by restrictive baffle designs. Typical design values of stripping steam superficial velocity are 0.15m/s-0.3 m/s and a catalyst mass flux of 30-75 kg/m^{2}s. (King, 1992). Flooding may result in carryover of injected steam to the regenerator by the catalyst particles due to its relative higher local velocity (Senior et al. 1998). Bridging is caused due to non-uniform steam distribution inside the stripper, which eventually leads to local defluidized zones of catalyst particles (Bi et al. 2004). Maldistribution is the result of channelling of phases, where steam flows up in region

of stripper and catalyst flows down in one region of stripper. All these problems can be minimized by good baffle design, even steam distribution and symmetrical stripper design.

Addition of simple baffles is a relatively low-cost measure to improve the performance of fluidized bed reactors (Jin et al. 1982; Kwauk, 1996). Various internal arrangements like disc-donut, V-shaped baffles, shades, trays, louver baffles, packing arrangements etc. have been proposed to avoid the common flow problems in stripper units. Horizontal or inclined baffles are used to increase gas–solid contacting, minimize short-circulating of solids, reduce gas bypassing in bubbles up the centre of the column and help distribute the gas uniformly over the cross-section. Reduction in the overall axial dispersion leads to an increase in the stripping efficiency (Cui et al. 2006b). In the following sections we briefly summarise the literature on FCC Stripper research.

Rivault et al.(1995) was among the first researchers to study the hydrodynamics of FCCU strippers. They used electrical capacitance tomography (ECT) to study the FCC stripper with operating conditions in the range of U_0 = 0.1-0.4 m/s and G_s = 28-108 kg/(m²·s), which are representative of commercial FCC operating conditions. The experiments were carried out in a stripper fitted with removable disc and donut baffles and monitored bubble diameters and bubble frequencies. Rivault et al.(1995) observed that baffled strippers provide effective bubble break-up, maintain a near constant bubble size over the stripper height when compared with non baffled strippers. Following this, Zhang et al. (2004) carried out mass transfer studies for the gas and solid phase in a 486×8000 mm plexiglass model stripper. The comparative study was carried out using oxygen tracing method for a general fluidized bed stripper and stripper fitted with disc and donut baffles for axial concentration distribution of oil and gas. It was found that the internal configuration and the gas-solid flow behaviour have an important effect on the stripping efficiency. Later Zhang et al. (2009) studied the effect of louver baffles on hydrodynamics and gas mixing in a fluidized bed of FCC particles using pressure transducers and Thermal Conductivity Detectors (TCD). Zhang et al. (2009) reported axial particle concentration profiles, bed expansion, pressure fluctuations and gas back mixing for a 2D column containing one layer of louver baffles and compared with the baffle free fluidized bed. Zhang et al. (2009) reported that the addition of louver baffles reduced back mixing. Apart from baffles, Rall and Demudler (2000) developed a new internal based on structured packing, named KFBE^{TM}. Rall and Demudler (2000) carried out pilot plant studies for stripper fitted with disc and donut trays and KFBE^{TM}. Their studies

indicated that stripper fitted KFBE^{TM} has performance advantages well beyond the capability of disc and donut trays. Despite the demonstration by Rall and Demudler (2000) on the superior performance of stripper fitted with packing internals, the key hydrodynamics of strippers fitted with packing's was not discussed in detail.

Modelling studies have also been carried out in the past on FCC Stripper units. Gao et al. (2008a), Gao et al.(2008b), McKeen and Pugsley (2003) have reported Computational Fluid Dynamics (CFD) based studies on the performance of FCCU strippers. McKeen and Pugsley (2003) modelled FCC stripper using a 2D (CFD) geometry and compared their results with Rivault et al. (1995). McKeen and Pugsley (2003) compared stripper hydrodynamics for different baffle types (standard disc and donut baffles, modified baffles and empty column) for different operating conditions. CFD model predicted improved break-up and redistribution of bubbles for a stripper fitted with baffles when compared to stripper with no baffles. Addition of down comers to the baffles reduces the onset of flooding. Although McKeen and Pugsley (2003) were able to get good agreement with Rivault et al. (1995) for some of the experiments, their model showed opposite trends for other data. This was attributed to the 2D approximation. Gao et al. (2008a) carried out hydrodynamics studies in FCCU strippers using a 2D CFD model. Gao et al. (2008a) compared bed density profiles for different stripper internal configurations (empty cylinder, V-baffled and disc and donut baffles) with experimental findings of Zhang (2003). Gao et al. (2008a) reported strippers fitted with disc and donut baffles give uniform distribution of gas and particulate phases in both axial and radial directions when compared with V-baffled strippers and empty cylinder. Gao et al. (2008b) studied mass transfer and stripping efficiency in an empty cylinder stripper and a stripper fitted with a V-shaped baffle, both experimentally and computationally. Gao et al. (2008b) reported that stripping efficiency depends strongly on operating conditions and also on internal structures. Increase in superficial gas velocity increases stripping efficiency. V-baffled strippers improve bubbles break-up and redistribution and enhance the gas-solids contact. Even though Gao et al. (2008a, 2008b) present radial and axial variation of bed density and get a reasonable agreement with experimental results, it is important to consider the simulations were performed for a 2D geometry. The effect of lack of symmetry in inlets and outlets design on the hydrodynamics of a stripper is difficult to predict using a 2D geometry.

Apart from FCC units, strippers are also used in fluid cokers. Fluid cokers are used in petroleum industry for thermal conversion of heavy hydrocarbons molecules into distillate products (Matsen, 1985; Kunii and Levenspiel, 1991). Bi et al. (2004) investigated the flooding behaviour in gas-solid counter current flow in fluidized beds. The experiments were carried out in a semicircular fluid coker cold model with a diameter of 0.61 m for FCC particles. Different baffle configurations were tested to study the flooding behaviour. The baffles tested included sheds, steeper sheds, cylinders of circular cross section and flat horizontal plates. Pressure transducers were used to monitor pressure fluctuations and pressure drop. Bi et al. (2004) found that, flooding is affected by superficial gas velocity, open area function, and open slot width and baffle shape. Usage of steeper sheds delays flooding. Later, Bi et al. (2005) examined the hydrodynamics of the stripper section for the same geometry by analysing pressure fluctuations and particle motion using pressure transducers and fibre velocimetry probe. Bi et al. (2005) observe that pressure drop over the stand pipe entrance is very sensitive to solid flux fluctuations'. Also pressure drop over the top rows of sheds was lower at higher solids circulation fluxes and at higher gas velocities due to formation of gas pockets between the top two shed rows. For the same geometry details of Bi et al. (2004, 2005), Rose et al. (2005) conducted further experiments on different stripper configurations to identify the best configuration, which will reduce stripper shed fouling and increase run length. Rose et al. (2005) determined the efficiency for different stripping configurations (empty stripper, gas-jet stripper and stripper with internal shed-baffles combined with jets) using TCD technique. The studies concluded that a combination of two mega sheds with gas jets/spargers attained better stripping efficiency and has a higher potential to reduce fouling effects, prevent flooding and increase run. This work was further extended by Cui et al. (2006a, 2006b). Cui et al. (2006a) examined the effect of different jet/steam configurations in a stripper fitted with mega sheds. The combinations tested were, 18 horizontal wall jets with two mega sheds; 12 horizontal wall jets and three spargers with two mega sheds and a combination of two mega sheds with 5 sweeping jets, 7 free jets). The stripping efficiency was determined for the each case using helium tracer concentration with the application of TCD technique. The results indicated that two mega sheds combined with steam injection via spargers, sweeping jets and free jets provide highest stripping efficiency. Then Cui et al. (2006b) studied the mixing characters of gas-solids in the fluid coker stripper. Stripping efficiency and gas-solid mixing behaviours was tested for different shed geometries (90^{o} top angled shed, 30^{o} top angle shed and Styrofoam fouled sheds). The studies concluded

that the stripping efficiency strongly depends on baffle geometries as wells operating conditions. The stripping efficiency increases with the superficial gas velocity at a constant solid solids circulation rate. Gas mixing is higher in the core region, when compared with the region near walls. The particles peclet number in the stripping section indicates the flow is neither plug flow nor perfect mixed. However, research of Bi et al. (2004, 2005); Cui et al. (2006a, 2006b); Rose et al. (2005) used the internals (predominately sheds) not common in FCC strippers. As most of the commercial FCC strippers use disc and donut baffle configuration for internals. The summary of different type of internals used in previous modelling studies is given below in Table 2.1.

Table 2.1: Summary of Internals used in previous modelling studies.

S.No	Internal Type	Reference
1)	V-Shaped	Gao et al. (2008a, 2008b)
2)	Disc and Donut	McKeen and Pugsley (2003), Gao et al. (2008a, 2008b)
3)	Louver Shaped	Zhang et al. (2009)
4)	Sheds	Bi et al. (2004, 2005), Cui et al. (2006a, 2006b), Rose et al. (2005)
5)	Structured Packing	Rall and Demudler (2000)

2.2. Summary of Research Gaps in the Literature

The above discussion on the available literature highlights the following:

1) The previous experimental scale studies have been mostly carried out for pilot scale or lab scale studies. Moreover, detailed data on the phase fraction map of the entire equipment (i.e. the distribution of the phases at different radial and axial locations in a stripper) is not available. Such data will be critical for understanding the hydrodynamics and will also be useful for validation of CFD models.

2) The CFD modelling studies have been conducted for 2D models. But 2D models fail to consider the effects of lack of symmetry in vessel design on the flow dynamics. Other than that 2D model predictions can often misguide in understanding the basic nature of flow.

3) Other than FCC strippers, the studies on fluid cokers concentrated on effect of steam injection patterns and different combination of internal arrangements. However, the fluid cokers predominantly use sheds as internals, which is not common in FCC stripper.

4) New type of internals like structured packing's are studied in pilot scale plants. Although, their superior performance to strippers fitted with baffles are reported, key hydrodynamic characteristics of stripper fitted with packing is not available in the open literature.

Therefore to address the several flow problems (flooding, bridging and maldistribution) and optimize the performance of industrial scale FCC Stripper, it is necessary to carry a complete 3D hydrodynamic study of an industrial scale FCC stripper. Hence the overall objective of this thesis was to conduct experiments and perform CFD simulations for both experimental and industrial scale FCC stripper with specific objectives.

3. NON-INVASIVE EXPERIMENTAL TECHNIQUES FOR FCC STRIPPER HYDRODYNAMICS

All the gas-solid multiphase system description and design largely rely on empirical correlations, which in turn are based on measurements made under conditions as relevant as possible to industrial practice. This practice is very much true for classic chemical engineering problems, where the quantities such as phase holdup and pressure drop are predicted via empirical correlations. Hence it is a necessity to have precise data, in the first place to obtain realistic empirical correlations (Boyer et al. 2002). Modern approaches such as CFD based models are used widely in design on multiphase reactors; however CFD models still require information on local and transient flow characteristics. Hence it is a prerequisite to have a relevant experimental data, of local characteristics of any multiphase system.

In the last two decades advances in instrumentation technology as well as high speed computers have led to a significant progress in the development of both invasive and non invasive measurements and flow visualization techniques for multiphase flow characterization. A list of these tools includes hot wire anemometry (HWA), laser Doppler anemometry (LDA), heat pulse anemometry (HPA), particle image velocimetry (PIV), computer automated radioactive particle tracking (CARPT) or simply radioactive particle tracking (RPT), computed tomography (CT), optical probes, and photographic techniques.

Depending on its level of interference with the flow field, the above techniques can be divided into two categories: (i) invasive and (ii) non-invasive techniques. Invasive methods (probe techniques) include optical filter probes, extraction probes, pitot tubes and isokinetic probes. These probes are easy to use at industrially conditions, but the drawbacks of these methods is that they require calibration, maintenance as fouling may occur on long term usage. In the past, invasive methods have been used for gas-solid systems such as Circulating Fluidized Bed (CFB), which is similar to the stripper system in terms of high solid flux. However, the measured quantities using probe techniques have resulted in appreciable errors when used in large-scale systems (Bhusarapu et al. 2006). Non-invasive techniques include optical methods such as PIV, LDV, and high speed cameras, and those which use radio

isotopes such as particle emission particle tracking (PEPT) and gamma-ray emitting radioactive particle tracking (RPT). All these techniques have been widely applied for different multiphase applications. Stellema et al. (1997) successfully employed PEPT for determining solids residence time distribution in interconnected fluidized beds. Godfrey et al. (1999) applied γ-ray emitting techniques for determining position and velocity of large particles in a gas-solid riser.

For a gas-solid system like stripper, application of optical methods would be not at all useful due to the opaqueness caused by the high solid mass flux and the presence of vessel internals. Bhusarapu et al. (2004a) have successfully used γ-ray emitting radioactive particle tracer methods for CFB systems which are similar to stripper in terms of high solid flux. Also in the recent past, Upadhyay and Roy (2010) have used densitometry and γ-ray emitting radioactive particle tracer methods to study binary fluidized beds. Bhusarapu et al. (2004a) reported solid holdup and particle Residence Time Distribution (RTD) for a CFB system using densitometry technique (CT) and RPT based Time-of-Flight technique respectively. The latter technique was also reported earlier for liquid-solid transport by Roy et al. (2002). As discussed in the following sections, an approach similar to Upadhyay and Roy (2010) has been used in this study to determine the solid holdup and particle average time of flight in the stripper system.

3.1. Experimental Setup

Based on the "estimated" mean residence time and solids holdup data from an industrial scale stripper, an experimental cold flow stripper was designed as shown in Table 3.1. A schematic of the experimental setup is shown in Figure 3.1. The construction material of the stripper outer body was perspex and the internals were made of stainless steel metal. Thus, the whole unit was designed in a manner (diameters adjusted such) that solid particles rolling down the outer (stripper) frustums roll down the sloping inverted frustums of the inner (stripper) inverted frustums.

To ensure a counter-current operation, the solid particles were fed from the top using hoppers with air being injected through a ring sparger from the bottom. The usual catalysts particles in the FCC systems are Geldart A type with average size of 80μm. These particles have cohesive inter-particle forces that lead to clustering of particles, resulting in larger effective particle sizes (Mckeen and Pugsley, 2003). These effective diameters are usually order of magnitude higher than the average particle diameter (Lettieri et al. 2002). Moreover, in the

follow-up work, the same experimental system was used to track trajectories of solids using radioactive particle tracking (RPT). It is difficult to obtain radioactive particles of sizes smaller than 500 μm due to the limitations posed by artificial transmutation in nuclear reactors. Therefore, glass particles (diameter: 800μm; density: 2600 kg/m^3) were used in this study instead of the usual FCC particles in industrial stripping operations. Two hoppers were placed above the stripper to store the glass particles. The particles were fed to the stripper at a constant rate through two pipe inlets. The solids flow rate was varied from 0.025 kg/s to 0.042 kg/s, and was controlled by a set of gate valves. The particles entered the stripper in the disengager section (Figure 3.1) and were made to move down the disc-donut baffles against the air flowing upwards, before exiting from the bottom of the stripper. The outlet flow rate was adjusted using a gate valve in order to achieve a steady.

Table 3.1: Dimensions of stripper.

All dimensions are in m	Experimental scale	Industrial scale
Column total height	0.44	10.227
Column diameter	0.14	3.2
Riser diameter	0.048	1.18
Disc baffle height	0.03	0.429
Disc baffle outer diameter	0.14	3.2
Disc baffle inner diameter	0.106	2.342
Donut baffle height	0.048	0.595
Donut baffle outer diameter	0.108	2.37
Donut baffle inner diameter	0.048	1.18
Particle inlet diameter	0.025	0.54

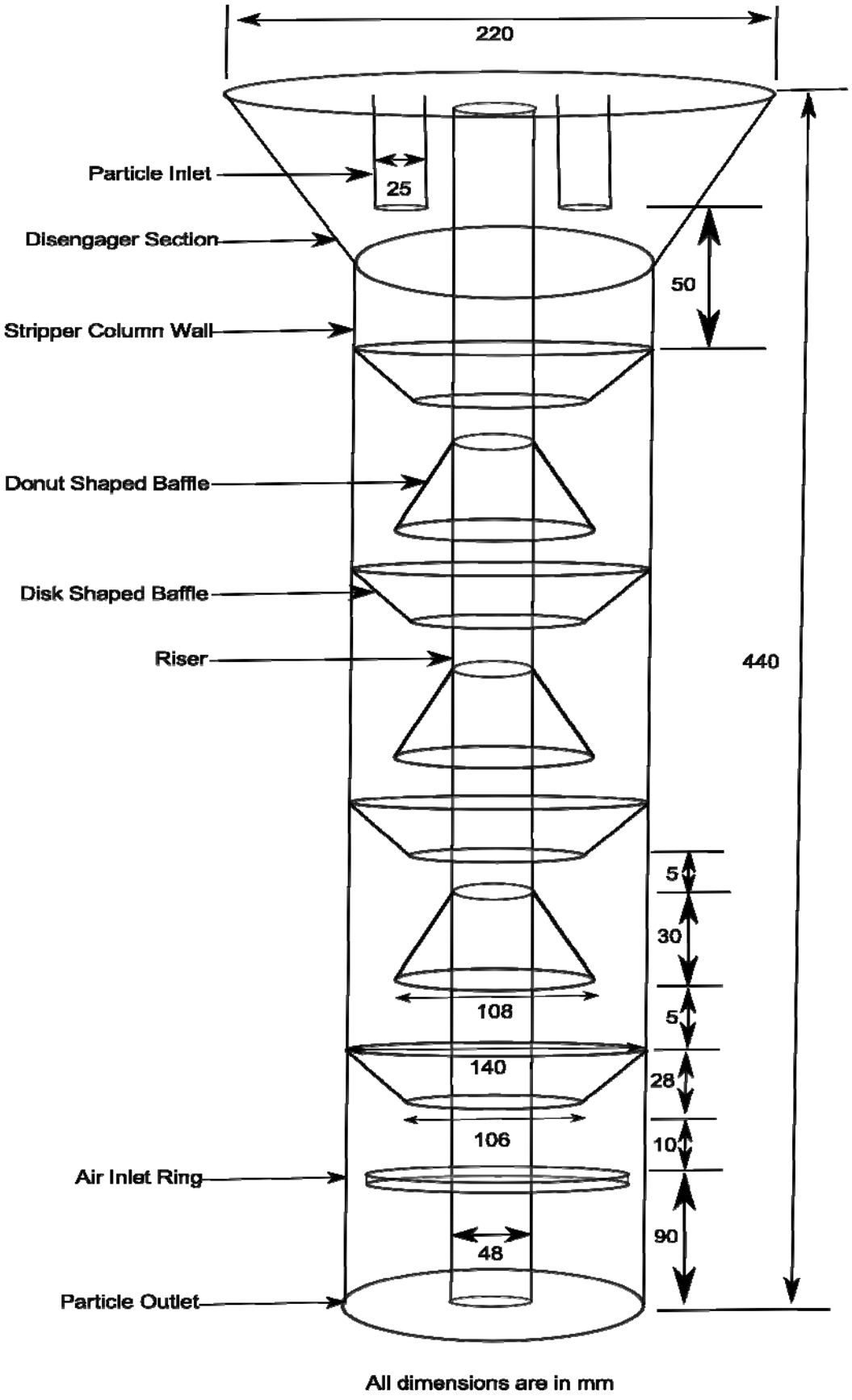

Figure 3.1: Design of stripper column.

state, such that this flow rate matched the inlet solids flow rate at the top. The solids were collected in a bin and were immediately transferred (manually) to the hoppers at the top in order to maintain a constant flow rates. Sufficient solids inventory was maintained in the hoppers such that at no point did the hoppers run dry and the rate of manual replenishment of the solids onto the hoppers was far quicker than the rate at which the solids level would change in the hoppers. The solids throughput was monitored and measured manually at regular intervals of equal duration at the bottom, so as to ensure that steady state conditions always existed in the system.

Air was used as a fluidizing medium, which was fed using a ring sparger with 1 mm nozzle diameter. A compressor at a constant pressure of 25 kg/cm^2 was used for the air supply. System was maintained at atmospheric pressure with the air being allowed to escape from the top of the disengager section. The air flow rate to the stripper was measured using a standard air flow meter which has a range from 100 lpm to 1000 lpm and controlled using a ball valve. Experiments were conducted at different air flow rates ranging from 600 lpm to 900 lpm corresponding to superficial velocities of 0.72 m/s and 1.1 m/s respectively. For these flow conditions radiation intensity in terms of attenuation was measured at different axial and radial positions. The experiments were conducted in batch with time duration of 3 hours ensuring data collection for one complete operating condition. The solids holdup was calculated by applying the Beer-Lamberts law. The details of densitometry techniques, its principles and calculation methodology are discussed in the following section.

3.2. Densitometry Experiments

When a narrow, parallel beam of mono-energetic γ rays (or any electromagnetic radiation) is transmitted through a closed system containing a two-phase mixture, the intensity of the radiation (radiation flux, or the number of photons per unit area per unit time) is attenuated in accordance with the Beer-Lambert's Law. This forms the basis of transmission tomography and densitometry, and in the recent past has been successfully employed for extracting phase holdups in various multiphase systems (Roy et al. (2002); Upadhyay and Roy (2010). According to of Beer-Lambert's Law, the attenuation of radiation intensity in any medium, *I*, is given by

$$I = I_0 e^{-\mu_{eff}\rho_{eff}l_{eff}} \tag{3.1}$$

Where, I_0 is the intensity of a collimated beam of radiation in free space; μ_{eff} is the mass attenuation coefficient; ρ_{eff} is the effective density and l_{eff} is the intervening distance between the source and the detector.

For this study, a single continuous collimated source aligned with a single detector on a moving horseshoe carriage (see Figure 3.2and Figure 3.3) was used. At one end of carriage, a lead-collimated source (Cs-137, 3 mCi strength) was fixed and at the other end a scintillation detector (NaI (Tl), from Bicron®). The source-detector assembly was suitably placed around the stripper shown in Figure 3.3. The carriage was designed to move both in horizontal and in vertical directions. Using the source-detector assembly, line-averaged attenuation of radiation intensity was measured for different radial locations along the height of stripper for different flow conditions.

The mass attenuation coefficient μ_{eff} is the sum of individual phase's attenuation coefficients' weighted by their respective volume fractions and it is given by,

$$-\ln\left(\frac{I_{g,m,s}}{I_{g,m}}\right) = \overline{\varepsilon_{s,l}}\left(\mu_s\rho_s - \mu_g\rho_g - \mu_m\rho_m\right)l_{eff} \tag{3.2}$$

Where, ε_{sl} is the line averaged solids holdup; μ_s, μ_g and μ_m are the attenuation coefficient for solid (glass), gas and metal respectively. The mass attenuation coefficient for solids and metal are 0.156 and 0.585 and the respective densities are 2600 kg/ m^3 and 7600 kg/ m^3. Therefore, knowing intensities ($I_{g,m}$, $I_{g,m,s}$), the effective chordal length (l_{eff}) values and the respective mass attenuation coefficients for the metal, gas and glass particles, the line (chordal) averaged solids holdup could be estimated at any given location using equation 3.2. A sample calculation is given in Appendix-I.

Note that when the source-detector assembly is moved in the horizontal plane at a fixed elevation, the line (collimated beam of γ-radiation) traced between the source and detector represents a chord, in general, in the circular cross-section of the cylindrical vessel. At different chords, the intervening distance l_{eff} is in general different, and hence what one obtains from a set of measurements made at one plane are a set of "chordal-average" measurements. Taken together, they represent the variation of phase holdup along a chord (and not the radius); thus representing a "chordal profile" and not a "radial profile".

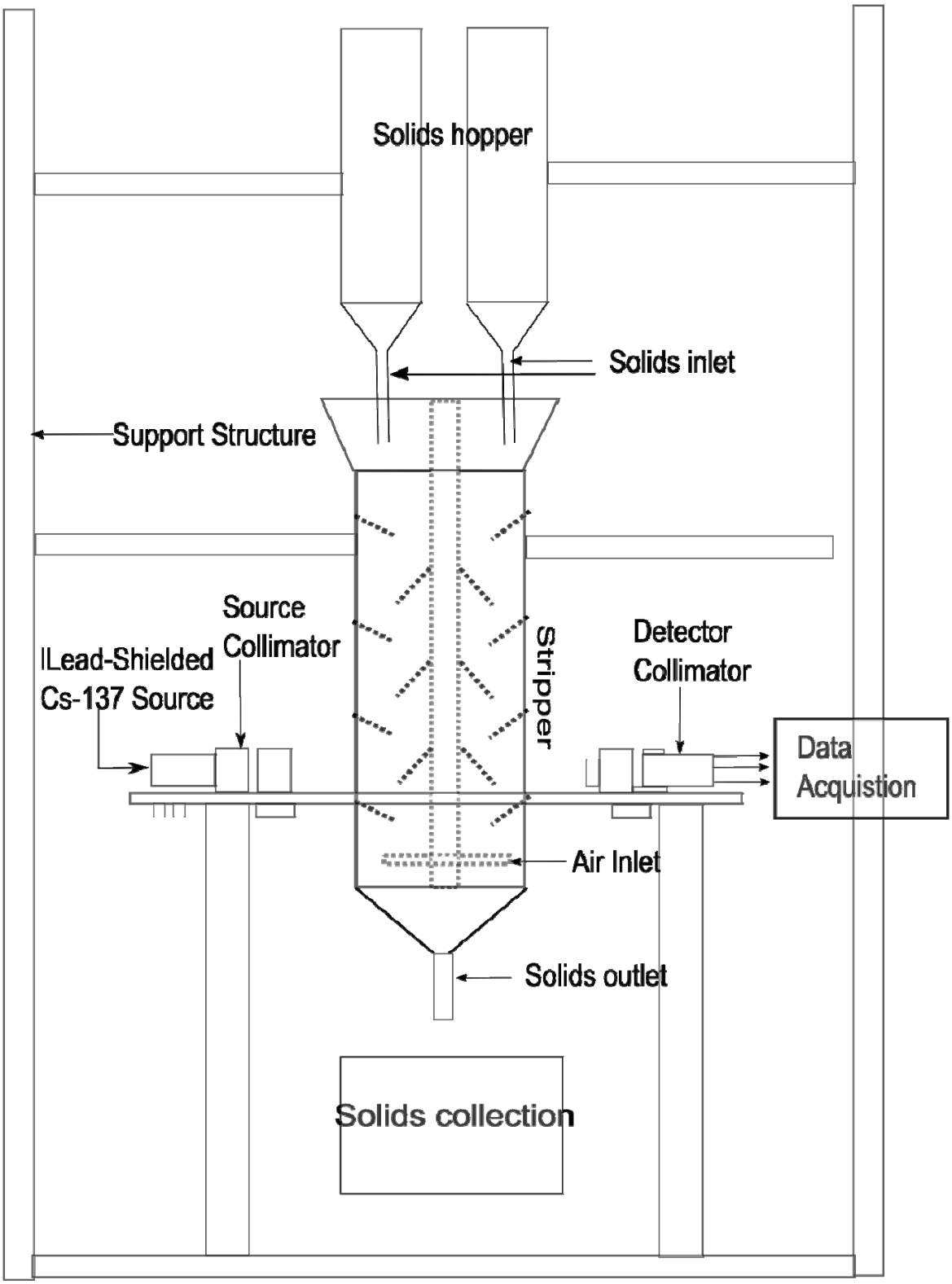

Figure 3.2: Schematic of experimental setup.

Figure 3.3: A photograph of densitometry experimental setup.

In the present work, solids holdup data was collected in the stripper column for various operating conditions at different axial locations. Figure 3.4 shows the measured I_0, I and the calculated solids holdup profiles for a typical case. The I_0 measurements (Figure 3.4 a) were taken with the empty column just fitted with the internal baffles. The I measurements (Figure 3.4 b) were preformed for a solid flow rate of 0.033 kg/s and superficial air velocity of 0.74 m/s. Each measurement scans through various chords on a cross section. The measurements were taken such that the chords pass through the centre of the baffles across it height. On a single cross sectional plane, thirteen equally spaced chordal measurements were recorded. The attenuation measured by the scintillation detector are inversely related (the projection measurement is inversely proportional) to the resistance offered by the medium as the radiation passes through it from the source (equation 3.2). Thus, more the resistance in the medium, lesser the attenuation detected by the detector.

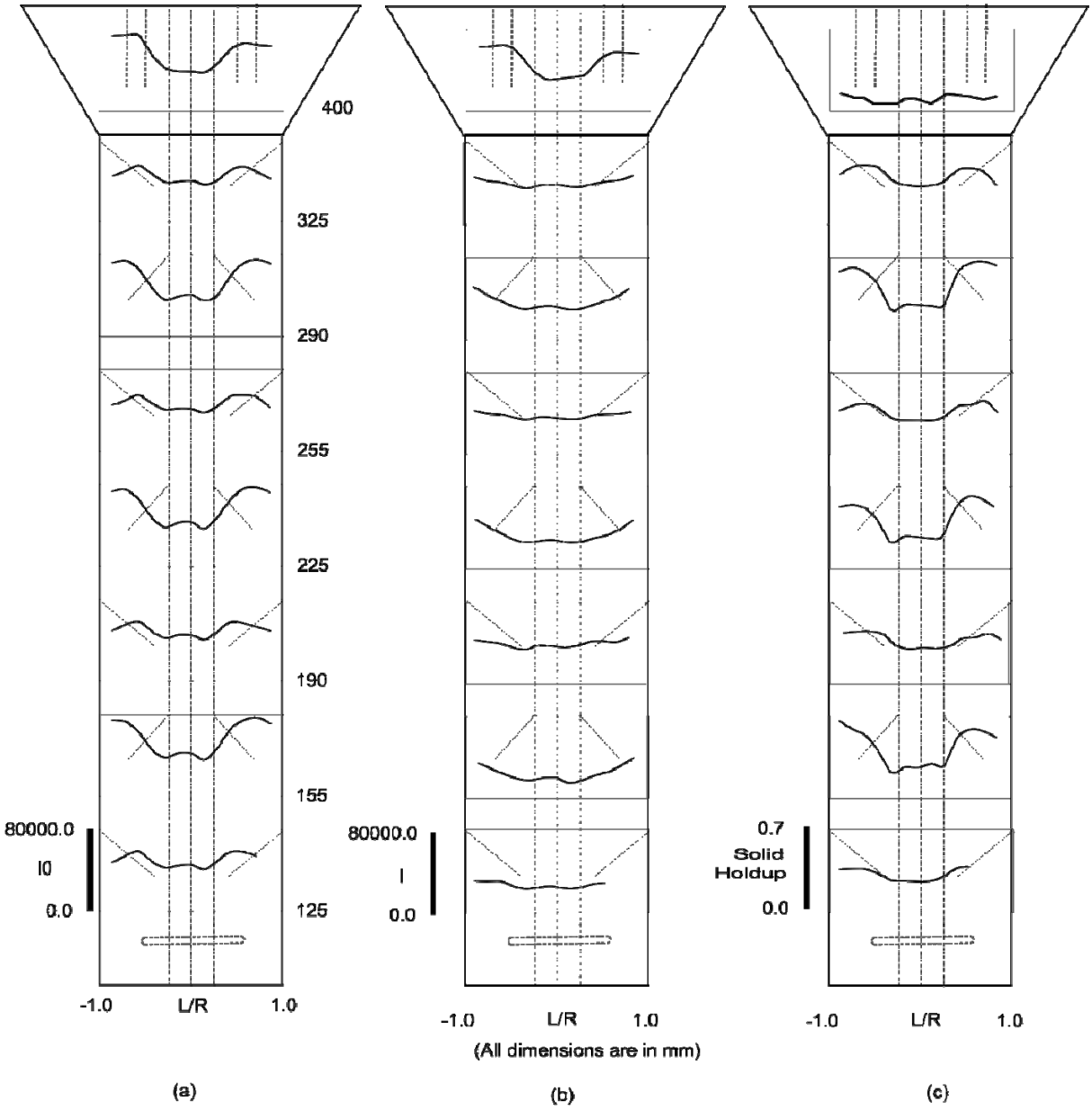

Figure 3.4: Preview of densitometry results. (a) Measured intensity when the column is empty, (b) Measured intensity with solids flow, (c) Calculated solid holdup.

Typically, two different shapes of the attenuation intensity profile were observed for the disc and donut baffles. In general, lower attenuation intensities were observed in the presence of metal, as it provides a stronger resistance to propagation of electromagnetic radiation. Thus, in case of the disc baffles (at heights 125, 190, 255 and 325 mm) lesser attenuation intensities are registered as the chord passes the baffle metal. There is steep rise in the attenuation intensity as it passes through the space between the disc baffle and the riser, as such a chord has less amount of metal (which is otherwise highly attenuating). This is followed by a fall in the attenuation in the riser section, which is basically a hollow cylinder. Thus, slight increase in the counts is observed at the centre of the riser column, even though this rise is not

dramatic since the path length (chordal length) is the highest here. In case of the donut baffles (at heights 155, 255 and 290 mm), higher attenuation is observed in the region between the baffles and the stripper wall. The counts dip drastically in the area near the riser walls as it is dominated by the riser walls as well as donut baffles. The top disengager section (at 400 mm) shows similar behaviour as the donut baffles with lower attenuation count at the centre and higher towards the periphery. However, the region of lower counts is limited to the riser section as there are no baffles present. In contrast to the empty stripper, the attenuation intensity observed in the presence of solids (Figure 3.4 b) was almost flat for the disc shaped baffles, where the profiles show a slight dip towards the centre of the stripper. In the disengager section, the profiles of both I and I_0 are similar indicating very small volume fraction of solids.

The phase fraction map calculated using the values of I and the I_0 using Equation 3.2 is shown in Figure 3.4c. The solids holdup profile at a given cross section resembles the I_0 profile as the profiles of I are almost flat. This clearly indicates that the solids holdup is influenced by the shape of the baffles. While analysing these figures one must note that these are line chordal averages at various radial locations and not radial averages. Thus, although there are no solids present in the riser section a non-zero volume fraction, corresponding to the holdup in the line of measurement, is observed. In the disengager section, the solids entering from top form a bubbling bed before the solids move down through the baffles. When the air passes through this bed of particles, some particles elutriate. The line of measurement in this experiments was above the bubbling bed in order to capture the elutriation. Very less elutriation was observed for the experimental conditions investigated in this study, and a very low solids volume fraction was observed in this section.

3.3. Time of Flight Measurements (TOF)

The second type of experiments was to determine the “time of flight” of the solids in the stripper section. To perform this measurement, a principle similar to Radioactive Particle Tracking (RPT) is followed. More details of RPT experiments in different systems can be found elsewhere (Roy et al. 2005, Dudokovic, 2002). However, unlike RPT, full velocity field reconstruction is not attempted owing to the complex geometry of the stripper. Rather, simpler time-of-flight measurements are made.

Accurate tracking of the particles necessitates the use of a radioactive tracer particle having physical properties similar to the glass particle used in this study. Therefore a single glass particle was irradiated with Sc-46 with a half life of 82.6 days and strength of 50 μCi in the reactor for a period of two days. This active irradiated glass particle (800 μm and 2600 kg/m^3) was used as a source. A set of scintillation detectors was used for simultaneous acquisition of photons emitted by the tracer particle. The photon counts recorded by these detectors were not used for positron construction, but were used for determining the time of entry and exit of the tracer particle.

Two batches of experiments were performed. In each batch, the detectors setup was aligned to the centres, to track radioactive tracer particle in the stripper. The first batch of experiments was performed to measure the overall TOF for the tracer particle in the stripper (Figure 3.5). A set of two detectors was used with one being at the particle inlet plane, and the other positioned at the particle exit plane with their centres aligned. Both detectors were positioned at 9 cm away from the columns centre. The next batch of experiments was performed to measure TOF of the tracer particle in each baffles zone, see Figure 3.6. The detectors were positioned to align with the top of each disc baffle. The tracer particle was introduced at the top in the hopper section and was collected at the bottom in the collection bin. A Geiger-Muller counter was used to ensure and detect that the tracer particle had entered the collection bin. This was followed by immediately turning the data acquisition system off. Once the particle was acquired, it was re-introduced at the top and the data acquisition was restarted again. The single tracer particle was introduced in each hopper alternatively, to reduce the effect of inlet position in the overall results. The same procedure was repeated for 50 times, for different operating conditions in each batch of the experiments. The Time of Flight (t) is defined by:

$$t = \overline{\tau^1} - \overline{\tau^2} \tag{3.3}$$

where,

$\overline{\tau^1}$, is the occurrence of the first peak in the average of first detector set called as particle entry time. While, $\overline{\tau^2}$ is the occurrence of the last peak in the average of second detector set, called as particle exit time. Roy et al. (2001) and Bhusarapu et al. (2004a), carried out similar TOF experiments for a CFB and determined Residence Time Distrubution (RTD), based on the distributions of TOF data. However, due to lack of sufficient statistics (50), the same

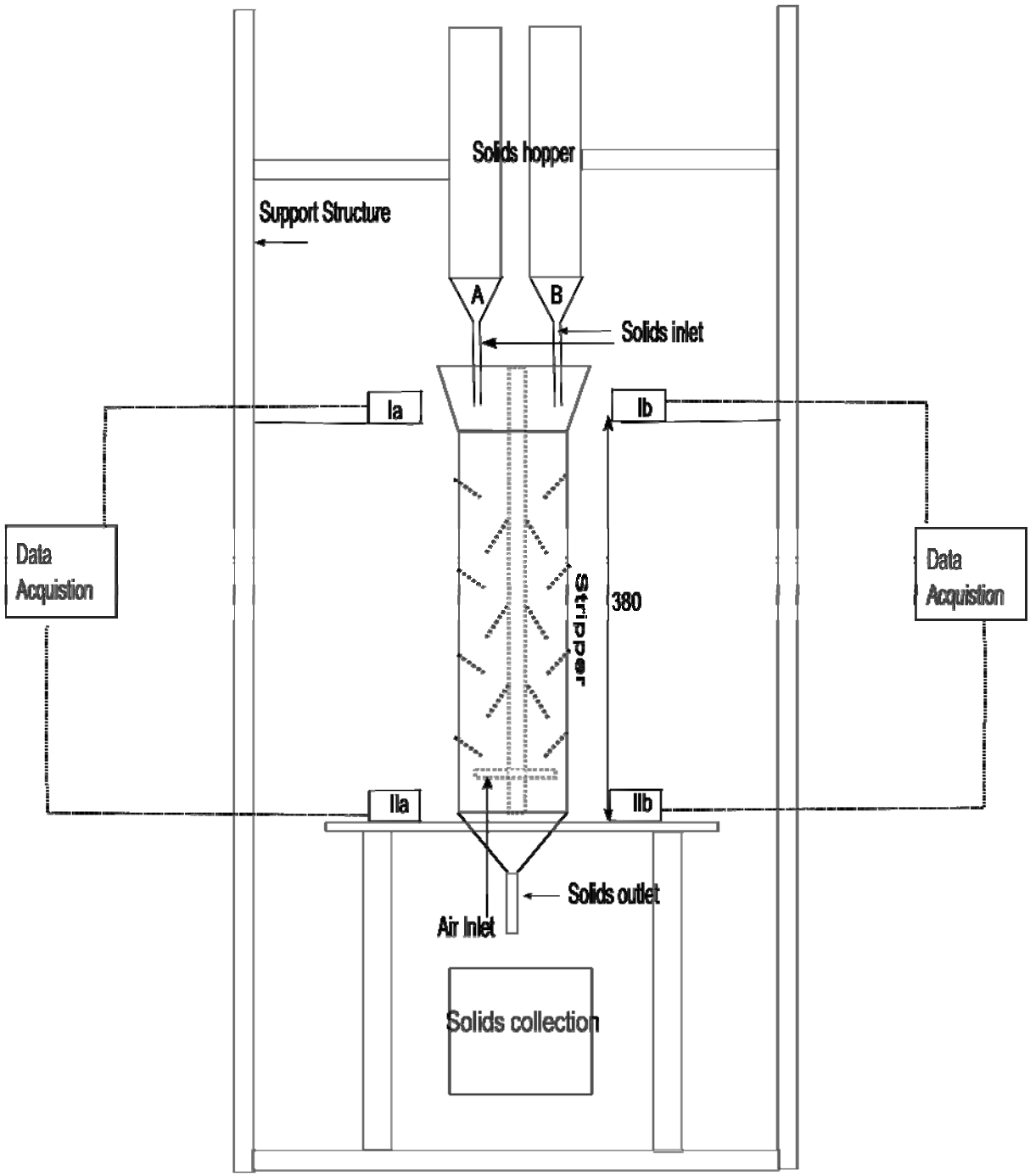

Figure 3.5: Schematic of experimental setup for over all time of flight experiments.

procedure was not followed for finding RTD of tracer particle in stripper. Instead a mean time of flight (T), which is an indicative of RTD, was determined. Where T is given by,

$$T = \frac{\sum_{i}^{n} t}{n} \qquad (3.4),$$

The variance in the TOF may be calculated as:

$$\sigma^2 = \frac{\sum_i^n (t-T)^2}{n-1} \tag{3.5}$$

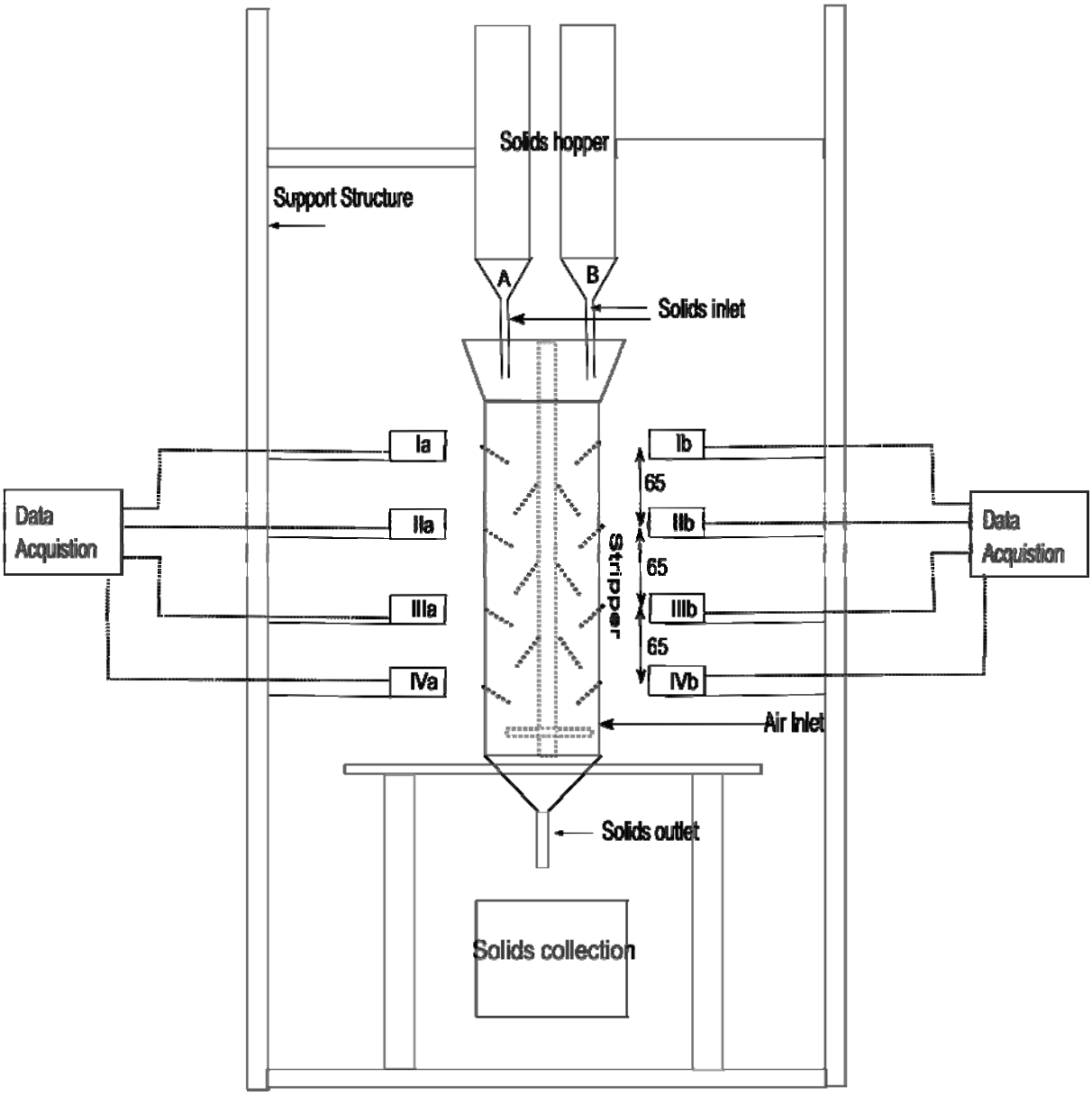

Figure 3.6: Schematic of experimental setup for time of flight study at the baffles section.

3.4. Results and Discussion

In the results and discussion section both densitometry experimental results and time of flight experimental results are discussed. First the effect of different operating conditions on solid holdup profiles is discussed. This is followed by time of flight experimental technique results.

3.4.1. Effect of Air Velocity on Solid Holdup

The effect of air flow rate on the solid volume fraction is shown in Figure 3.7a and Figure 3.7b. Figure 3.7a shows a profile of a typical disc baffle at axial location of 190 mm and Figure 3.7b of a typical donut baffle at an axial location of 225 mm. For solids flow rate of 0.025 kg/s, the solids volume fraction is plotted as a function of radial coordinate. Data are plotted for two different superficial air velocities of 0.74 m/s to 1.10 m/s. The solid particles flow downwards in counter current fashion with respect to the air. At the disc donut shaped baffle (Figure 3.7a), higher solids volume fraction is observed in the area between the baffle and the riser. Owing to the 45° angle of the baffle, the solid particles moved into the contracting area between the riser column wall and baffle's wall, which resulted in an increase in the solids volume fraction in the middle section.

The upward moving gas was obstructed by the disc baffle and a dead zone was formed near the stripper wall region below the disc baffle. As this zone is predominantly occupied by gas, lower solids holdup was observed near the stripper walls. It should be noted that the densitometry results tend to be marginally less accurate in the near wall and the dead zone regions due to the presence of thick welding material on the baffles in this region. In reality, the volume fraction will be still lower than that reported by the densitometry studies. It is observed that the increase in air flow rate had a significant effect on the solids volume fraction. Lower solids hold up was observed for higher superficial air velocities. As the superficial air velocity was varied from 0.74 m/s to 1.10m/s the observed maximum solids holdup falls from 35% to 25% in the disc shaped baffle region. At the donut baffle (Figure 3.7b), a higher solids volume fraction was observed in near wall region. As the particles flow through the donut shaped baffle region, they enter the open region between the disc shaped baffle and the riser wall. The 45° angle of the donut shaped baffle ensures that the solids flow smoothly down to the next succeeding disc shaped baffle. The upwards rising air from the disc baffle is obstructed by the donut baffle creating a recirculation of air below the donut baffle. This leads to formation of a dead zone for solids below the donut baffle near the riser wall region. Therefore, a lower solids volume fraction was observed in this region. Similar to

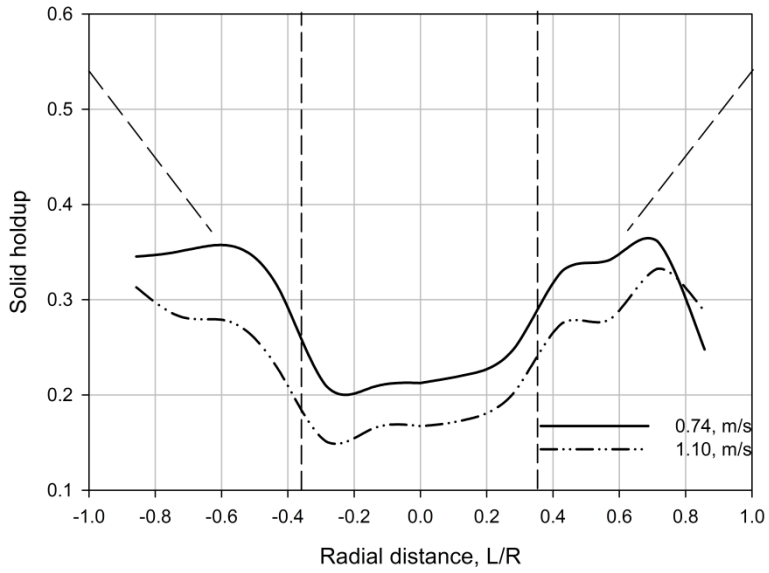

(a)

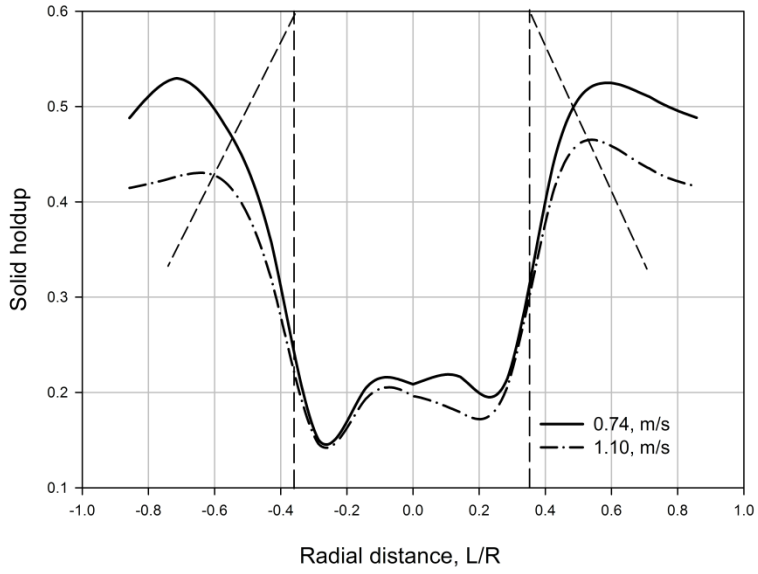

(b)

Figure 3.7: Effect of air flow rate on solid holdup: (a) 190 mm, (b) 225 mm.

the disc baffles, an increase in the superficial gas velocity leads to a decrease in the solids volume fraction in the donut baffle region. The maximum solids holdup decreased from 52 % to 42% when the superficial gas velocity was increased from 0.74 m/s to 1.10 m/s. The decrease was more pronounced near the stripper walls as the gas velocity was higher in this area.

It is known that an increase in superficial gas velocity makes the bed dilute and can eventually lead to flooding (Mckeen and Pugsley, 2003). Due to limitations on the superficial gas velocity in the experimental setup, experiments in this regime could not be conducted, even though such an exercise would have been really useful. In general, higher solids volume fraction was observed in the donut baffle region compared to the disc baffle. Moreover, the solids volume fraction was minimum in the areas beneath the baffles, indicating dead zones, whereas the solids volume fraction was highest near the baffle walls indicating segregation of solids along the walls. Due to alternating arrangement of the disc and donut baffles, a zigzag pattern was observed for the both phases.

3.4.2. Effect of Solids Flow Rate on Solid Holdup

The effect of solids flow rate as a function of radial coordinate for the disc and donut baffles is shown in Figure 3.8 and Figure 3.9 respectively. In both figures, the solids flow rate was changed from 0.025 kg/s to 0.042 kg/s for a constant superficial gas velocity of 0.74 m/s. For both the disc and the donut baffle, there was a minimal effect of solids flow rate on the solids hold up.

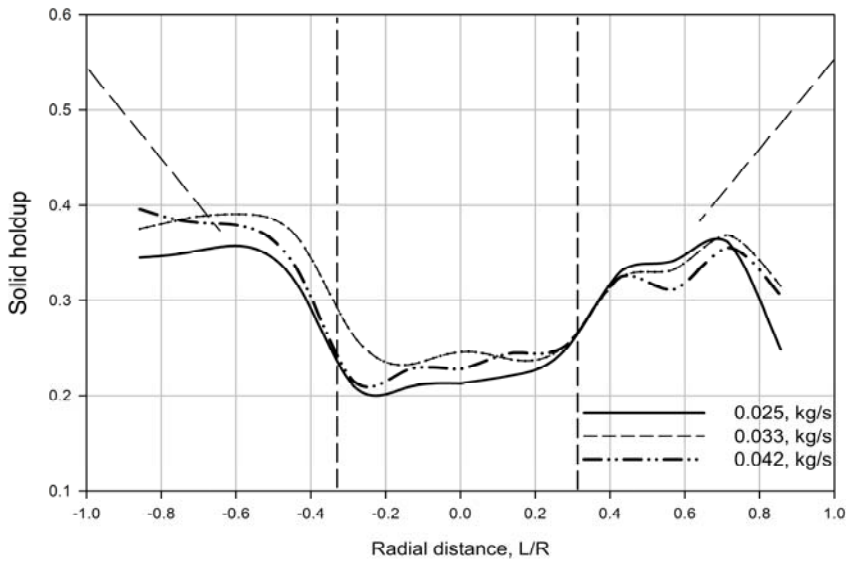

Figure 3.8: Effect of solid flow rate on solid holdup at 190 mm.

At higher solids flow rate, the channelling and bridging might occur. However, due to experimental limitations, higher solids flow rates could not be achieved. Furthermore, the chosen solids flow rates in this study may be so close to each other to have any significant impact on solid holdup. Unlike previous studies (Rivault et al. (1995) and Gao et al. (2008a)), we observed that for all the experimental conditions, the radial holdup profile is asymmetric

at both the disc and donut baffles. This indicates that the axi-symmetry assumption often considered to model these systems is not completely valid and a full three-dimensional model should be used to study the hydrodynamics.

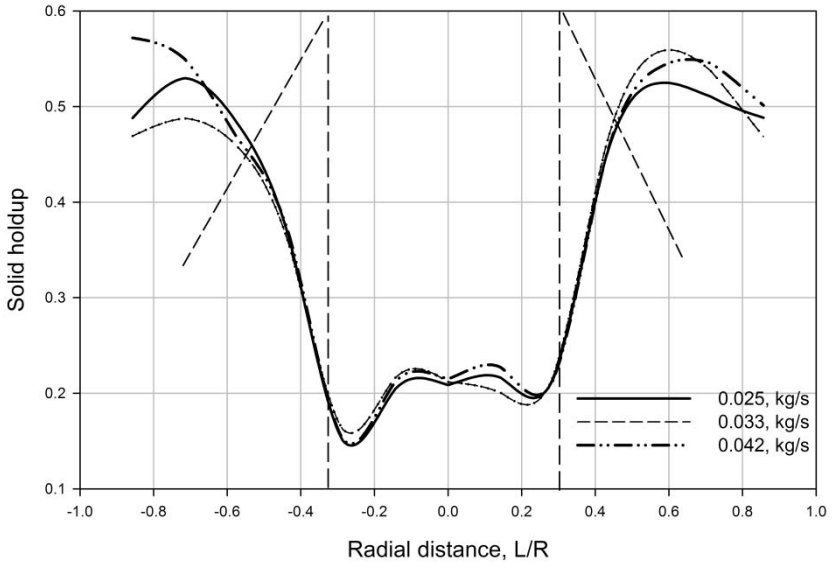

Figure 3.9: Effect of solid flow rate on solid holdup at 225 mm.

3.4.3. Solid Phase Fraction Map

Figure 3.10 shows solids phase fraction map for the entire stripper at two different superficial gas velocities. The variation in solids holdup along the height of the stripper for two different solids flow rates of 0.025 kg/s and 0.042 kg/s is shown in Figure 3.10a and Figure 3.10b respectively. At lower solids flow rate of 0.025 kg/s (Figure 3.10a), the solids holdup decreased on increasing the superficial gas velocity. Near the gas inlet (at first disc baffle), the difference in the solids holdup for the two superficial gas velocities was significant. This difference was more pronounced at the lower half of the stripper than the upper half because the lower region is more strongly influenced by the air inlet. Higher local superficial air velocities are experienced in this region leading to considerably lower solids volume fraction compared to the other regions of the stripper. The alternate arrangement of the disc and the donut baffles acted as a restriction for free flow of both the phases and enforced a good contact and mixing. In the disengager region, opposite behaviour to that observed in the stripper is seen. The solid holdup in this region increased with the superficial gas velocity. This is due to the increase in entrainment at higher superficial gas velocities.

The solids phase fraction map for higher solids flow rate of 0.042 kg/s is shown in Figure 3.10b. Three distinct behaviours are observed in the radial solids holdup profile. In the lower

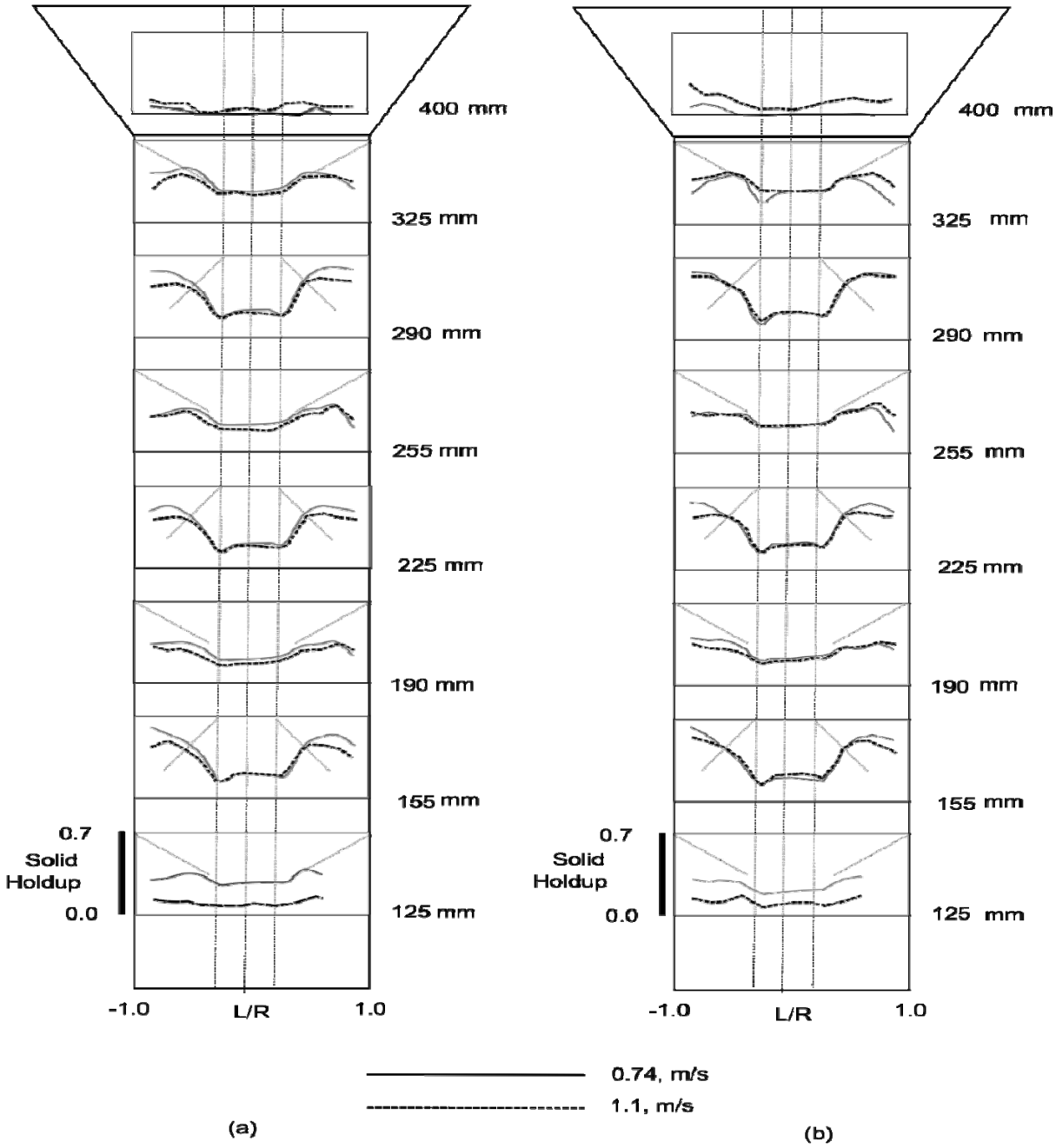

Figure 3.10: Comparison of solid holdup across the stripper: (a) 0.025, kg/s solid loading, (b) 0.042, kg/s solid loading.

region of the stripper (up to 190 mm) similar behaviour to lower solids flow rate was observed as the solids flow rate was increased from 0.025 kg/s to 0.042 kg/s. In this region, the solid holdup decreased on increasing the superficial gas velocity. However, the difference is not as pronounced as in case of lower solids flow rates. In the central region of the stripper (from 190 mm to 290 mm), the superficial gas velocity has minimal effect on the solids volume fraction. In the top region (from 290 mm to 400 mm), the opposite trend is observed. The solids volume fraction increased with the superficial gas velocity. This region is

influenced by the solids inlet. Increasing the solids flow rate increased the solids mixing zone due to an increase in the local solids flux. At higher superficial gas velocity, segregation and channelling was observed in the top baffle region.

3.4.4. Axial Variation of Solid Holdup

The line averaged solids holdup is plotted against the axial location at three different radial locations in Figure 3.11. Axial variation of solids holdup for a constant solids flow rate of 0.033 kg/s is shown for two different superficial gas velocities of 0.74 m/s and 1.1 m/s in Figure 3.11a and Figure 3.11b respectively. The three radial positions are L/R=0.00, L/R=0.57 and L/R=0.85 that correspond to the centre, stripper midsection and the region near stripper wall respectively.

For lower superficial gas velocity of 0.74 m/s (Figure 3.11a), lower solids holdup was observed in the central region with average holdup being about 22%. The holdup increased gradually along the height of the stripper; however, the variation is minimal. The holdup profile closely followed the stripper geometry for radial locations L/R=0.57, and L/R=0.85. For these locations, a minimum is observed near the disc baffles and a maximum is observed near the donut baffles. For the disc baffles, the chord at L/R=0.57 mostly passes through the empty space between the baffle walls and the riser while the chord at L/R=0.85 passes through a region below the baffle for most of its length. In the annular space between the riser and the disc, the solids phase was more dilute and hence lower holdup was noticed at L/R=0.57. As described previously, dead zones were also observed below the disc baffles. Since at L/R=0.85 most of the chord lies in the region of dead zone, a lower solids volume fraction was observed. For the donut baffles, the chord at L/R=0.57 passes above the donut wall, whereas the chord at L/R=0.85 passes through the region near stripper walls. Higher solids holdup was observed in this region compared to the disc baffle and the central region. The solids holdup near the donut baffle (L/R=0.57) was higher compared to the solids holdup near the stripper wall indicating a segregation of solids. The segregation was more pronounced in the upper section of the stripper (above a height of 190 mm).

While a lower solids holdup was observed for all the locations at higher superficial gas velocity, the trend with respect to axial position was similar (Figure 3.11b). The solids holdup was lowest in the central region (L/R=0), while it fluctuated between lower and higher values for alternative disc and donut baffles respectively.

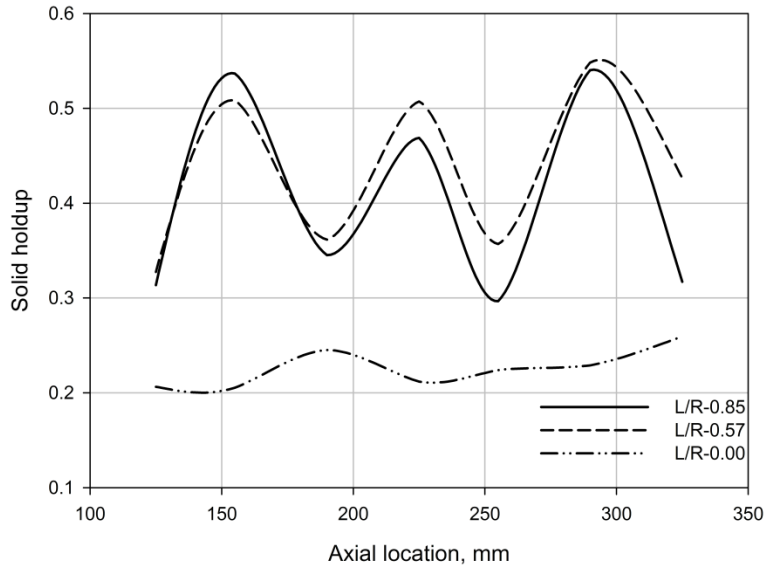

(a)

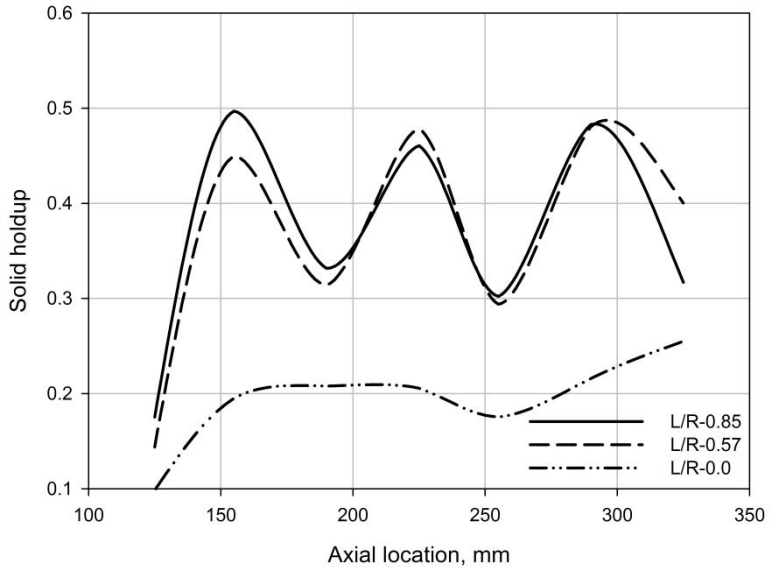

(b)

Figure 3.11: Effect of air flow rate on solid holdup at a single radial location along the height of stripper for 0.033, kg/s solid loading: (a) 0.74, m/s, (b) 1.1, m/s.

In contrast to the lower superficial gas velocity, the solids holdup was lower near the gas inlet due to an increase in the superficial gas velocity. Moreover, the difference between solids holdup at L/R=0.57 and L/R=0.85 diminished, indicating lesser radial segregation at higher superficial gas velocity. The difference in solids holdup was more pronounced in the bottom section which was influenced by the gas inlet. In the following sections, the time of flight experimental results are discussed.

3.4.5. Time of Flight Measurements

This experimental work is the first of its kind in applying RPT based technique for a system like stripper in terms of complex geometry, due to the riser part and internals. It was a challenge to acquire, process the report the data without affecting the accuracy. However a valid attempt was made to get the best results. The difficulties and limitations of applying a RPT based technique for a system like stripper is discussed below.

The actual raw data from the detectors had to be filtered using a low pass filter to remove unwanted noises in the recorded signal. Figure 3.12 displays the filtered data for the overall "time of flight" experiments obtained from the two detector setup for flow conditions of 0.033 kg/s of solid flow rate and an air flow rate of 1.1 m/s. As the tracer particle entered the stripper from the particle inlet dipleg, the first set of detectors positioned at the inlet plane recorded a high peak in the count. This occurrence of first peak was the time at which the particle enters the stripper, and is denoted as the particle entry time ($\overline{\tau^1}$). Similarly, the exit of the particle from the stripper was recorded by a second set of detectors position at the particle exit plane. The occurrence of last peak recorded by the second set of detectors was denoted as the particle exit time ($\overline{\tau^2}$). In Figure 3.12, the first peak in detector Ia was recorded at 35th second for a count magnitude of 38, while detector Ib recorded a lower count of magnitude of 29 at the same time. This difference is due to detector Ia's close proximity to the hopper A inlet, and in this data set, the particle was entering the stripper from the hopper A. However, for the calculation of '$\overline{\tau^1}$', the average of the counts was taken into account, as shown in Figure 3.12c, where the average of the first peak counts magnitude was 33.5. It is noticed that the peak of the counts varies from 35 to 60. Also the peaks were noticed for a period of 210 seconds, while the data were recorded for 520 seconds. The particle inside the stripper could traverse at different radial and azimuthal position and also there were more chances that the particle was circulating inside the stripper in the axial direction also. These movements make it probable that the particle comes in close vicinity of the detectors; and hence maximum peaks are observed at different times. This was very much similar to observation by Bhusarapu et al. (2004a). With the progress of time, the particle slowly moved down the stripper, far off enough from detector set I, and hence the detector set I did not detect the particle movement after 210 seconds. The detector set II, which was positioned at the particle exit plane, started to detect the particle as the particle descended down towards the exit at t = 210 second as can be seen in Figure 3.12.

A similar procedure of averaging of counts recorded by each detector was followed to determine the particle exit time. The occurrence of the last peak recorded by the second set of detectors is denoted as the particle exit time ($\overline{\tau^2}$). Figure 3.13 shows the representation of data recorded by the second set of detectors, where the last peak occurred with a magnitude of 8 at 435th second. Appling equation (3.3) to this data, we obtained a time of flight (t) of 401.5 seconds. The same procedure was followed for another 49 instances. With this 50 different (t) data's, distributions can be derived to obtain a Residence Time Distribution (RTD), (Figure 3.14). The calculated RTD or Mean Residence Time (MRT) for these distributions was 396 seconds.

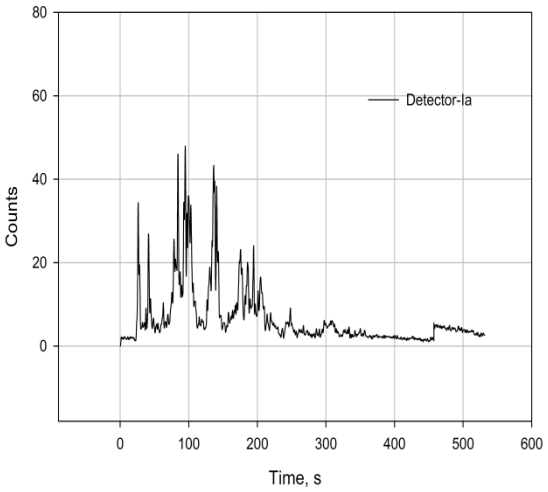

(a)

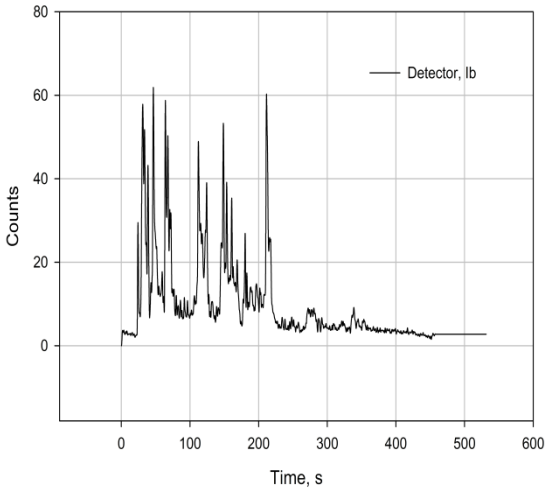

(b)

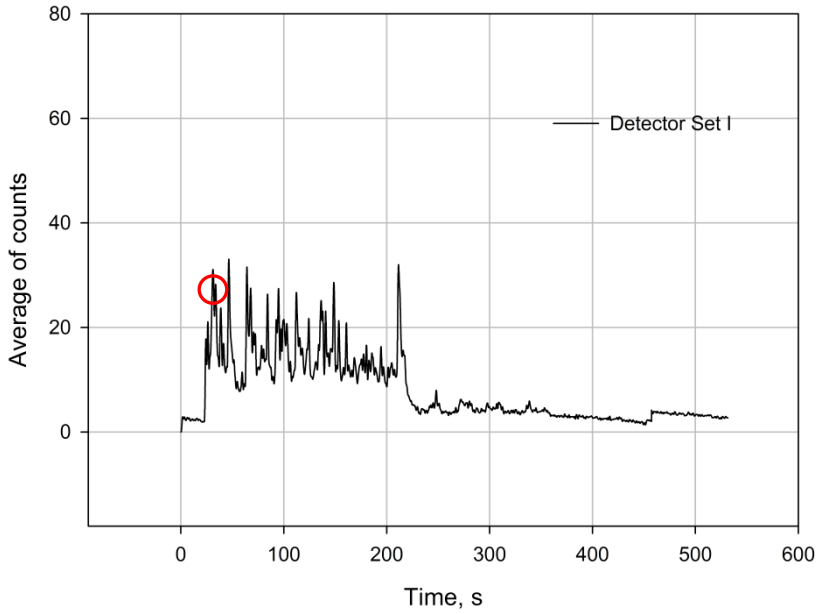

(c)

Figure 3.12: Recorded data from detector set I.

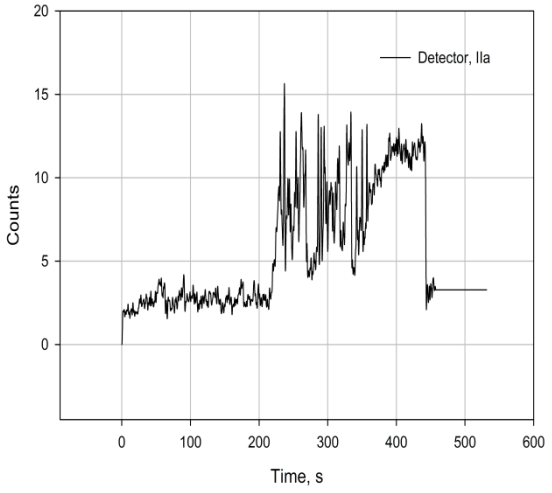

(a)

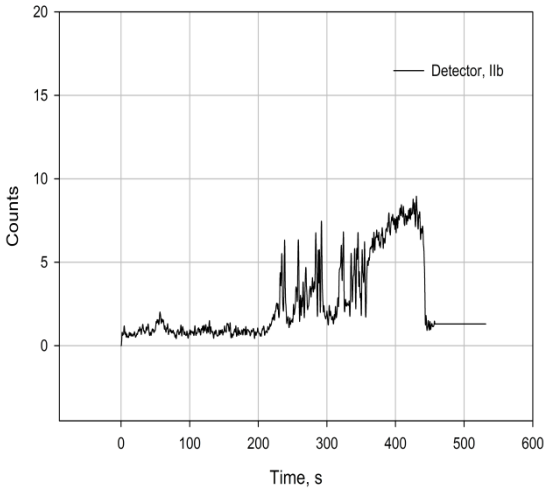

(b)

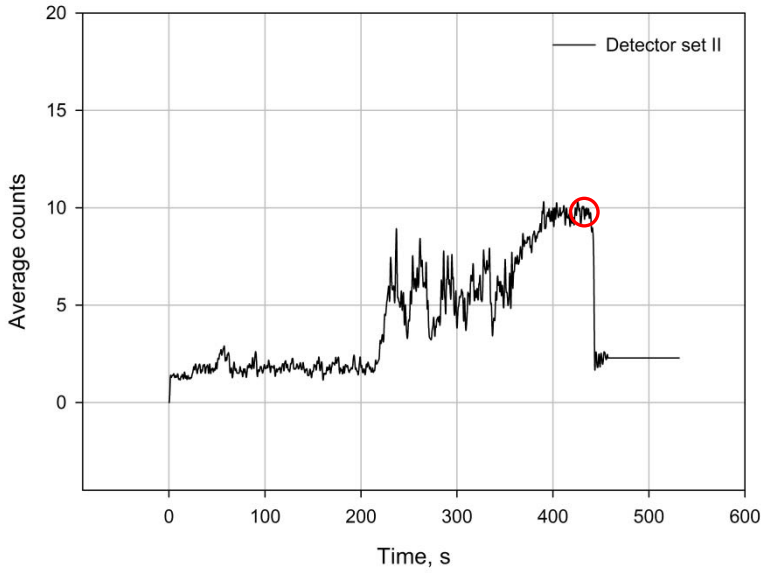

(c)

Figure 3.13: Recorded data from detector set I.

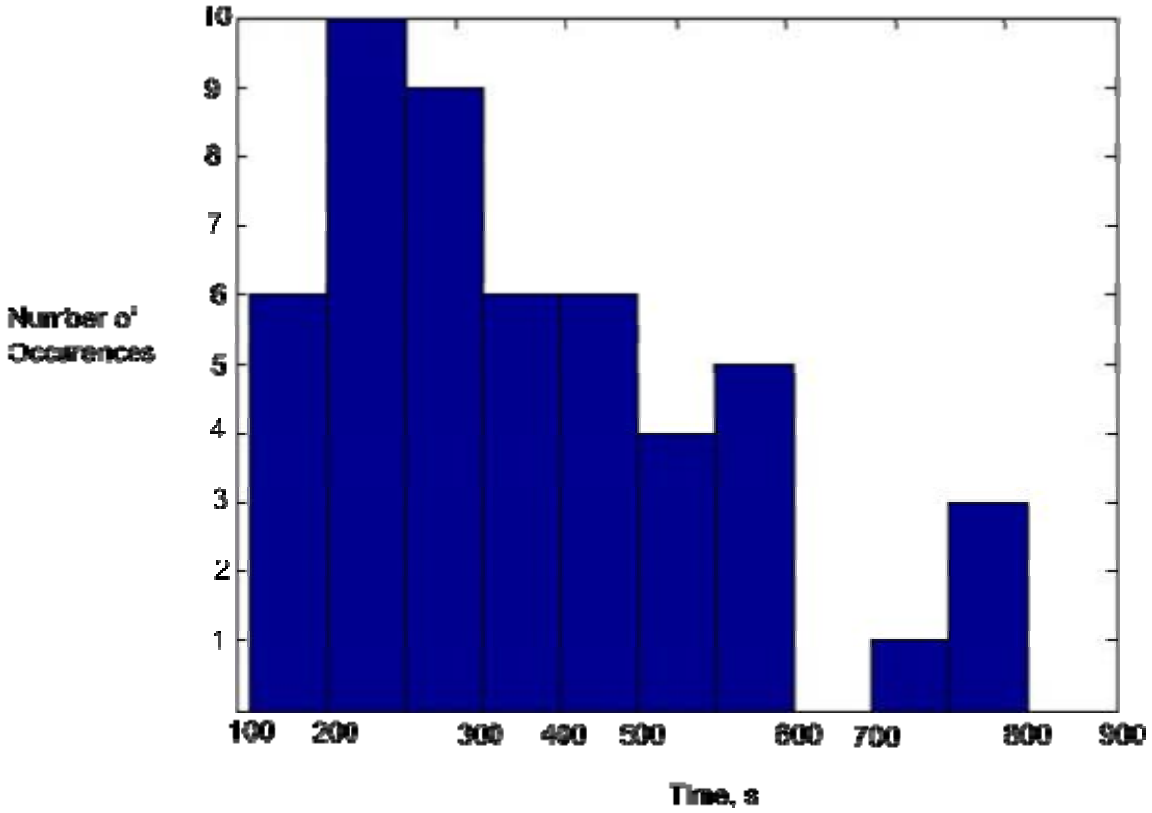

Figure 3.14: Histogram plot showing the number of occurrences at different times.

It is noticed that the particle mostly spent its time in the range between 200 to 300 seconds. There were also occurrences of a long tail, where the particle spent around 800 seconds, which indicates that the particle might have been trapped in the dead zone region due strong recirculation of air in this region. It was also observed that there was an empty bin in the duration of 600 to 700 seconds and also there was only one occurrence in the duration of 700 to 800 seconds in Figure 3.14. If there had been sufficient statistical data, the MRT should be equal to the arithmetic average time (T). However due to less number of available data, the calculated T was 368 seconds (equation 3.4) and the MRT was 396 seconds. Notably, this range of error is less than 10%, which is not too high in these chaotic gas-solid systems. Therefore, to avoid these statistical errors or lack of sufficient samples, the same procedure (equation 3.4) was followed to determine the mean time of flight (T) of the particle for the rest of data samples.

Figure 3.15 shows the effect of airflow rate on mean time of flight for different solid flow rates. It is noticed that for a solid flow rate of 0.025, kg/s the mean T increased from 334 seconds to 364 seconds as the airflow rate was increased from 0.74 to 1.1, m/s. This indicates

that at higher airflow rates, higher residence time in the stripper is achievable. On the other hand, when the solid flow rate was increased to 0.033 kg/s from 0.025 kg/s, the mean T dropped to 236 seconds for an air flow rate of 0.74 m/s. This was expected as more solids entered the stripper, the time spent by the particle in the system would decrease. The effect of increase in airflow rate was also felt significantly in this case as the mean T increased by 26 seconds, when the airflow rate was increased to 1.1 m/s. However, at a much higher solid flow rate of 0.042, kg/s, it was observed that the change in air flow rate had least effect on the mean T; although the mean T was much lower when compared to the previous two cases (Figure 3.15).This shows that the measured mean T was independent of the air flow rat**e** at higher solid flow rates. A similar observation was made for solid holdup in the axial section 3.5.3 (solid phase fraction map).

Figure 3.16 shows the effect of air flow rate on $\sigma_\theta^2$for different solid flow rates. Irrespective of solid flow rate, it is seen that the $\sigma_\theta^2$was around 0.2 at lower air flow rate. This indicates that in general, the particles followed a plug flow pattern with a possible channelling of particle phase occurring inside the stripper. On the other hand, at higher a air flow rate, the σ^2_θincreased linearly when solid flow rate was increased from 0.025 kg/s to 0.033 kg/s and it became constant when solid flow rate further increased to 0.042 kg/s. This implies that at higher air flow rates, the reactor can tend to behave like a CSTR as σ_θ^2approaches towards 1.

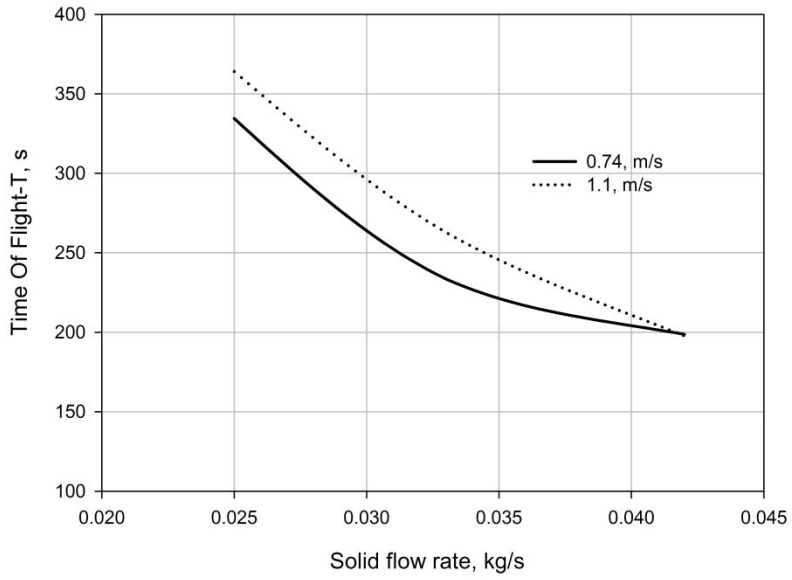

Figure 3.15: Effect of air flow rate on mean T for different solid flow rates.

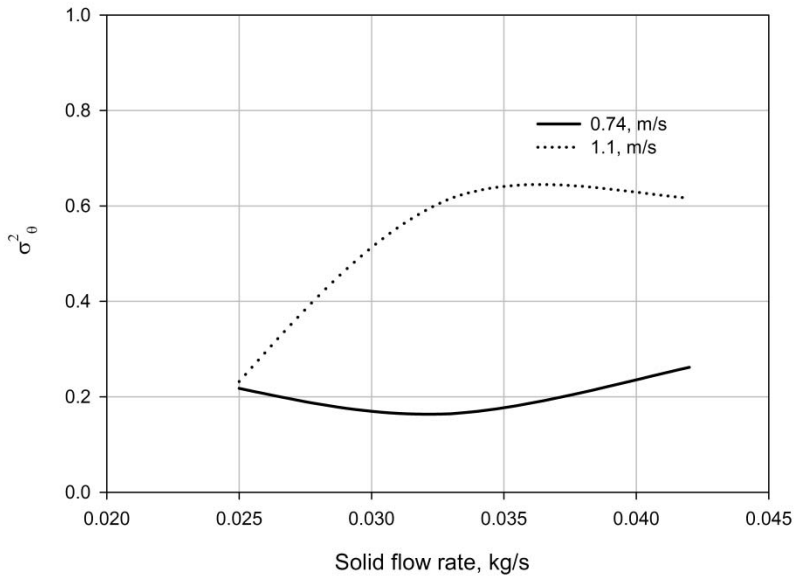

Figure 3.16: Effect of air flow rate on σ_θ^2 for different solid flow rates.

3.4.6. Time of Flight Measurements Across Baffles

Experiments were also conducted to determine the mean T of the particle in each of the baffle zones. The main principle for tracking the particle in each baffle zone was to treat each zone as a separate unit connected to each other in a tanks in series manner. The occurrence of first peak in the first detector set denoted the inlet of the particle into that baffle zone. While the occurrence of first peak in the second detector set marked the inlet time of particle in second baffle zone, while consecutively marking the exit time from the previous baffle zone. However, the processing of data for this exercise was a tedious task.

Figure 3.17 shows the filtered data for all of the 8 detectors for 0.025 kg/s of solid flow rate and the air flow rate of 1.1 m/s. In Figure 3.17, it can be observed that the magnitude of peaks vary from 14 to 122. The baffle detector-Ia and baffle detector-Ib, were positioned at the top baffle to detect or record the entry time of particle. The counts in the baffle detector-Ia and baffle detector-Ib record a maximum count peak of 17, which is much below the average of the rest of peaks (~60) in Figure 3.17. Hence, an assumption has to be made, in spite of a very low count peak, that the particle has entered the detection zone, at that particular instance.

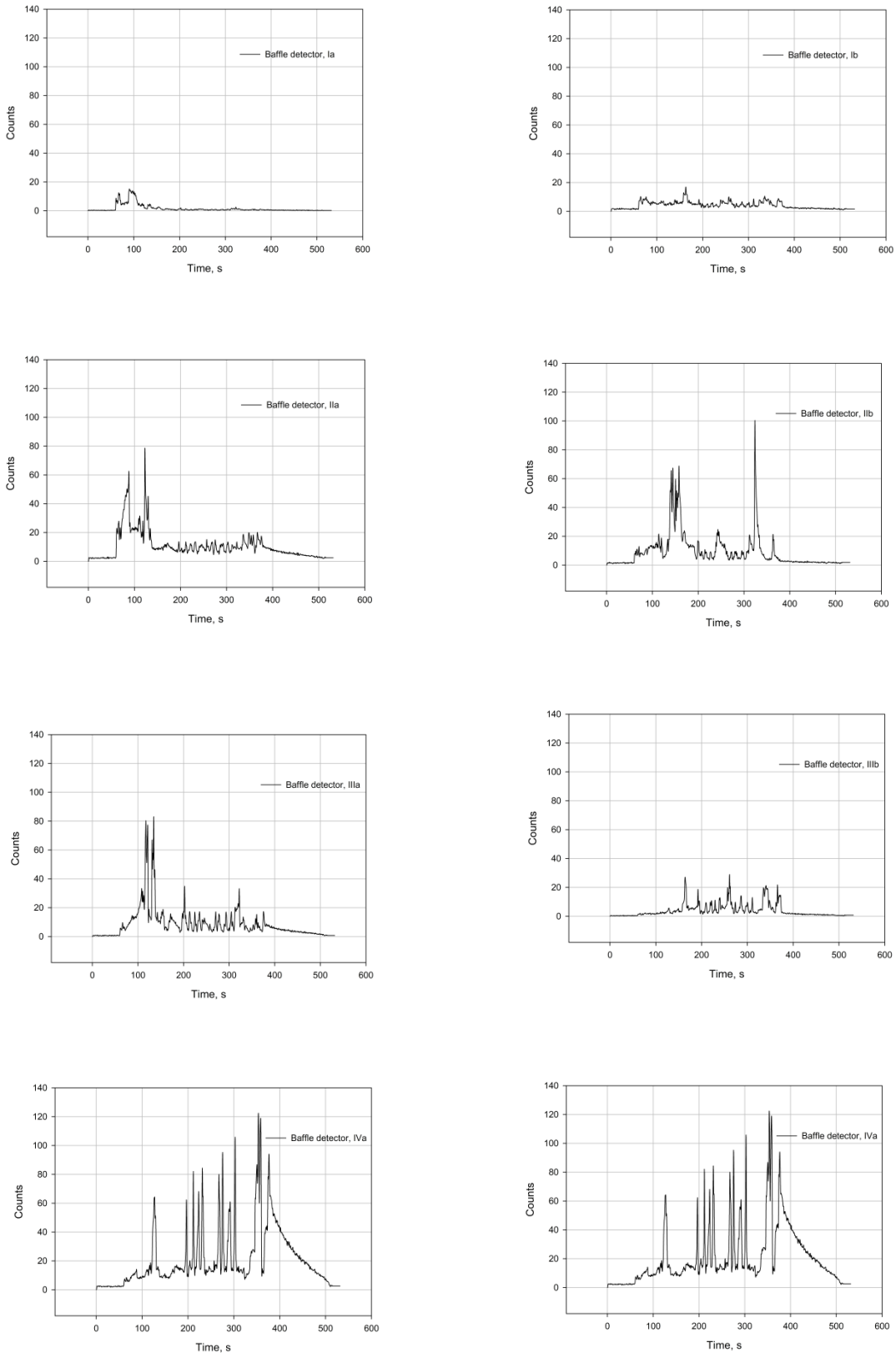

Figure 3.17: Recorded data from all 8 detectors positioned at baffles.

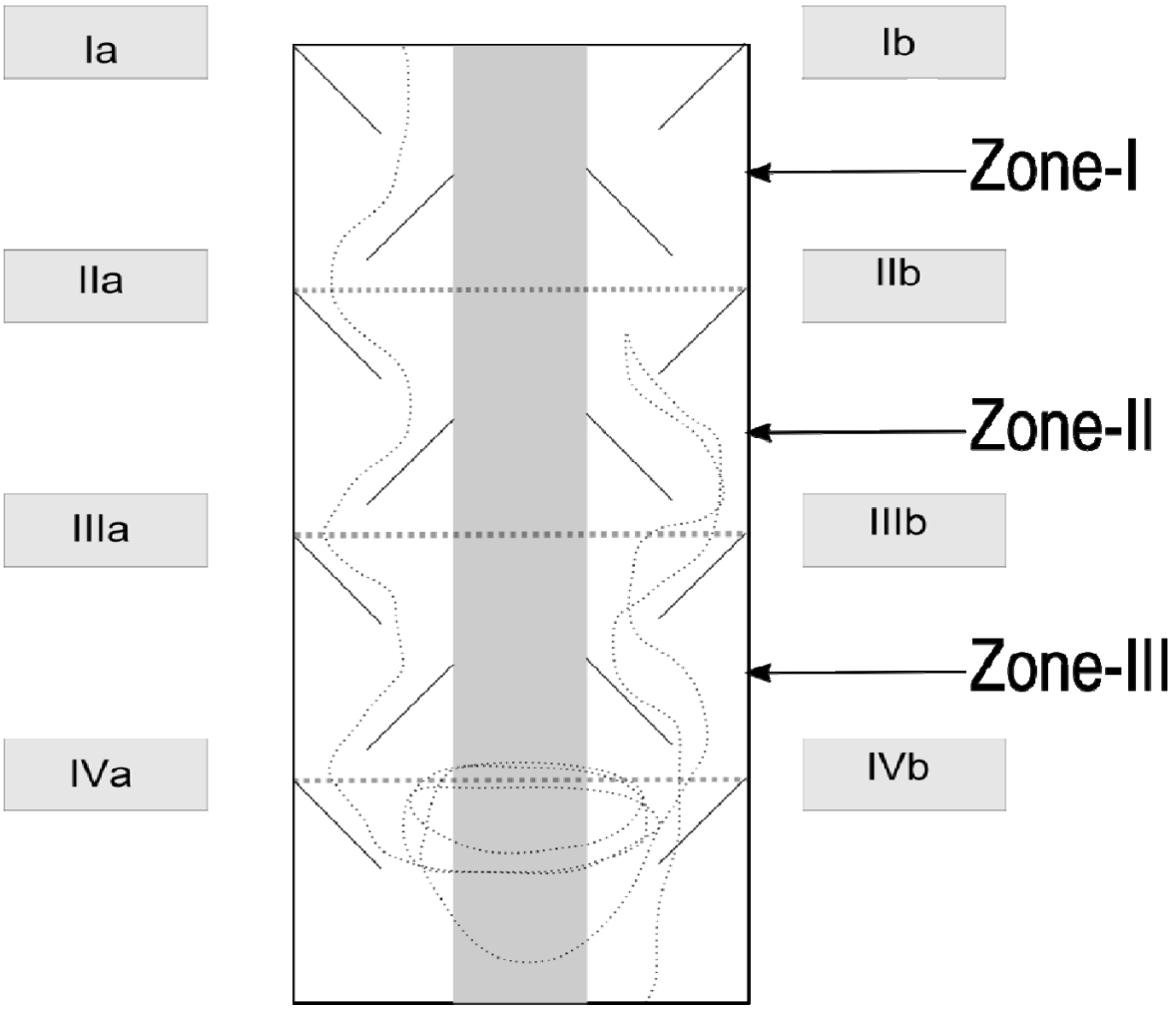

Figure 3.18: Probable schematic of particle path line (based on TOF data analysis).

It was observed in Figure 3.18 that the particle traversed mostly through the zones detected by baffle detector set Ia, IIa and IIIa. The particle also spent some time in the zone detected by detector set IV. Later the particle was carried up by the air to Zone II, because a big peak with a count of 98 was noticed for detector-IIb in Figure 3.17. This occurrence occurs at 330 seconds in detector-IIb. Then the particle moved to the last baffle before exiting the stripper, when a peak was noticed in detector set IV at 370 seconds. In this scenario, a question arises that at what time the particle crossed the detector set III while coming down towards the exit. Since there was no noticeable peak in either of the detector set-IIIa nor in detector set-IIIb, it becomes more complicated to assume or calculate the time spent by the particle in zone-III in Figure 3.18. Owing to all these uncertainties, the time spent by the particle in the baffle zone has not been reported in this thesis.

However, above mentioned issues cannot be considered as shortcomings of the RPT based experimental technique, but can be avoided in future works by following the guide lines listed below:

1) A prior calibration of the system by placing the tracer particle at different locations in the column operated under the actual experimental conditions would have avoided the degree of discrepancy in the available data.

2) The photon counts recorded by the detector are a function of not only of the distance between the radioactive source and the detector, but also the density of the intervening medium (Roy et al. 2005). In the case of experimental scale stripper, it was fitted with a thick SS-made hollow riser and an arrangement of disc and donut baffles in SS. However, even the use of Perspex material would not have guaranteed a decrease in the level of uncertainty because the accuracy of tracer experiments is also influenced by the way detectors are packed around the column (Larachi et al. 1994; Roy et al. 2001). To accommodate the detectors (50 mm diameter) in each baffle zone, where, the axial distance between the baffle zones was 65 mm, an arrangement as shown in Figure 3.19 was used.

3) To minimize errors in the calculation of residence times and to increase the resolution, the distance between the detectors must be carefully selected (Bhusarapu et al. 2004b). This distance is usually achieved by trial and error procedure to match correlation of time series between the detectors. In previous studies, the minimum distance between successive detectors zone was above 150 mm. (Roy et al. 2005-150mm, Bhusarapu et al. 2004a-400mm, Bhusarapu et al. 2006-720 mm). However in the current work, due to experimental limitations, a small scale stripper was used, and hence a very low distance of 65 mm between the baffle zones was chosen.

4) The use of collimated detector could have ensured in the reduction of error percentage levels. However it is still debatable since the source is coming from a single particle, unlike a group of particles in RTD experiments.

Figure 3.19: A photograph showing the arrangement of detectors in the baffle section.

3.5. Conclusions

Cold flow experiments were performed to understand the hydrodynamics of FCC strippers. γ-ray densitometry method was used to quantify the effect of gas velocity and solids flow rate on the solids holdup. Solids holdup was measured at different radial locations along the height of the stripper. Due to the design of disc and donut baffles, the solid particles moved through the stripper in a zigzag manner. The holdup profiles were asymmetric in nature highlighting the need for 3D modelling. Clear radial segregation was observed at lower superficial gas velocity. At higher superficial gas velocity, lower solids holdup was observed. The solid holdup profiles along the height of stripper are greatly influenced by the shape and position of baffles. Higher gas volume fraction was observed in areas beneath the baffles,

indicating dead zones. In general the holdup was observed to be higher near the donut baffle regions and lower near the disc baffle.

RPT based Time of Flight Technique was used to determine the average time 'T' of the particle inside the stripper column for different operating conditions. The overall average time 'T' of the particle increased with the air flow rate, but at the same time it decreased with the solid flow rates. The time of flight experiments provided new insights on the importance of the quantity of statistical data from RPT experiments. The data provided here gives clear insight into the FCC strippers and will be critical for understanding the effect of stripper internals on the hydrodynamics. The data presented here will also be useful for validating computational fluid dynamics models.

4. HYDRODYNAMICS OF SMALL SCALE FCC STRIPPER

Although the overall objective of this study was to conduct hydrodynamic characterization of an industrial-scale FCC stripper, initially, CFD simulations were conducted on the experimental-scale FCC stripper so that CFD models could be validated before applying them to industrial-scale simulations. Therefore, simulations were conducted on the small-scale FCC stripper discussed in the previous chapter (Chapter 3). In addition to presenting results of CFD simulations, this chapter also focuses on validating the multiphase models using experimental solid holdup data for various operating conditions. Unfortunately, there are only a limited number of studies specific to FCC strippers in open literature. However, since an FCC stripper is essentially a fluidized bed, all the literature pertinent to general fluidized beds is directly relevant to hydrodynamics of FCC strippers. Therefore, before discussing CFD results, a brief literature survey on the hydrodynamic modelling of fluidized beds has been presented. The computational model for the experimental geometry, boundary conditions, and numerical parameters are discussed next. Finally, appropriate conclusions have been made on the basis of qualitative and quantitative comparison between CFD and experimental results.

4.1. Hydrodynamics of Fluidized Beds

In a fluidized bed reactor, typically, gas is sparged through a distributor plate at the bottom of a container containing solid particles. Depending on operating conditions, different flow regimes may prevail in the reactor. Figure 4.1 depicts different contacting regimes that might be encountered. These regimes (and thus operating behaviour of the reactor) are affected by the operating conditions, solids flow rate, gas flow rate and system configuration (reactor hardware). Besides, the regimes are also a strong function of the properties (size distribution, shape, density and restitution coefficient) of solid particles. In these reactors, global characteristics like conversion, residence time distribution, degree of back-mixing, mass and heat exchange between phases depend on parameters such as characteristic mean bubble size, size distribution, rise velocity, spatial distribution of particles etc. A lot of empirical knowledge has been accumulated over the years about these parameters and their effects.

Conventional modelling methodology makes use of this empirical information to develop reaction engineering models.

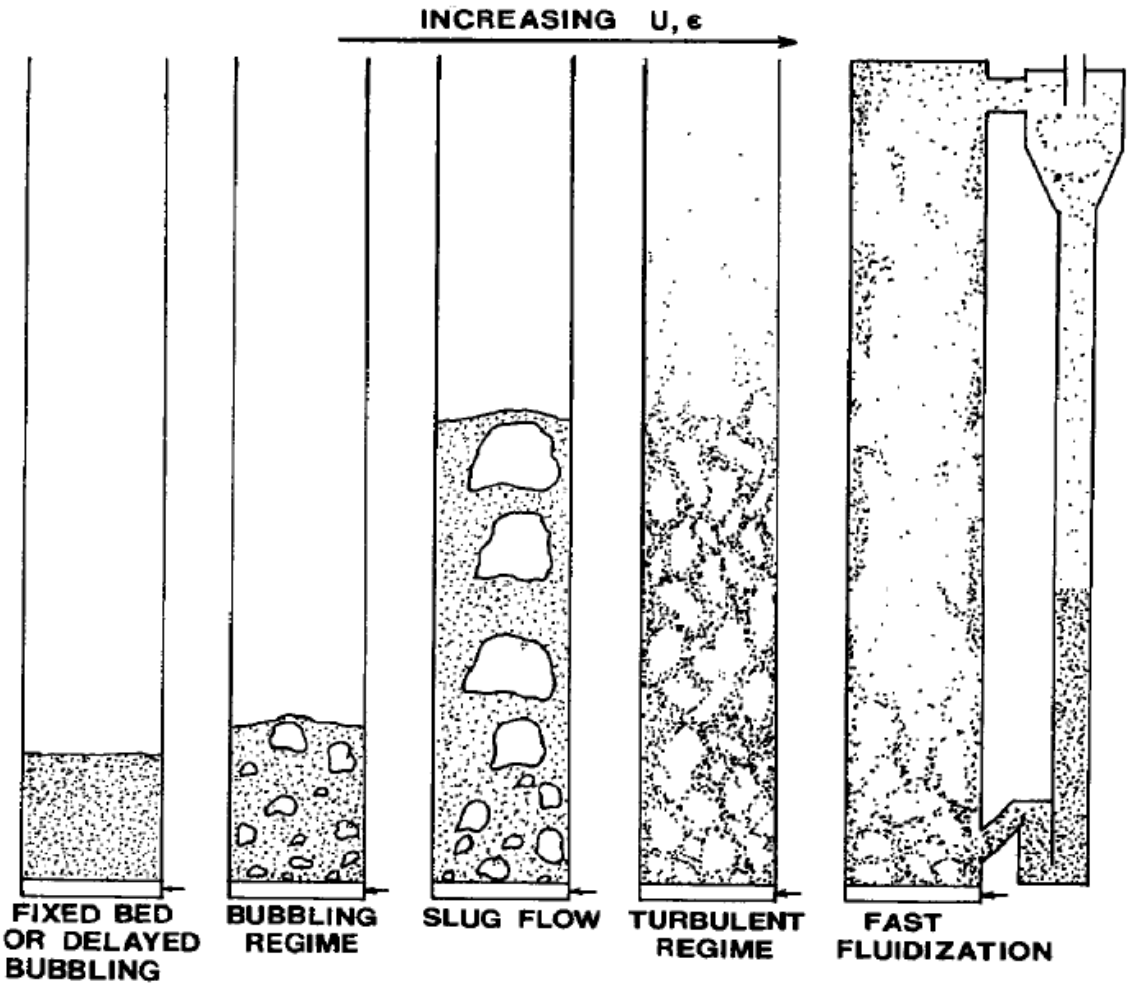

Figure 4.1: Flow regimes in fluidized beds (Grace, 1990).

Most of the conventional/ phenomenological models are variations of two-phase models, which consider a bubble phase and an emulsion phase. Such models are based on a simplified fluid dynamics and are typically used to understand the sensitivity of reactor performance to operating and model parameters (Ranade, 2002). However, these models have generally proven unsuccessful when it comes to detailed understanding of the system as they are typically limited to the database used to develop them. Furthermore, these models are not useful to understand the influence of details of hardware configuration on reactor performance. Therefore, detailed hydrodynamic models are required to resolve hardware related issues.

During the last decade, numerical simulations of fluidized beds using CFD techniques have gained considerable interest. The models developed can be broadly categorized into Eulerian–Eulerian or continuum models (e.g. Huilin et al. (2003b), Goldschmidt et al., (2002), Mathiesen et al. (2000)) and Eulerian–Lagrangian or discrete models (e.g. Hoomans et al. (2000), Kaneko et al. (1999), Tsuji et al. (1993)). In the Lagrangian approach, a separate equation of motion must be solved for each particle in the flow field. This approach, therefore, is computationally expensive and not well suited for simulating large and complex industrial fluidized bed reactors which might contain billions of solid particles. On the other hand, in the Eulerian approach, the gas and solid phases are treated as separate, continuous and fully interpenetrating.

4.1.1. Classes of Hydrodynamic Models

As mentioned previously, for CFD simulations, two modelling approaches can be identified viz. Eulerian–Lagrangian models and Eulerian–Eulerian models. In gas–solid flow modelling terminology, usually Eulerian–Lagrangian models are called discrete particle models (DPMs) and Eulerian–Eulerian models are called granular flow models (GFMs). DPMs can be adopted in simulations where the number of particles in the system is rather low (i.e. less than 10^5 particles). Whereas, GFMs are more suitable for simulating large and complex industrial fluidized bed reactors containing billions of solid particles. The interrelationship between various models is schematically shown in Figure 4.2. Due to their continuum description, GFMs require additional information about solid phase rheology and particle–particle interaction laws.

In theory, it is possible to deduce all the necessary closure laws and parameters required for GFMs using more fundamental approaches like Lattice Boltzmann Models (LBM), direct solution of Navier-Stokes equation (DNS) and contact theory. LBM and DNS are, nevertheless, computationally too demanding, even for thousands of solid particles. Discrete particle models solve the Newtonian equations of motion for each individual particle, taking into account the effect of particle collisions and forces acting on the particle by gas. Particle collisions are described by collision laws, that account for energy dissipation due to non-idea particle interactions by means of the empirical coefficient of restitution and friction (hard sphere approach) or an empirical spring stiffness and a friction coefficient (soft sphere approach). Eulerian models considered all phases to be continuous and fully interpenetrating. The equations employed are a generalization of the Navier-Stokes equations. Implicit to the

continuum description of the discrete phase, Eulerian models require additional closure laws to describe the rheology of particle phase. In most recent continuum models constitutive equations according to the kinetic theory of granular flow are incorporated. This theory is basically an extension of the classical kinetic theory of gases to dense particle flow, which provides explicit closures that take energy dissipation due to non-ideal particle–particle collisions into account by means of the coefficient of restitution. With the present state of knowledge, complete a priori simulations are not possible (Ranade 2002). It is necessary to use different models discerningly. DPMs are usually used to gain an insight into various vexing issues such as bubble or cluster formations and their characteristics or segregation phenomena. The understanding developed and simulation results can then directly or indirectly be used to develop GFMs. For full scale simulations of industrial fluidized beds, DPMs are computationally too demanding and GFMs should be preferred. Owing to the continuum representation, the Eulerian approach requires additional closure laws to describe the rheology of the fluidized particles (Goldschmidt et al. 2001). In most recent continuum models constitutive equations according to the kinetic theory of granular flows (KTGF) are incorporated. In the next subsection, these models involving KTGF are reviewed.

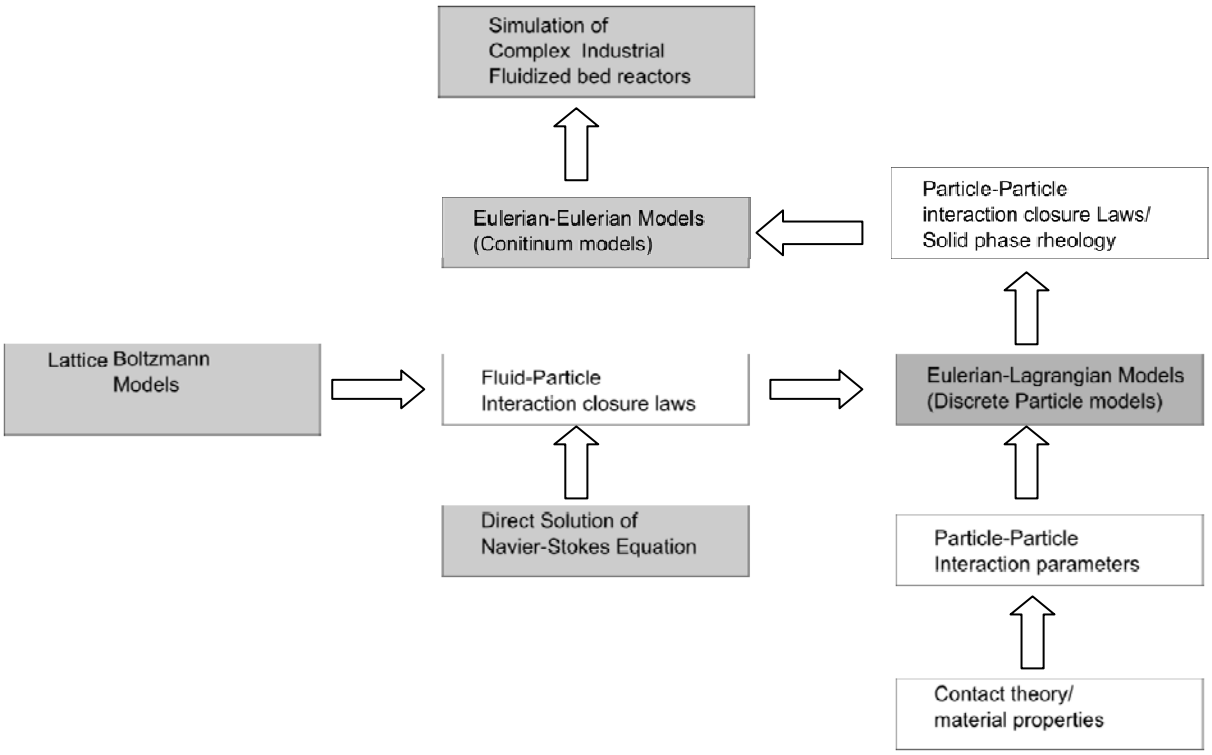

Figure 4.2: Hierarchy of models for the simulation of gas-solids fluidized bed reactor.

4.1.2. Application of KTGF to Fluidized Bed Modelling

Industrial fluidized bed reactors usually are characterized by a very large number of solid particles (of the order of 10^6 particles). In such situations continuum models are the obvious choice for detailed study of the hydrodynamics of the reactor. The main difficulty in applying the continuum model lies in "how to treat inter-particle collisions?". Or in other words, how to deduce constitutive equations for the solids phase (which is assumed to be continuous) that is otherwise dispersed. In recent years, approach based on KTGF has been used to answer this question. The basic principles and constitutive relations deduced from KTGF have been described by Gidaspow (1994). In this section, we look at some of the recent efforts to model the hydrodynamics of fluidized bed using KTGF. A number of investigators have studied the Hydrodynamics of fluidized beds using the continuum approach. These investigations can be classified into dilute flows (risers) and dense bed flows (bubbling beds). Enwald. et al.(1996) gives a thorough literature survey of all these models. Boemer et al. (1997), studied the process of bubble formation at single orifice using KTGF approach. They compared their results with experimental data obtained from instantaneous image processing. They used an average granular temperature formula proposed by Moseley and O'Brien (1993).

Gera et al. (1998) compared bubble formation, motion and eruption using a discrete particle model and two fluid model. They found the inter-particle friction (and thus solids pressure) to be the key sensitive parameter. Gustavsson and Almstedt (2000) studied the fluid dynamics and erosion for a two-dimensional fluidized bed containing two horizontal heat exchanger tubes, using a curvilinear two-fluid model solver. The local instantaneous kinetic energy dissipation rate was compared with the local fluid dynamic behaviour at the surface of the target tube for a bubble passage cycle to understand erosion mechanisms. The wake passage was found to contribute most to the time averaged erosion. They concluded that tube erosion models should take into account the wake properties such as wake size and velocity. Schmidt and Renz (1999) and Schmidt and Renz (2000) used the Eulerian approach to calculate the fluid dynamics and the heat transfer in a particle-gas fluidized bed. They adopted an approach in which effective thermal conductivity was calculated from an idealized arrangement of the particles in the bed, and compared it with the KTGF approach. They found that the kinetic theory approach estimates larger thermal conductivity values than the standard approach, due to an increase in the granular temperature. They also compared their results with the penetration model. They found that, in the stagnant cap at the upper part of the tube the

particle motion was very low, so that the time dependent solution of the penetration theory was valid.

Goldschmidt et al. (2001) studied the effect of coefficient of restitution on bed dynamics. They found that the hydrodynamics of dense fluidized beds strongly depend on the amount of energy dissipated in particle–particle encounters and the effect of non-ideal particle–particle encounters should be taken into account order to obtain realistic simulations. They emphasised the need for further development of the kinetic theory of granular to improve the constitutive equations for multi-fluid continuum models. Goldschmidt et al. (2002) compared the kinetic theory of granular flow with 3D hard-sphere discrete particle simulations. They used the discrete particle models as a tool to provide detailed information about the basic particle flow characteristics. They validated many key assumptions of KTGF. However, for highly inelastic and rough particles an anisotropic maxwellian particle velocity distribution was observed. This is attributed to the formation of dense particle clusters, which became stronger as more inelastic were the particles.

Peirano et al. (2001) carried out numerical simulations of a stationary bubbling fluidized bed using three dimensional Eulerian approach. They observed significant differences between 2D and 3D simulations. With the same configuration (if all numerical parameters are kept constant), they found that only 3D simulations can predict the statics (bed height) and dynamics (pressure spectra) of the bed. They observed that for the mono-dispersed non-spherical particles, at least the bed height could be accurately represented by calculations using an empirical maximum packing coefficient. Further, the issue of the accurate prediction of the drag force was less important if accurate empirical correlations were available.

Lathouwers and Bellan (2001) presented a multi-fluid model for dense gas-solid biomass pyrolysis in a fluidized bed. The model captured the key features of the pyrolysis process, and was general enough to be used for the optimization of reactor geometries and operating parameters. Peirano et al. (2002) performed numerical simulations of a freely bubbling fluidized bed with an emphasis on the influence of the pressure drop of the air distributor on the state of fluidization. The air distributor and the air plenum were included in the computational domain. Their results showed that when the pressure drop of the air distributor was high, predictions of the dynamics of the bed were in good agreement with the experiments. However, when the pressure drop of the air distributor was low, the predictions were not reproducible. This indicates that in the low pressure drop configuration, not only the

air distributor and the plenum should be included in the simulations; the influence of the whole air supply system should also be investigated. Srivastava and Sundaresan (2003) described frictional–kinetic constitutive model for particle phase stresses by assuming that the frictional and kinetic stresses are additive. They modelled frictional stresses by invoking the critical state hypothesis, whereas the kinetic stresses are modelled using the kinetic theory of granular flow. By simulating a rising bubble in a fluidized bed, they demonstrated the significance of the frictional stress on the bubble shape. The shape of the bubble changed appreciably when the frictional stresses were dropped. Hong et al. (2003) studied the formation and coalescence of jets in gas–solids fluidized beds with two vertical jets numerically and experimentally and found that the power law differentiation with first order upwind difference scheme was numerically more stable. It was also found that the Froude number and Reynolds number were dominant parameters in determining the jet penetration height. They concluded that the jet penetration height increases with the increase of superficial gas velocity, and presented correlations for estimating the jet penetration height for the isolated, transitional, and interacting jet regions. Huilin et al. (2003a) studied the behaviour of a binary mixture in a gas bubbling fluidized bed using the kinetic theory of granular flow. Their simulation results indicated that the particle segregation depends on the particle size distributions in the gas bubbling fluidized beds. They emphasised the need for experiments for which the collision parameters and rheology of particles have been accurately determined. Patil et al. (2003) simulated a single rising bubble through an incipiently fluidized bed. They found that the transfer of the gas into the bubble was mainly by convection (through flow) rather than diffusion. This also proved that the usual assumptions of constant diameter and uniform tracer concentration for the prediction of the bubble-to-emulsion mass transfer coefficient are not valid. Their simulations results showed an increase in the initial bubble-to-emulsion phase mass transfer coefficient, and found a good agreement with the experimental measurements for low jet velocities. However, for higher jet velocities, the concentration of tracer gas was over predicted. This was attributed to the under-prediction of the meandering of jet.

Chandrasekaran et al. (2005) validated the KTGF based two fluid model by simulating the fluidizing behaviour of non spherical particles. Polyethylene beads were considered in their study. The simulated results were compared with both pressure fluctuations and average bubble properties. Their work showed that significant improvements need to be done before successful implementation of two fluid granular models for non-ideal particles. Hulme et al.

(2005) validated the KTGF based on two fluid model of commercial CFD package FLUENT with experimental data from a scaled down cold flow bubbling fluidized bed polyethylene reactor. Parametric study showed that time step, numerical differencing scheme for conservations equations and the frictional stress models significantly affect the average bubble diameter. Their simulations were performed on 2D computational domain to reduce computational time. Taghipour et al. (2005) also carried out a similar investigation of KTGF based granular TFM code in FLUENT. The effect of inter phase exchange coefficients was also studied in their work. Johnson et al. (2006) modelled the slugging fluidized bed using the Eulerian Eulerian approach with different closures for particle phase stress and air feed system. The results from kinetic theory based model were in better agreement with the experiments than the constant viscosity models for the particle phase stress. They concluded that the further modelling of air feed system is essential for predicting the overall bed dynamics. Pandit et al. (2007) studied the effect of imposed inter particle force on bubble formation in 2D system using DEM simulations with 36000 particles. The mechanism of first bubble formation was found to be different from successive bubble formation. With imposed cohesive inter particle force, time delay was observed in the bubble formation. Further successive bubble formation required higher gas velocities than that required for the first bubble formation. The shape and growth of bubbles was found to be influenced by the magnitude of the inter particle forces.

McKeen and Pugsley (2002) and McKeen and Pugsley (2003) simulated a freely bubbling bed and, a 2D FCCU stripper column of FCC catalyst for Geldart A particles, using two-fluid CFD code MFIX and a modified drag law based on Gibilaro et al. (1985). They reiterated the theory that cohesive inter–particle forces are a significant contributor to the fluidization behaviour of fine Geldart A particles. Gao et al. (2008a) studied a 2D FCCU stripper column fitted with different type of internals using a modified Gidaspow drag force model. This modification combines the influence of inter-particle forces, and hence the effect of particle agglomeration on the drag force.

It can be seen from the literature survey that the numerical simulation of gas–solid bubbling fluidized beds using KTGF is still in its infancy. Main focus of the research has been the development and validation of the fundamental hydrodynamic models that accurately predict the behaviour of the flow phenomena inside the reactor. Application to realistic industrial systems is, however, not very widely reported in the literature. Firstly, most models have

been applied to over-simplified rectangular geometries (2D columns). This can be attributed to (i) the lack of confidence in the KTGF theory, which is still not foolproof and depends on many assumptions and empirical inputs, (ii) limitation of computational resources and (iii) difficulties in ensuring validation data from plant-scale fluidized beds. Secondly, most of the simulations are performed using two-fluid model with only mono-dispersed solids (which is generally not the case in reality). Recently, however, theory for multi-particle system has been developed (Huilin et al. (2003a), Mathiesen et al. (2000)). Some attempts of incorporating heat (Schmidt and Renz (2000), Boemer et al.(1997)) and mass transfer (Patil et al. 2003), and chemical reaction (Lathouwers and Bellan, 2001) have been made. However, most simulations have been performed on relatively coarse grids, and the results of modelling attempts strongly depend on how well the gas-fluidized bed hydrodynamics is captured. Considering all these issues discussed above, a 3D model using Eulerian-Eulerian model of two phase flow has been used in this study for simulating the experimental scale FCCU stripper. In the following section the 3D computational model is discussed along with corresponding equations.

4.2. Computational Model

In the Eulerian–Eulerian continuum model, each phase is considered as an interpenetrating continuum. Integral balances of continuity, momentum and energy for both phases, with appropriate jump conditions for phase interfaces are then derived. Since the continuum approximation for the solid phase has no equation of state, closures are required for the internal momentum transfer in the particulate phase (solid phase viscosity and solid phase pressure gradient). Closures based on the kinetic theory of granular flows (KTGF) (Ding and Gidaspow, 1990) are widely used for fluidized bed modelling. It should be noted that the two fluid model along with the KTGF contains several modelled terms (stress tensors, solid phase bulk and shear viscosity, radial distribution function and so on). Several different versions for each of these have been proposed and a general consensus on the selection of appropriate version has not yet emerged (Ranade, 2002). Van Wachem et al. (2001) have provided a condensed summary of the governing equations and closure equations that are commonly used. In recent studies a frictional contribution to the momentum transfer in the solid phase has been accounted for by using empirical correlations (Srivastava and Sundaresan, 2003). In the present work, we have used a two fluid model with KTGF closures. The governing equations of which are summarized as follows:

Gas-phase continuity

$$\frac{\partial}{\partial t}(\varepsilon_g \rho_g) + \nabla \cdot (\varepsilon_g \rho \vec{v}_g) = 0 \tag{4.1}$$

Solid-phase continuity

$$\frac{\partial}{\partial t}(\varepsilon_s \rho_s) + \nabla \cdot (\varepsilon_s \rho \vec{v}_s) = 0 \tag{4.2}$$

Gas-phase momentum

$$\frac{\partial}{\partial t}(\varepsilon_g \rho_g \vec{v}_g) + \nabla \cdot (\varepsilon_g \rho_g \vec{v}_g \vec{v}_g) = -\varepsilon_g \nabla P_g - \nabla \cdot \tau_g + K_{gs}(\vec{v}_g - \vec{v}_s) + \varepsilon_g \rho_g \vec{g} \tag{4.3}$$

Solids-phase momentum

$$\frac{\partial}{\partial t}(\varepsilon_s \rho_s \vec{v}_s) + \nabla \cdot (\varepsilon_s \rho_s \vec{v}_s \vec{v}_s) = -\varepsilon_s \nabla P_g - \nabla \cdot S_s - K_{gs}(\vec{v}_g - \vec{v}_s) + \varepsilon_s \rho_s \vec{g} \tag{4.4}$$

The thermal energy equations have not been included due to the anticipated negligible heat effects in cold-flow fluidized beds. Constitutive equations for the gas-phase stress τ_g, granular stress S_s, gas-solids drag K_{gs} etc. are needed in order to close the above set of equations. Previous studies have suggested that in dense phase bubbling beds, gas phase turbulence is for the most part damped due to the presence of the particle inertia (Enwald, 1996). The granular stress is accounted for mainly due to inter particle collisions for ε_g when the voidage is above the maximum packing value, otherwise frictional forces dominate. The interphase momentum transfer is an important term in the modelling of gas–particle interactions, since particle fluidization results from the drag exerted by the interstitial gas on the particulate phase. One of the requirements of the drag coefficient is to properly predict the minimum fluidization velocity. The Syamlal and O'Brien's drag model (Syamlal and O'Brien, 1989) can be adjusted easily to match the minimum fluidization velocity (Utikar and Ranade, 2007). Therefore, in the present study we have used the Syamlal O'Brian drag model. The gas–solid exchange coefficient for this model is given by

$$K_{sg} = \frac{3\varepsilon_S \varepsilon_g \rho_g}{4 {v_{r,S}}^2 d_s} C_D\left(\frac{\mathrm{Re}_s}{v_{r,S}}\right)\left|\vec{v}_s - \vec{v}_g\right| \tag{4.5}$$

The terminal velocity of solid particle $v_{r,s}$ is calculated as,

$$v_{r,S} = 0.5(A - 0.06\,\mathrm{Re}_s)^2 + \sqrt{(0.06\,\mathrm{Re}_s)^2 + 0.12\,\mathrm{Re}_s(2B - A) + A^2} \tag{4.6}$$

Where,

$$A = \varepsilon_g^{\,4.14} \tag{4.7}$$

and ,

$$B = 0.281632\varepsilon_g^{\,B_1} \text{ for } \varepsilon_g \le 0.85,$$
$$\text{else } B = \varepsilon_g^{\,B_2} \tag{4.8}$$

The coefficients B_1, B_2 in equation 8, were set to 0.911 and 1.856 respectively, so that the predicted u_{mf} was equal to the experimentally observed value of 0.58 m/s for a glass particle size of 800μm.

The solids pressure (p_S) is composed of two parts: a kinetic term that dominates in the dilute flow regions and a collision contribution that is significant in the dense flow regions:

$$p_s = \varepsilon_s \rho_s [1 + 2(1+e)\varepsilon_s g_0]\Theta \tag{4.9}$$

Where, e is the restitution coefficient. The radial distribution function, $g_{0,}$ a correction factor that modifies the probability of collisions between grains when the granular phase becomes dense is expressed as:

$$g_0 = \left[1 + \left(\frac{\varepsilon_s}{\varepsilon_{s,\max}}\right)^{1/3}\right]^{-1} \tag{4.10}$$

Where, Θ is the granular temperature, defined by,:

$$\Theta = \tfrac{1}{3}\overline{\langle u'_s\, u'_s \rangle} \tag{4.11}$$

Solids phase shear viscosity:

$$\mu_s = \frac{2\mu_{s,dil}}{(1+e)g_0}\left[1+\frac{4}{5}(1+e)g_0\varepsilon_s\right]^2 + \frac{4}{5}\varepsilon_s^2\rho_s d_s g_0(1+e)\sqrt{\frac{\Theta}{\pi}} \quad (4.12)$$

Solids phase dilute viscosity:

$$\mu_{s,dil} = \frac{5}{96}\rho_s d_s\sqrt{\pi\Theta} \quad (4.13)$$

The solids bulk viscosity accounts for the resistance of the granular particles to compression and expansion. It has the following form:

$$\xi_s = \frac{4}{3}\varepsilon_s^2\rho_s d_s g_0(1+e)\sqrt{\frac{\Theta}{\pi}} \quad (4.14)$$

The diffusion coefficient for the particulate phase energy fluctuation is:

$$\Gamma_\Theta = \frac{2\Gamma_{\theta,dil}}{(1+e)g_0}\left[1+\frac{6}{5}(1+e)g_0\varepsilon_s\right]^2 + 2\varepsilon_s^2\rho_s d_s g_0(1+e)\times\sqrt{\frac{\Theta}{\pi}}, \quad (4.15)$$

$$\Gamma_{\Theta,dil} = \frac{75}{384}\rho_s d_s\sqrt{\pi\Theta}. \quad (4.16)$$

The collisional dissipation of energy fluctuation is:

$$\gamma = 3(1+e^2)\varepsilon_s^2\rho_s g_0\Theta\left[\frac{4}{d_s}\sqrt{\frac{\Theta}{\pi}-\frac{\partial u_{sk}}{\partial x_k}}\right] \quad (4.17)$$

When two particles collide energy is lost. This loss of energy is accounted by introducing a coefficient of restitution (e) (Jenkins and Savage, 2006). The coefficient of restitution quantifies the elasticity of particle collisions between one, for fully elastic collisions, and zero for fully inelastic collisions. A decrease in the coefficient of restitution results in less elastic collisions generating more fluctuating kinetic energy (Goldschmidt et al. 2000). Accordingly a restitution coefficient of 0.9 was used in this work.

4.2.1. Boundary Conditions and Numerical Parameters

Simulations were conducted using commercial CFD software Fluent 6.3.16 (of Ansys Inc). The geometry and mesh were created in Gambit 2.3.16 (of Ansys Inc) for the same experimental dimensions of Figure 3.1. QUICK discretization scheme was used for the

momentum and volume-fraction differencing scheme, and time discretization was first order. The solution of the pressure from the momentum equations uses a pressure correction equation that corrects the pressure and the velocities after every iteration according to the SIMPLE algorithm. At each time step, 20 internal iterations were given. Table 4.1 gives a list of numerical parameters and closure relations used in the model. Simulations were carried out for different operating conditions. Velocity inlets boundary conditions were used for both solid and gas inlets. A pressure outlet boundary condition was specified at the top of the stripper. Solids were free to leave if entrained and are not returned to the computational domain.

Table 4.1: Simulation parameters.

Gas phase (Eulerian approach)	
Flow Regime	Laminar
Solid phase (Eulerian approach)	
Shear viscosity	Gidaspow et al.(1990)
Bulk viscosity	Lun et al. (1984)
Frictional viscosity	Schaeffer et al. (1987)
Frictional pressure	Based KTGF
Granular temperature	Algebric
Radial distribution function	Lun et al. (1984)
Solid pressure	Lun et al. (1984)
Drag model	Syamlal-O'Brien (1989)
Maximum packing limit	0.60
Restitution coefficient	0.9
Angle of internal friction	30°
Time step size	1×10^{-4}
Discretization	QUICK
Pressure-velocity coupling algorithm	SIMPLE

Based on preliminary numerical computations for grid dependency, a mesh with an average cell size of 4mm was used. Figure 4.3, shows the simulated geometry and the computational grid for the domain. The simulations were carried out in transient manner. Volume fraction and velocity of both the phase were monitored across the domain. The simulations were deemed converged once these quantities reached steady state. It took approximately 60 seconds to achieve convergence. Time averaged data on the phase velocities and volume fraction was then collected for 110 seconds.

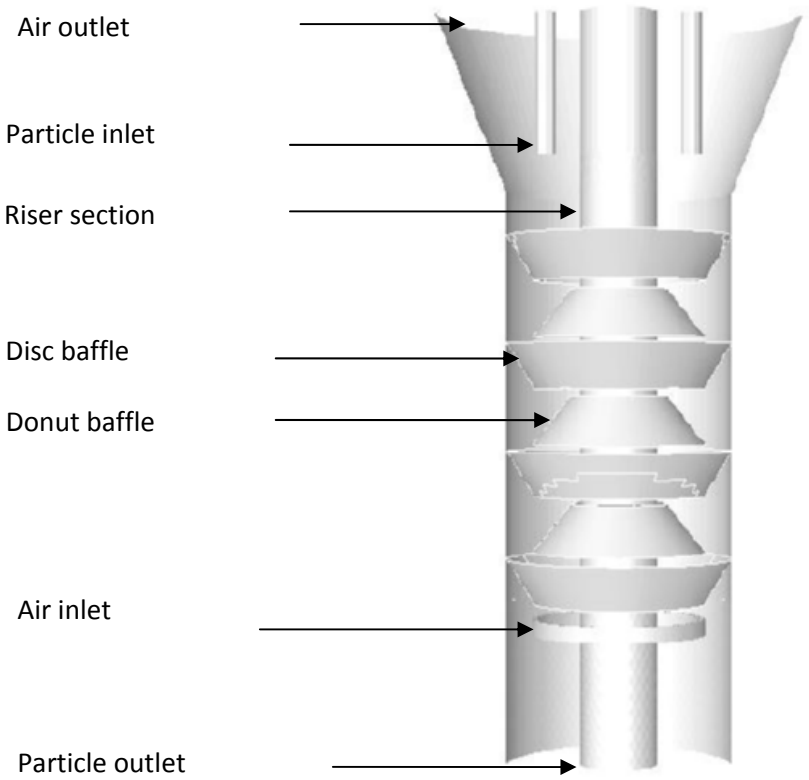

(a)

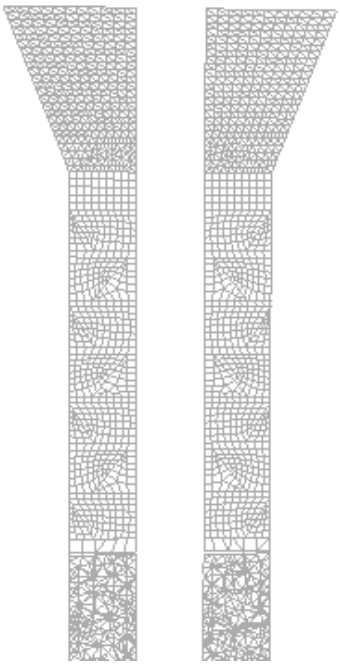

(b)

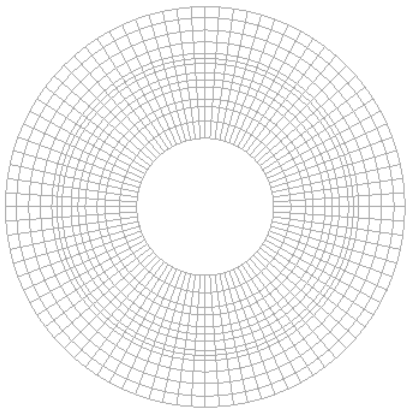

(c)

Figure 4.3: Computational domain. (a) Geometry of stripper, (b) A vertical cross-sectional view of grid, (c) A horizontal cross-sectional view of grid.

4.3. Results and Discussion

In the following sections, the comparison of CFD predictions with the experimental results and the effect of operating condition on solid holdup and the flow is analysed in detail.

4.3.1. Comparison of CFD model with Experimental Data

Figure 4.4 shows a comparison of predicted holdup from the CFD model against the experimental data for 3rd and 4th baffles from bottom (at heights 190 mm and 225 mm respectively). The solid flow rate was 0.033 kg/s and air superficial velocity was 0.74 m/s. The chordal line average solid holdup at different radial locations is plotted and is compared with the CFD results. The CFD results were in semi-quantitative agreement with the experimental findings. Since there are no solids present in the riser section, the line chordal averages were lower in the riser region. As the glass particles enter the stripper from the inlet at the top, they descent towards the outlet at the bottom against a counter flow air. When the particles reached a donut shaped baffle (Figure 4.4a), the particles moved into the contracting annular space between the stripper wall and baffle. Thus exhibiting higher volume fraction near the stripper wall compared to the riser wall. As the particles continued their descent to the disc shaped baffle below (Figure 4.4b), the particles were forced to move towards the center of the stripper. Thus, at these locations, the volume fraction around the riser was higher than that at the walls. Higher volume fractions were observed in both experiments and CFD simulations for the donut shaped baffle compared to the disc shaped baffle.

The CFD simulations also showed asymmetric profiles same as the asymmetric experimental results at the two locations. A 2D model was unable to capture this behaviour and only 3D models should be used to characterize the hydrodynamics of these systems. While the CFD simulations show reasonable quantitative and qualitative agreement for the dead region near below the disc shaped baffle, the simulations predicted much lower volume fraction near the downward baffles compared to the experimental findings (Figure 4.4). This was probably due to the presence of thick welding material on the downward baffle in this region, which rendered the densitometry results some what less accurate.

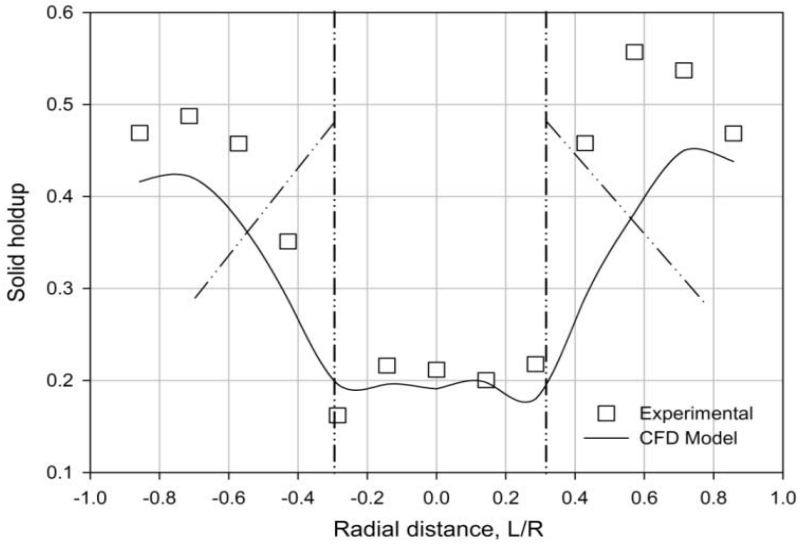

(a)

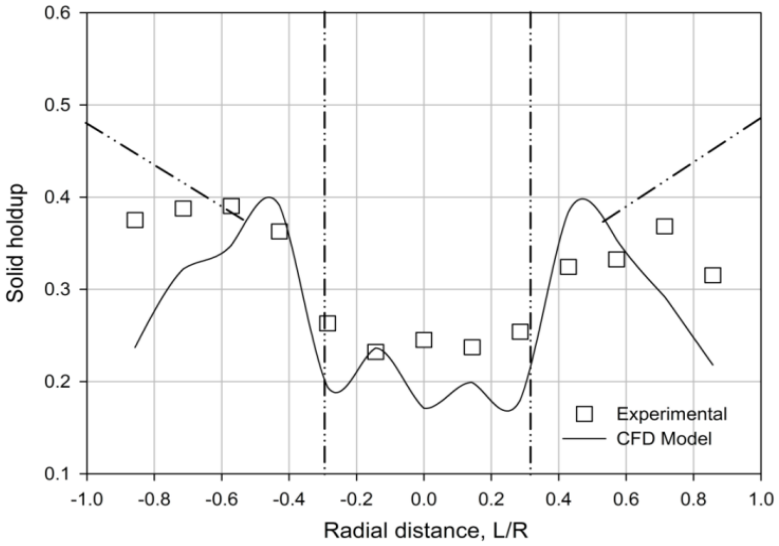

(b)

Figure 4.4: Comparison of CFD model prediction with experimental results (air flow rate = 0.74m/s and solid flow rate = 0.033 kg/s at: (a) 225 mm, (b) 190mm.

4.3.2. Flow Patterns in FCC Stripper

The contours of the mean volume fraction of gas are shown in Figure 4.5a. Due to alternating arrangement of the disc and donut baffles, a zigzag pattern was observed. The air volume fraction was highest in areas beneath the baffles indicating dead zones. Whereas the volume fraction was minimum near the baffle walls representing segregation of solids along the baffles. In the top region, the air holdup dropped as the air encountered the glass particles

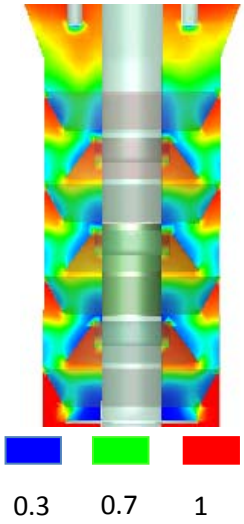

(a)

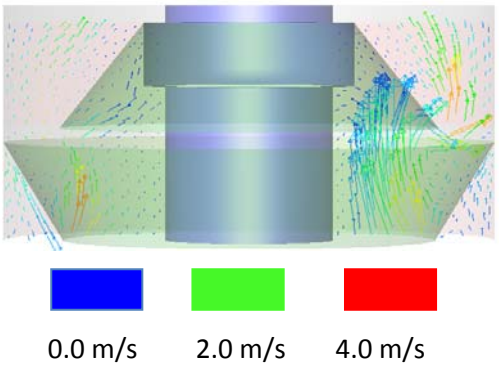

(b)

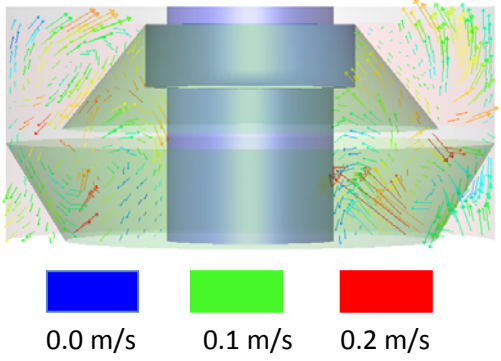

(c)

Figure 4.5: Time averaged contours and velocity vectors (air velocity = 0.74 m/s and solid flow rate = 0.033 kg/s). (a) Contour plot of gas volume fraction, (b) Vector plot of air velocity, (c) Vector plot of particle velocity.

entering the stripper. In order to reveal more details of the flow pattern, velocity vectors of the gas and solid phase with higher resolution at the 3rd and the 4th baffle from bottom are plotted in Figure 4.5b and Figure 4.5c respectively. The primary path of the air can be clearly seen in the vectors of the high magnitude. Although majority of air passes through the cavity between the riser walls and disc baffle, some portion enters the space beneath the baffle. This air hits the walls and recirculates back to region between the baffle and riser wall creating a dead zone.

The solid velocity vectors in Figure 4.5c show higher degree of recirculation compared to those of air flow. The upwards rising air from the disc shaped baffle carries solids along with it creating a recirculation zone on the outside of the donut baffle. Some of the air leaving the disc baffle directly goes in to the dead region of below donut baffle. Particles influenced by this motion of air form another recirculation zone below the donut baffle. However, the volume fraction (and hence the amount) of solids in this region was very low.

4.3.3. Effect of Gas Velocity and Solid Flow Rate

The effect of air velocity on solid holdup is shown in Figure 4.6. The points represent the radial variation of solid holdup measured along different chordal lengths at a height of 190 mm across the stripper. The lines represent CFD predictions. The experimental data shows solid holdup decreased with increase in airflow rate, the CFD results are also able to clearly show that the solid holdup decreased with increase in gas flow. For the particular location, as the superficial airflow rate is varied from 0.74 m/s to 1.1 m/s the observed maximum solid holdup falls from 0.44 to 0.29. The decrease was more pronounced near the riser walls as the gas at higher velocity tries to push through the small annular gap. It is known that increase in air flow rate makes the bed dilute and can eventually lead to flooding (McKeen and Pugsley (2003)). Due to limitations on the air flow rate in the experimental setup, experiments in this regime were not conducted. The numerical simulations in this regime are recommended for future work.

The effect of solid flow rate on the solid holdup at the same location (190 mm) is shown in Figure 4.7. Experiments were conducted for three different solid flow rates 0.025 kg/s, 0.033 kg/s and 0.042 kg/s for a fixed air velocity of 0.74 m/s. The simulations were conducted for 0.025 kg/s and 0.033 kg/s solid flow rate. From the figure, it can be seen that the solids flow rate did not have a significant effect on the solids holdup. For all the solids flow rates examined, the qualitative profile of the holdup at different flow rates remained identical. The

CFD simulations were able to capture the profile adequately. As the solid flow rate increased, more solids circulated through the system. More numerical simulations should be performed at higher solid flow rates in order to completely understand the dependence of solid holdup and the stripper hydrodynamics on the solid flow rate.

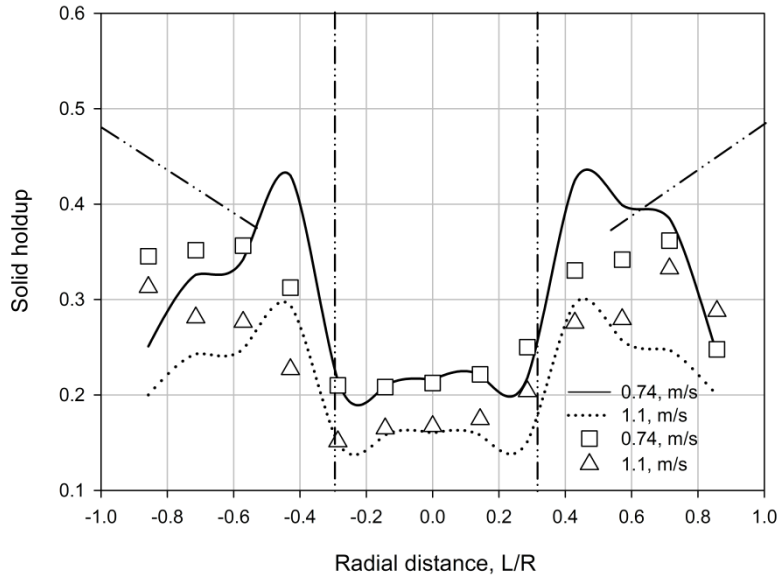

Figure 4.6: Effect of air flow rate on solid holdup.

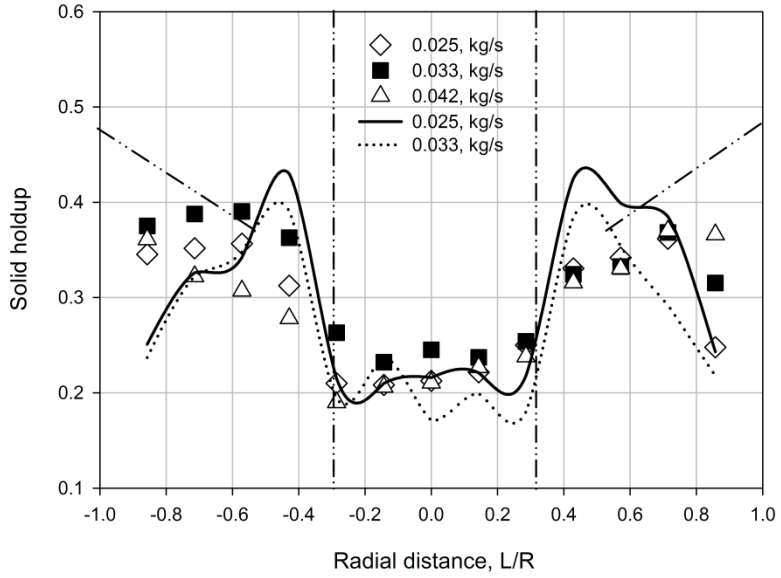

Figure 4.7: Effect of solid flow rate on solid holdup.

Figure 4.8 shows the contours of mean solid holdup for different air flow rates for a solid flow rate of 0.033, kg/s in the baffle regions. At lower air flow rates it is clearly seen that,

solids slide on the baffle walls and descend down. High solid holdup was observed on top of each donut baffle regions leading to formation of local defluidized zones. The main reason for this behaviour is that, when the air rises upward in the narrow region between donut baffle wall and stripper column, the air pushes the solid particle toward the top surface of donut baffle. However this behaviour decreased with increase in air flow rate. This was because, at higher air flow rates, local recirculation zones are formed under the donut baffle region and this recirculating air, aids in increasing the fluidization at those regions.

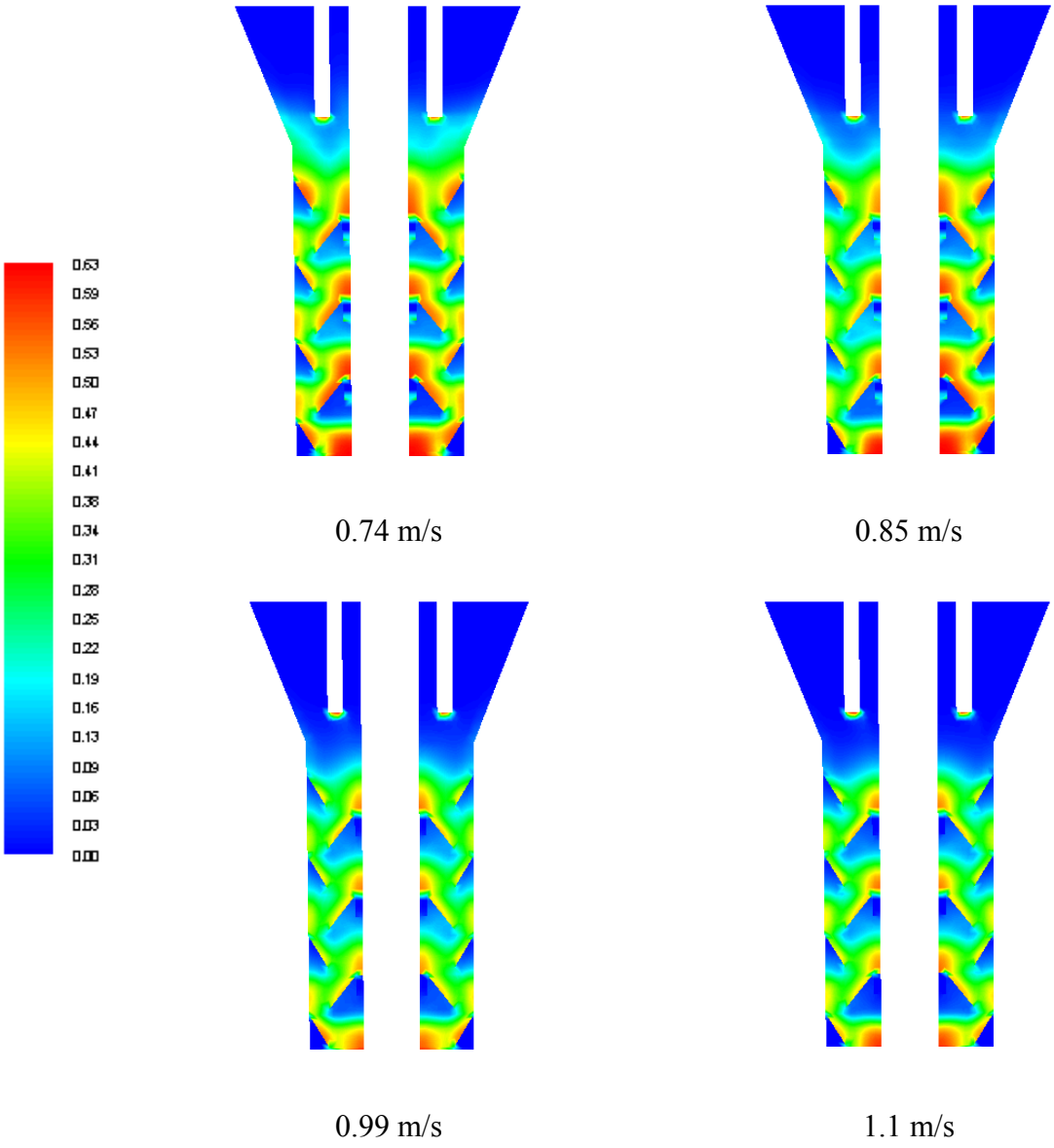

Figure 4.8: Contour plots of time-averaged solid holdup in the baffle regions (solid flow rate = 0.033, kg/s).

4.3.4. Solids Axial Velocity and Solids Holdup along the Height of the Stripper

The axial variation of solid axial velocity and solid holdup obtained using CFD simulations along the height of the stripper are shown in Figure 4.9a and Figure 4.9b respectively. The simulations were carried out for a solid flow rate of 0.033 kg/s and air velocity of 0.74 m/s. The particles descended from the inlet at the top and reached the first disc shaped baffle from top (at 325 mm). As they entered the baffle region, the particles moved along the baffle wall and were forced towards the central riser. Thus, a maximum axial velocity was observed in this open region between the riser wall and disc baffle. Then the particles moved down against the upward motion of air and then entered the donut baffle region (at 290 mm). In this region, the particles are forced to enter a narrow cross sectional region between stripper wall and donut baffle. This contraction gives rise to a steep peak in the axial velocity in this region. This pattern continued alternatively till the particles reached the steam inlet region. The solid axial velocity pattern was dominated by the air velocity. Higher solid axial velocity was observed at locations where the air velocity was higher. In the dead zones below the baffle walls, almost zero or negative axial velocities were observed. The minimum velocities observed in the dead zones indicate that the unused area in stripping operation reduces the efficiency of this design. The solids holdup profiles (Figure 4.9b) showed similar profiles. Higher holdup was observed in the regions where the particle axial velocities were higher. The overall average solids holdup in the stripper was around 0.35.

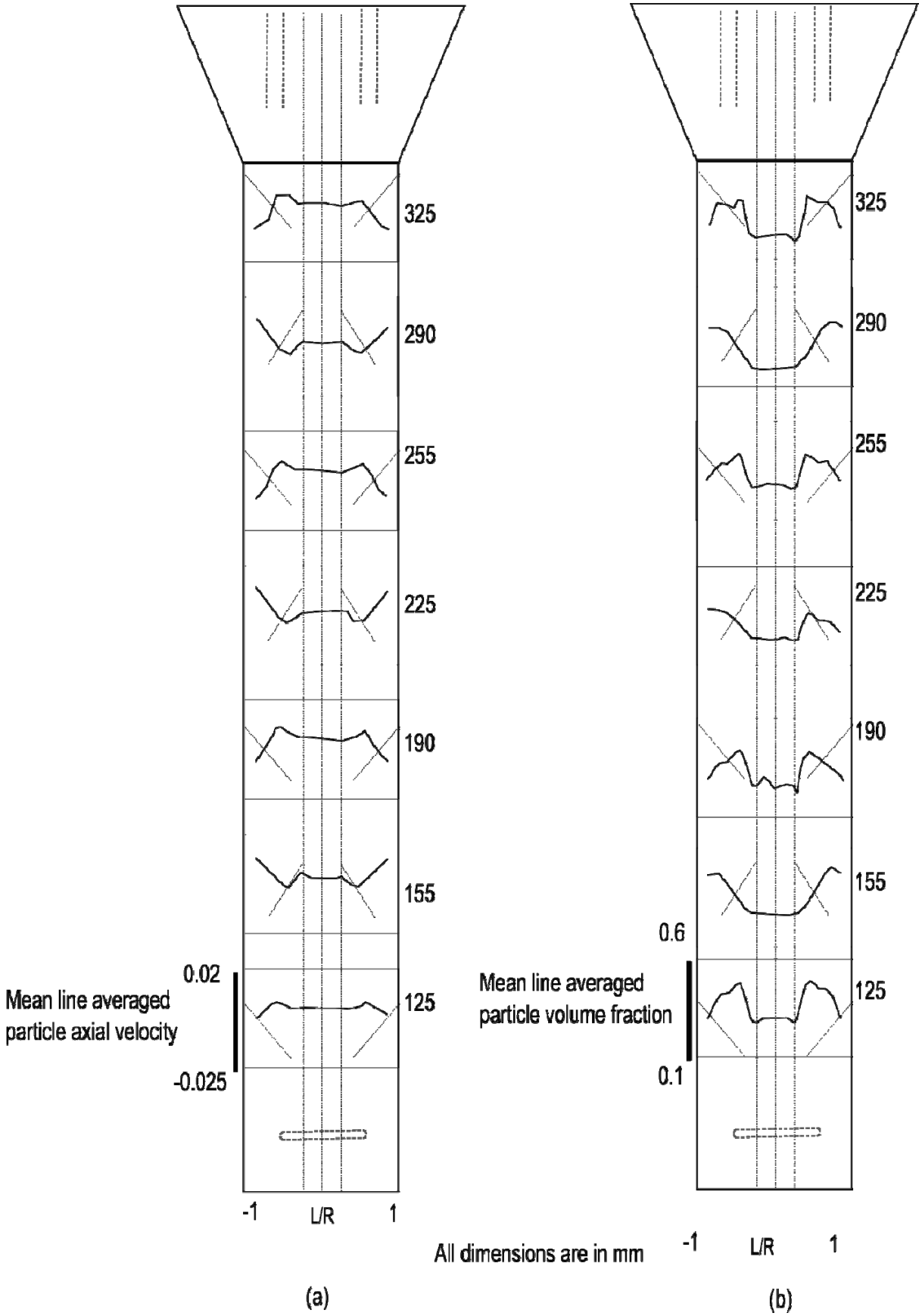

Figure 4.9: Variation of time averaged solid axial velocity and solid holdup along the height of stripper for solids flow rate of 0.033 kg/s and air velocity of 0.74 m/s.

4.3.5. Radial Distribution of Solid Axial Velocity and Solids Holdup

Using FLUENT's post processing tools, we computed the area weighted average of a quantity over a specified area by circumferential isocliping the specified surface area in to equal bands of axial and radial coordinates and also plotted the average against the coordinate. Figure 4.10 shows a comparison of radial distribution of solid axial velocity and solid holdup for two different air flow rates (0.74 m/s and 1.1 m/s) for a solid flow rate of 0.33 kg/s. From Figure 4.10a it is observed that the radial particle axial velocity magnitude is higher at all axial locations for the stripper case operating with superficial air velocity of 1.1 m/s. The difference is easily noticed in the first baffle (disc) immediately above the air inlet ring when compared to other axial locations. This was due to higher local velocity of air near the air inlet sparger, which was similar to the observation made in the previous chapter. It can be observed in Figure 4.10a that irrespective of air flow rates, the particle axial velocity was less in the dead zone regions. The catalyst axial velocity was also less near the baffle wall regions indicating that the particles slide on the baffles walls while slowly descending down.

The CFD model predicted a decrease in the holdup with increase in air flow rate. The overall hold up distribution in radial direction for an air flow rate of 1.1 m/s was lower than the case with air flow rate of 0.74 m/s in Figure 4.10b. In the disc baffle region, a flat hold up profile was seen in the annular gap between the baffle wall and the riser at all sections, except the top disc baffle near the particle inlet. This was due to the influence of high particle velocities at the particle inlet. Also it was noticed that the maximum holdup was near the baffle wall regions for both the air flow rates in the donut baffle regions. However, on re-examining Figure 4.10a, at these locations, it became apparent that the particle axial velocity was low in this regions. This signifies the presence of local defluidized zones near the donut baffle wall region. This confirms the observations made in the earlier section 4.3.3.

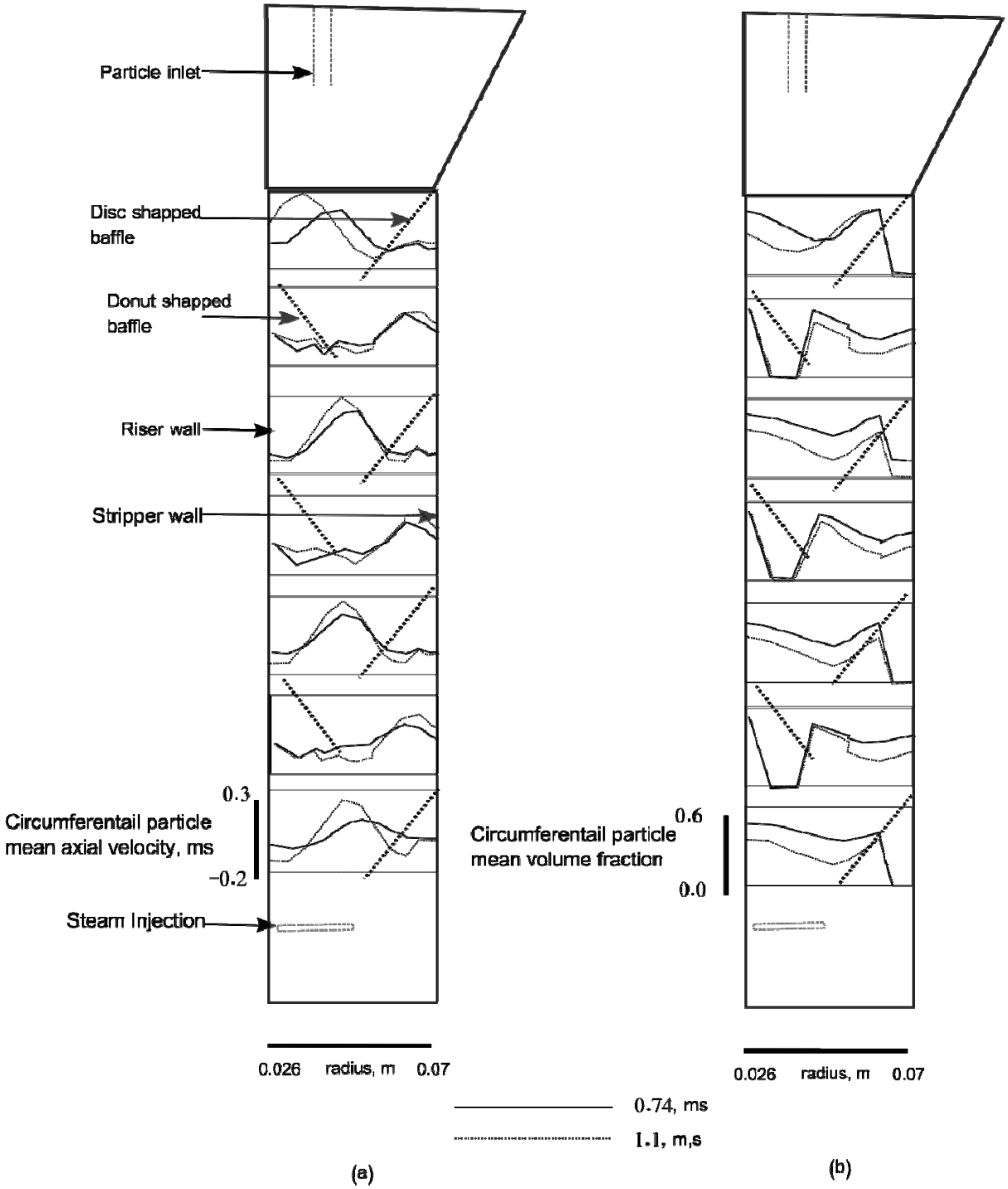

Figure 4.10: Comparison of time averaged radial profiles along the height of stripper: (a) Axial velocity, (b) Volume fraction.

The line average solid holdups are plotted against the axial location at three different radial locations in Figure 4.11. Average solid holdup at a constant solid flow rate of 0.033 kg/s and gas velocity of 0.074 m/s were measured and plotted along the height of the stripper. Three radial positions L/R=0.00, L/R=0.43 and L/R=0.85 that correspond to the center, stripper midsection and the stripper wall respectively were selected. At the center of the column, the line averaged solid holdup did not vary significantly along the stripper height. An average value of 0.19 was observed at this location. In the stripper mid section, high solids holdup was observed near the air inlet region. The volume fraction then oscillated between 0.28 and 0.4 depending on the location of disc or donut baffle. A disc shaped baffle showed maximum solids holdup whereas a donut shaped baffle showed minimum solid holdup at this radial location. Whereas for the region near stripper walls, a disc shaped baffle exhibited lower solid holdup and a donut shaped baffle showed higher solid concentration. Near the stripper wall, maximum variation in the solid holdup was observed in the entry region of the stripper, whereas the holdup was reasonably constant (between 0.21 to 0.26) in the central region of stripper.

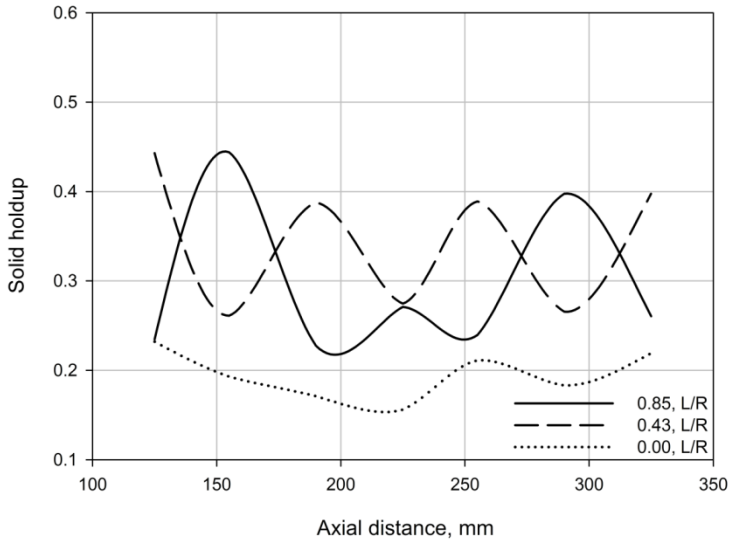

Figure 4.11: Variation of time averaged solid holdup on a single radial location along the height of stripper.

4.4. Conclusions

In this study, 3D CFD simulations on an experimental scale stripper for different operating have been carried out using a two-fluid Eulerian approach. The CFD simulations predicted asymmetric radial profiles, thus necessitating the need for 3D simulations. The CFD models

were validated using experimental data from Chapter 3. The CFD simulations predicted semi-quantitatively with the experimental analysis. The validated 3D CFD models then provided detailed data on the axial and radial variation of particle holdup and velocity. Due to the design of disc and donut baffles, the solids flow through the stripper in a zigzag manner. Recirculation was noticed under the baffle regions for both gas and solid phase. The CFD simulations predicted that the solid holdup decreases with increase in air flow rate.

The model predicted that the solid holdup profiles along the height of stripper are greatly influenced by the shape and position of baffles. At lower air flow rates, the particle phase accumulates over the donut baffle leading to local defluidization zones. Change in solid flow rate had very little effect on solid phase holdup. The solid axial velocities and the volume fractions were observed to be influenced by the gas velocity. The particle axial velocities were low near the wall region, indicating particles slide down on the baffle walls. In the region near the stripper column walls, the lower solid holdup was observed for disc baffle and higher solid holdup was noticed for the donut baffle region. The steam entry had a major impact on velocity and holdup profiles. In summary the CFD simulations along with the densitometry data provide a valuable insight into the FCC stripper operations and can be used to device novel stripper internals.

5. CFD SIMULATIONS OF INDUSTRIAL SCALE DISC AND DONUT FCC STRIPPER

In the previous chapter, the hydrodynamics of strippers fitted with disc and donut baffles was analysed for an experimental/small scale stripper with Geldart B particles. The prime motive for conducting CFD simulations for experimental scale stripper was to study and understand the hydrodynamics of FCC stripper along with insights from experimental results. The literature studies have shown that there is presence of dead zones and bypassing in stripper fitted with disc and donut baffles. The experimental scale CFD model results showed the presence of dead zones and bypassing nature of the phases. Importantly the experimental scale CFD simulations predicted asymmetric nature of flow, which were also observed in the experimental analysis. This ability of the CFD model for small scale stripper to capture these key hydrodynamic features of FCC stripper gives us the confidence for using the CFD model for the industrial scale also. With the increase in computational power it is possible to simulate and study larger computational domains. In this chapter, the focus of work is on studying the effect of steam inlet configuration and lack of symmetric outlet design on the stripper hydrodynamics for an industrial scale stripper fitted with disc and donut baffles. Two different steam inlet configurations; a full ring steam inlet (FRSI) and a simple pipe steam inlet (SPSI) were studied and compared in detail. Also the effect of lack of symmetry in catalyst outlet design on the hydrodynamics of the stripper system was examined. The schematic of the industrial scale FCC Stripper is shown in Figure 5.1. The stripper in this study had seven baffles (four disc and three donut), which were placed alternatively around the riser column. The steam is injected using a ring sparger at the bottom. The catalyst particles enter at the top in the disengager section. The computational model for the experimental geometry, boundary conditions, and numerical parameters are discussed next. Finally, appropriate conclusions have been made on the basis of qualitative and quantitative comparison between CFD and experimental results.

5.1. CFD Model

The two fluid model with KTGF closures as used in chapter 4 is used in this simulation. The governing equations can be summarized as follows:

Gas-phase continuity

$$\frac{\partial}{\partial t}(\varepsilon_g \rho_g) + \nabla \cdot (\varepsilon_g \rho \vec{v}_g) = 0 \tag{5.1}$$

Solid-phase continuity

$$\frac{\partial}{\partial t}(\varepsilon_s \rho_s) + \nabla \cdot (\varepsilon_s \rho \vec{v}_s) = 0 \tag{5.2}$$

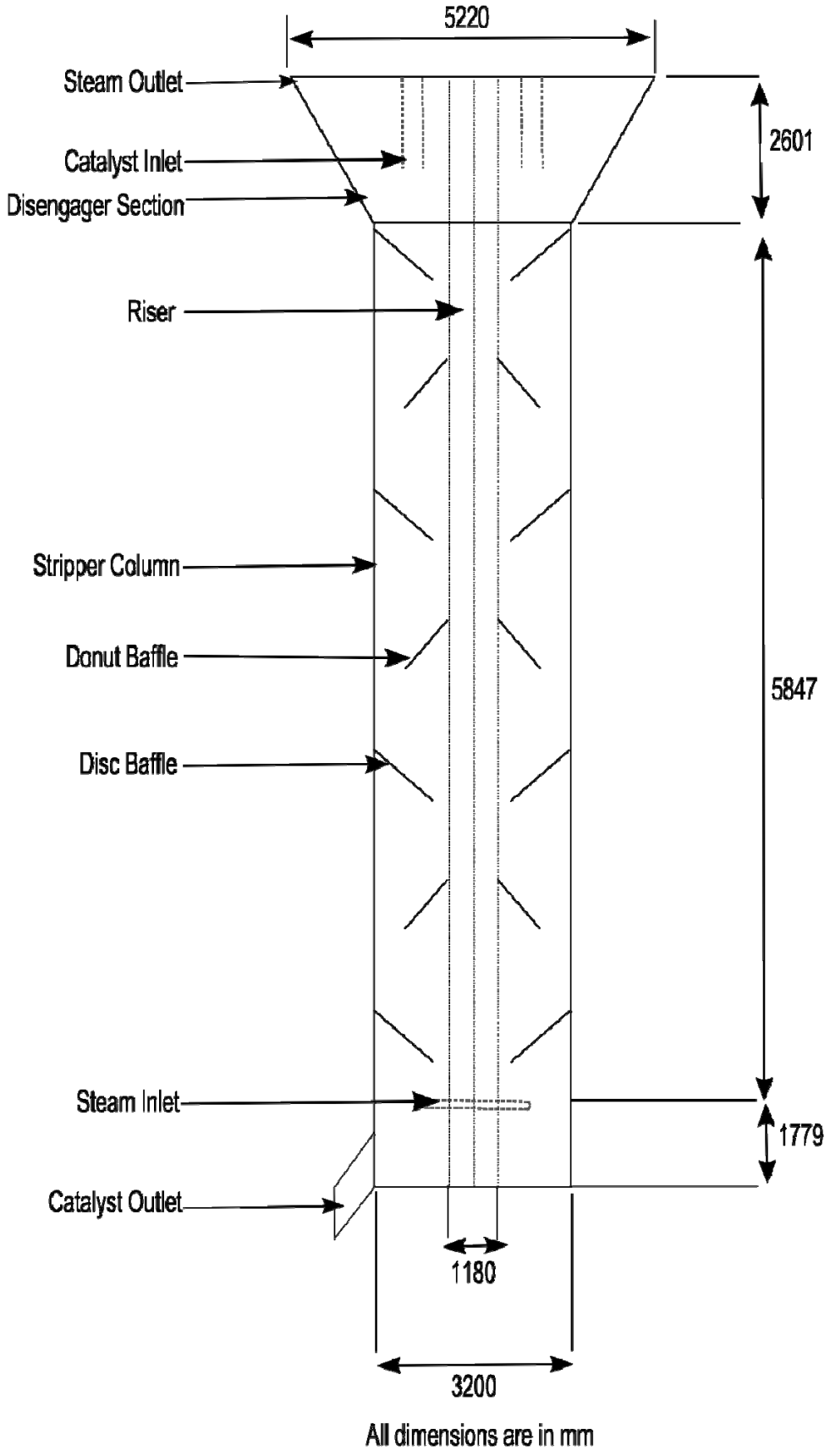

Figure 5.1: Schematic of industrial scale FCC stripper.

Gas-phase momentum

$$\frac{\partial}{\partial t}(\varepsilon_g \rho_g \vec{v}_g) + \nabla \cdot (\varepsilon_g \rho_g \vec{v}_g \vec{v}_g) = -\varepsilon_g \nabla P_g - \nabla \cdot \tau_g + K_{gs}(\vec{v}_g - \vec{v}_s) + \varepsilon_g \rho_g \vec{g} \quad (5.3)$$

Solids-phase momentum

$$\frac{\partial}{\partial t}(\varepsilon_s \rho_s \vec{v}_s) + \nabla \cdot (\varepsilon_s \rho_s \vec{v}_s \vec{v}_s) = -\varepsilon_s \nabla P_g - \nabla \cdot S_s - K_{gs}(\vec{v}_g - \vec{v}_s) + \varepsilon_s \rho_s \vec{g} \quad (5.4)$$

The thermal energy equations have not been included due to the anticipated negligible heat effects in cold-flow fluidized beds.

Table 5.1: Material Properties

Steam density	0.77, kg/m^3
Steam viscosity	1.13× 10^{-5}, kg/m.s
Steam Superficial velocity	0.25, m/s
Catalyst density	1600, kg/m^3
Catalyst particle size	80, μm

The material properties are listed in Table 5.1. In general drag laws are derived from both ends of the voidage scale; the pressure drop correlations are extended for a packed bed into a fluidised bed condition with the Ergun equation (Ergun, 1952). Under dilute conditions, the single particle drag laws are modified to account for the influence of neighbouring particles as in the Gidaspow equation. The limitation of these gas–solid drag laws in the context of the present study is that they were all derived from data obtained for particles much larger than the fine Geldart A particles, which are used in FCC unit. When applied to fine FCC catalyst, the effect of inter-particle forces leading to particle agglomeration and hence reduced drag force is not automatically accounted in the drag law. Gas–solid drag laws are all derived from data at uniform voidages (packed bed, fixed expanded bed, or sedimentation data), and hence are only applicable when the voidage within a computational cell is uniform. In the case of the formation of particle clusters smaller than a computational cell, the standard gas–solids drag correlations are no longer valid. The use of the standard drag laws with FCC catalyst results in overestimates of the level of bed expansion (McKeen and Pugsley, 2002).

Therefore, it is important to use appropriate drag law model, to account for the cohesive nature of Geldart A particles and subsequent cluster formation. Direct implementation of the modified Syamlal O'Brian drag model for Geldart B particles (Ref-Chapter 4) was not possible in this industrial scale stripper having Geldart A particles. To overcome these issues, a modified diameter factor has been used to account for the agglomeration of fine particles according to equation (5.5).

$$d_m = d_s(1 + F_D * \sin((1-\varepsilon_g)\pi / \varepsilon_{\max}) \tag{5.5}$$

Where, d_m is the modified diameter and the diameter factor (F_D) used for this work is 1.75. The Wen and Yu equation (5.6) is accurate at low solids packing where it approaches Stroke's Law and at high solids packing where it approaches the Ergun equation (5.9).

$$K_{sg} = \frac{3}{4} C_D \frac{\varepsilon_s \varepsilon_g \rho_g \left|\vec{\upsilon}_s - \vec{\upsilon}_g\right|}{d_m} \varepsilon_g^{-2.65} \tag{5.6}$$

Where, C_D is given by;

$$C_D = \frac{24}{\varepsilon_g \operatorname{Re}_s}\left[1 + 0.15\left(\varepsilon_g \operatorname{Re}_s\right)^{0.687}\right] \tag{5.7}$$

$$\operatorname{Re}_s = \frac{\rho_g d_s \left|\vec{\upsilon}_s - \vec{\upsilon}_g\right|}{\mu_g} \tag{5.8}$$

$$K_{sg} = 150 \frac{\varepsilon_s\left(1-\varepsilon_g\right)\mu_g}{\varepsilon_g d_s^2} + 1.75 \frac{\varepsilon_s \left|\vec{\upsilon}_s - \vec{\upsilon}_g\right|}{d_s} \tag{5.9}$$

In this work, the modified diameter was used with the Wen-Yu equation. The momentum coefficient from the modified Wen-Yu drag models was compared with that using the modified Gidaspow drag force (Gao et al., 2008a) for the conditions shown in Table 5.2. The momentum coefficient using the modified Wen-Yu drag law matched well with the momentum coefficient of the modified Gidaspow drag force for solid packing of 20% to 50% as shown in Figure 5.2. Then the modified Wen-Yu drag law was benchmarked with industrial solid holdup percentage distribution data for the stripper case fitted with full ring steam inlet (FRSI) configuration. Also, it was compared along with model predictions from

modified Syamlal O'Brian drag model for Geldart A particles with industrial solid hold up percentage at different sections (Figure 5.3 and Figure 5.4) of stripper.

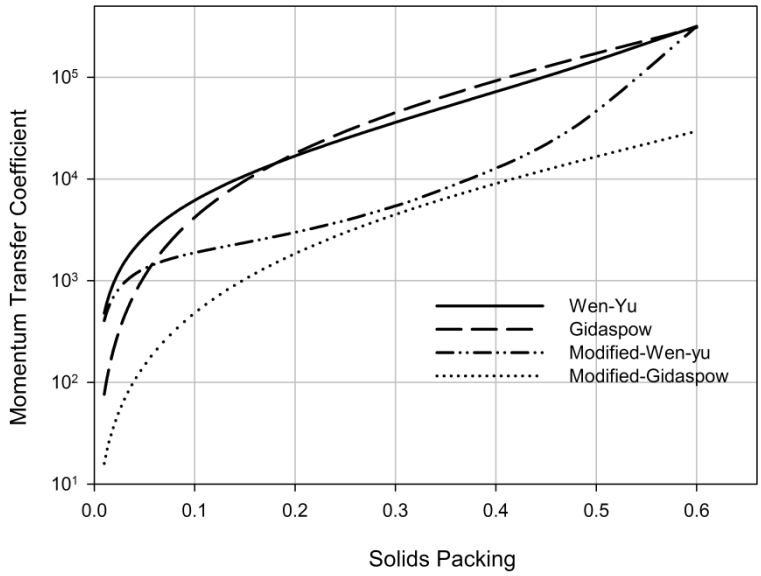

Figure 5.2: Comparison of drag models.

From Figure 5.4, it is clear that in general both modified Wen-Yu and modified Syamlal-O'Brian drag models compared the industrial data well within acceptable limit with a maximum deviation of 10%. In the top half of the stripper, there was not much difference in predictions from both the drag law models. However, in the bottom and middle sections, the modified Wen-Yu drag model compared better with the industrial data at two locations each, when compared with the Syamlal-O'Brian drag model. Therefore, the rest of the simulations in this study were carried out using the modified Wen-Yu drag model. The summary of the closure equations used in this work is given in Table 5.2. The rest of closure equations can be found in Chapter 4.

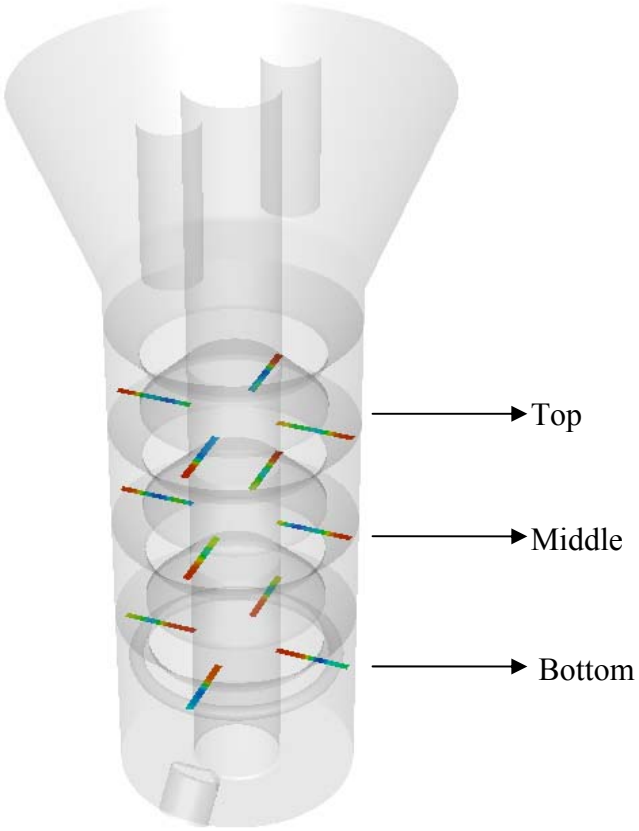

Figure 5.3: Locations at which industrial data was sample and compared with industrial data.

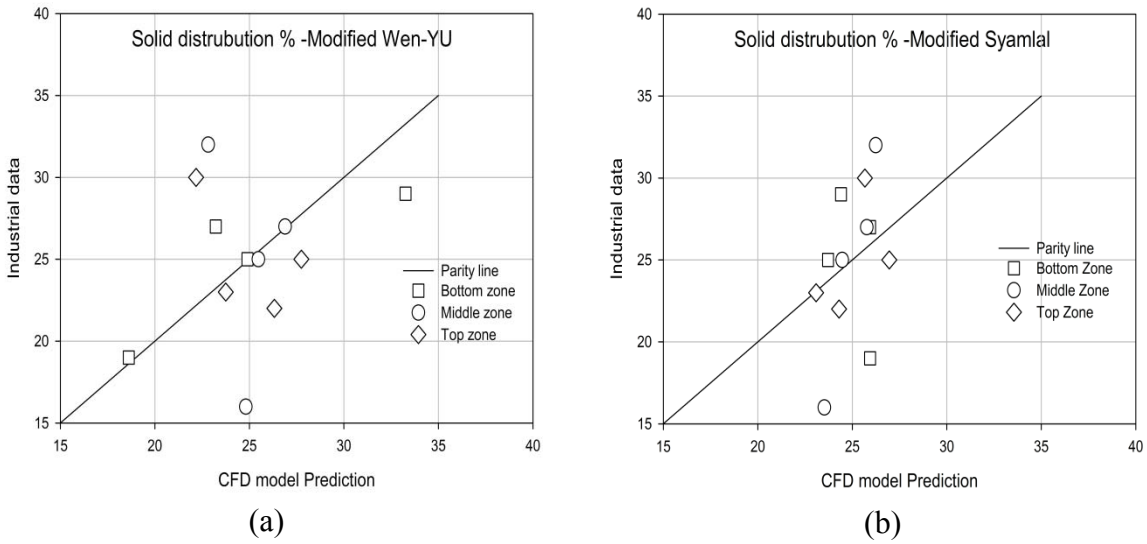

Figure 5.4: Solid distribution % comparison: (a) Modified Wen-Yu drag model, (b) Modified Syamlal-O'Brien drag model.

Table 5.2: Simulation parameters.

Gas phase (Eulerian approach)	
Flow Regime	Laminar
Solid phase (Eulerian approach)	
Shear viscosity	Gidaspow et al.(1990)
Bulk viscosity	Lun et al. (1984)
Frictional viscosity	Schaeffer et al. (1987)
Frictional pressure	Based KTGF
Granular temperature	Algebric
Radial distribution function	Lun et al. (1984)
Solid pressure	Lun et al. (1984)
Drag model	Modified Wen-Yu
Maximum packing limit	0.60
Restitution coefficient	0.9
Angle of internal friction	30°
Time step size	1×10^{-4}
Discretization	QUICK
Pressure-velocity coupling algorithm	SIMPLE

5.1.1. Simulation Method and Boundary Conditions

Simulations were conducted using commercial CFD software Fluent 6.3.16 (of Ansys Inc). The geometry and mesh were created in Gambit 2.3.16 (of Ansys Inc). The geometry of the strippers with different steam inlet configurations is shown in Figure 5.5. The full ring steam inlet configuration is denoted as FRSI and the simple pipe steam inlet configuration is denoted as SPSI. QUICK discretization scheme was used for the momentum and volume-fraction differencing scheme, and time discretization was first order. The solution of the pressure from the momentum equations uses a pressure correction equation that corrects the pressure and the velocities after every iteration according to the SIMPLE algorithm. Simulations were carried out for a solid flux of 45 kg/m^{2}s and a superficial steam velocity of 0.25 m/s was used FCCU catalyst particles of size 80 microns. Velocity inlets

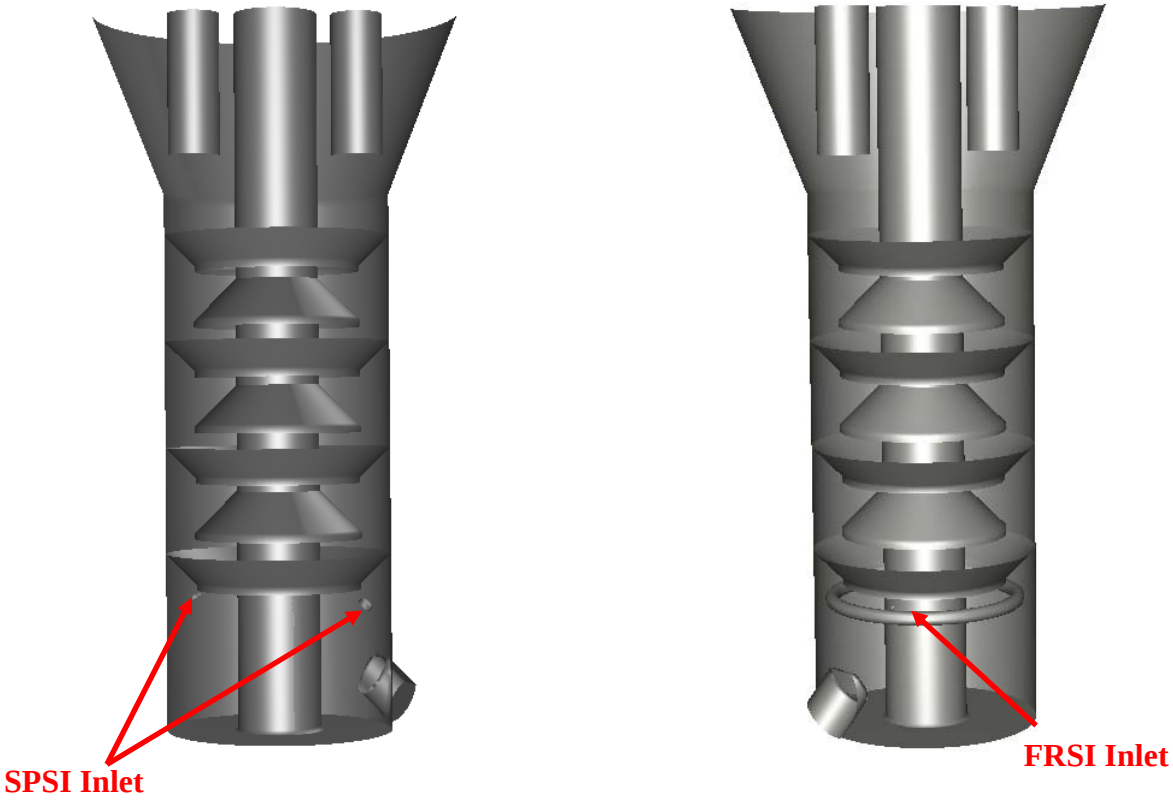

Figure 5.5: Stripper geometry with different steam inlet configurations.

boundary conditions were used for both solid and gas inlets. The catalyst phase was allowed to enter elutriated along with air at catalyst inlet, where the catalyst inlet velocity was 1.4 m/s with a phase hold up of 0.165. A pressure outlet boundary condition was specified at the top of the stripper. Solids were free to leave if entrained and were not returned to the computational domain. The simulations were carried out in transient manner. Volume fraction and velocity of both the phase were monitored across the domain. The simulations were deemed converged once these quantities reached a steady state. It took approximately 60 seconds of computational time to achieve convergence. Time averaged data on the phase velocities and volume fraction was then collected for next the110 seconds.

Preliminary numerical experiments were carried out for FRSI using two different computational grids to assess the grid dependency (Figure 5.6). The coarse grid had an average cell size of 70 mm (Figure 5.6a, c), whereas the grid size for finer mesh was 45 mm (Figure 5.6b, d). A comparison of the bed density and catalyst mean velocity profiles for the two different grids is shown in Figure 5.7. The profiles for the bed density in two cases were identical. The values of mean catalyst velocity magnitude differed slightly along the height of

the stripper. However, this difference was considered to be in acceptable limit considering industrial scale geometry configuration. Therefore, in order to save computational time, the relatively coarser average cell size of 70 mm was used in the remaining simulations.

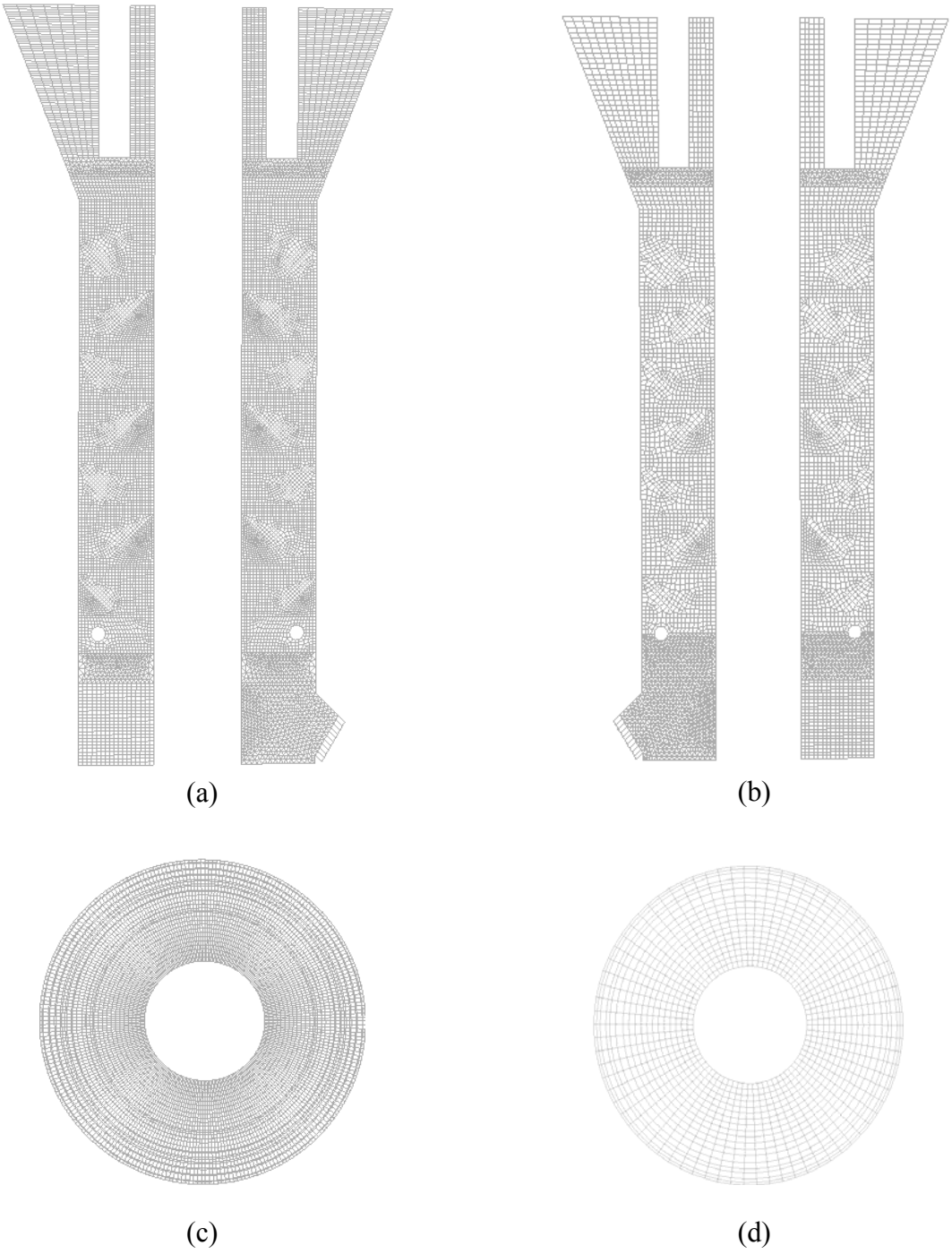

Figure 5.6: Different grid sizes: (a) Vertical cross sectional view of 45 mm cell sized grid, (b) Vertical cross sectional view of 70 mm cell sized grid, (c) Horizontal cross sectional view of 45 mm cell sized grid, (d) Horizontal cross sectional view of 70 mm cell sized grid.

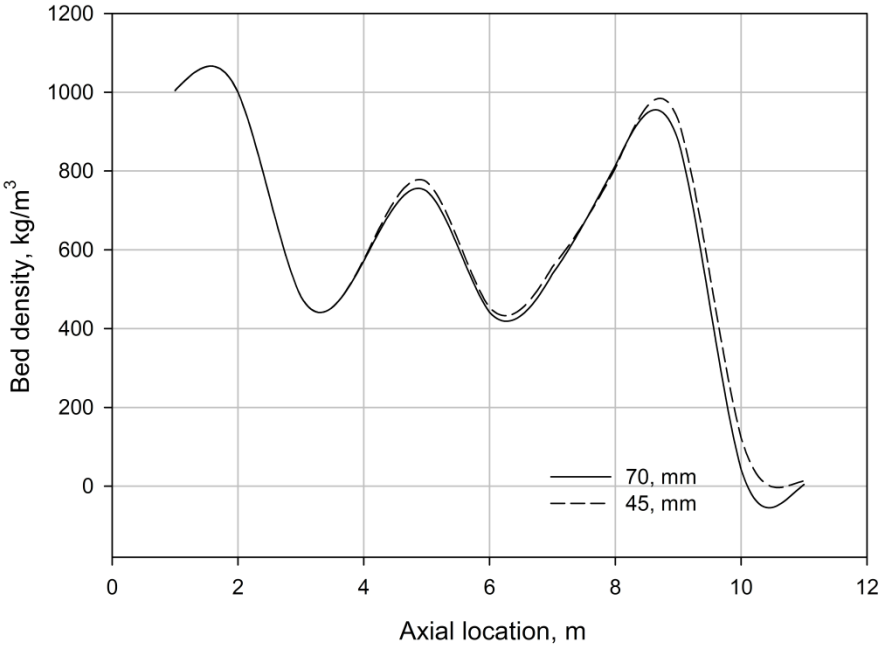

(a)

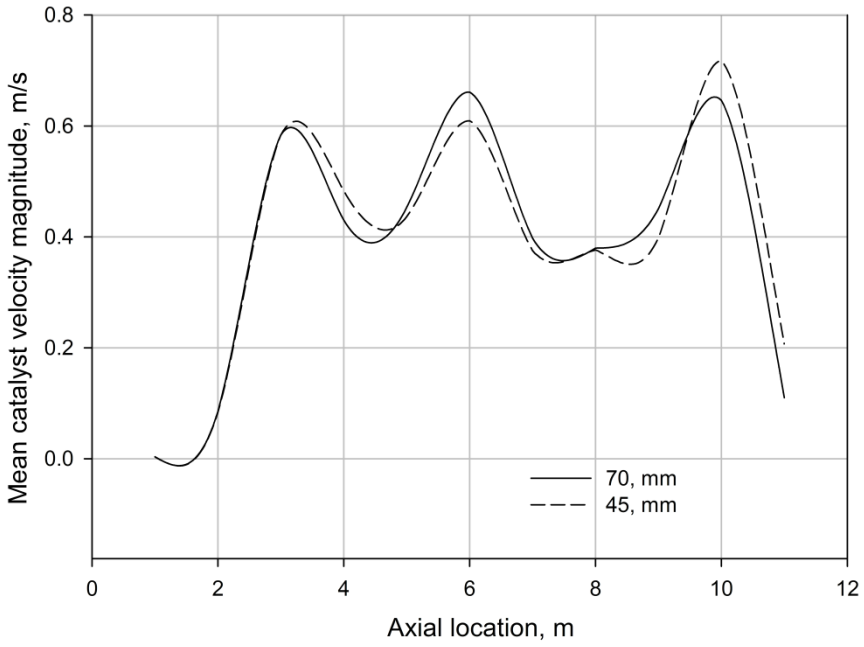

(b)

Figure 5.7: Time averaged (mean) results from grid independency study: (a) Bed density, (b) Catalyst velocity magnitude.

5.2. Results and Discussion

The following section discusses the hydrodynamics of stripper fitted with simple pipe steam inlet (SPSI) and full ring steam inlet (FRSI) configurations. Simulations were conducted for a steam superficial velocity of 0.25 m/s and catalyst mass flux of 45 kg/m^{2}s.

5.2.1. Hydrodynamics of stripper with SPSI Configuration

The contours of mean volume fraction of steam are shown in Figure 5.8a. Transverse planes passing through the centre of the stripper at four different angular positions were selected for plotting the contours. The position of these planes is shown schematically in Figure 5.8c. The 0^o plane passed through the centre of the two steam inlets and the 45^o plane passed through the catalyst outlet. The 3D contours of mean catalyst hold-up across the stripper are shown in Figure 5.8b. Contours are draw` n for different iso values ranging from 0.2 to 0.6.

For SPSI, using 2D simulations Gao (Gao et al. 2008a) predicted a uniform radial distribution of the two phases. However, using 3D simulations, it was clear that the steam flow was highly segregated with widespread bypassing and channeling as seen in Figure 5.8a. Maximum steam holdup was observed under the baffles, reflecting the presence of dead zones or unused area for stripping operation. Severe maldistribution was also apparent from the iso surface plots shown in Figure 5.8b. The down flow path of catalyst was noticed only in one section of stripper, where the holdup varied from 20% to 50 %. This mode of catalyst flow in one section of the stripper would adversely affect the performance of stripping operation. Higher volume fraction of steam was observed in the regions adjacent to the steam inlet pipe 1 (Figure 5.8c); whereas the steam distribution was very poor in the region influenced by steam inlet pipe 2 (Figure 5.8c). This can be attributed to the asymmetric catalyst outlet which is located near the steam inlet pipe 2. Due to the high catalyst (and associated steam) flow rate from the outlet, a large amount of steam (equivalent to 17 % of steam coming in from steam inlet pipe 2) was carried over by with the catalyst to the catalyst outlet pipe. This resulted in lower volume fractions of steam in the region near the steam inlet 2. However, some mixing was also observed at the top region of the stripper, where the steam maldistribution was not as severe as at the bottom.

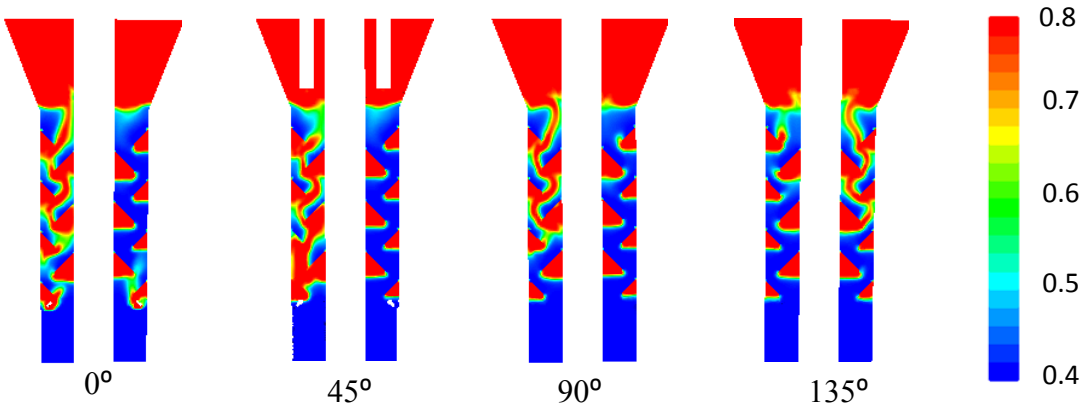

(a)

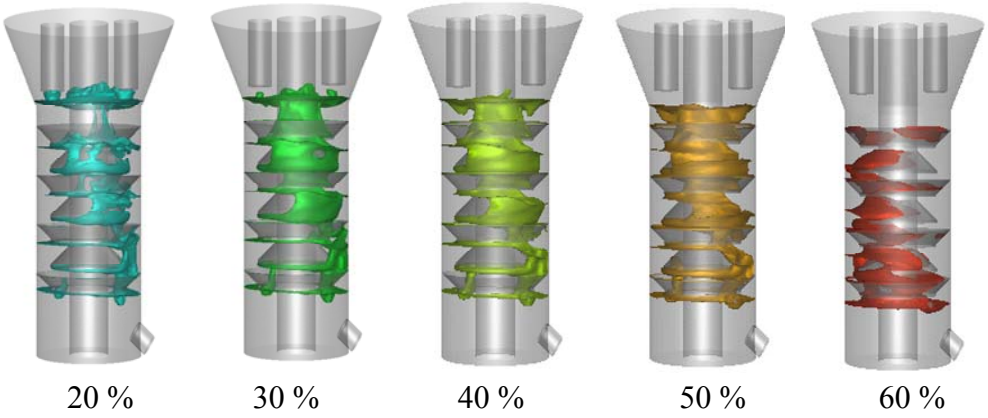

(b)

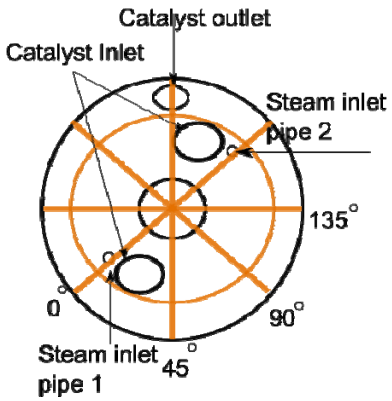

(c)

Figure 5.8: Simple pipe steam inlet stripper: (a) Contours of time averaged (mean) volume fraction of steam, (b) 3D contours of time averaged (mean) volume fraction of catalyst, (c) Top view of stripper.

Figure 5.9 shows the mean steam velocity vector plot in the catalyst outlet region located near the steam inlet pipe 2. The asymmetric design of catalyst outlet affects the steam distribution, as a large portion (17%) of the steam injected from the steam inlet pipe 2 is carried along with the catalyst towards the outlet. Either a common outlet at the centre or two outlets symmetric to each other can be used to get a better steam distribution across the entire stripper. However, due to design constraints on industrial FCCUs, this might not be possible in practice. A better steam inlet configuration such as a full ring, multiple single nozzles, sparger, or a combination thereof can help in reducing the steam mal-distribution.

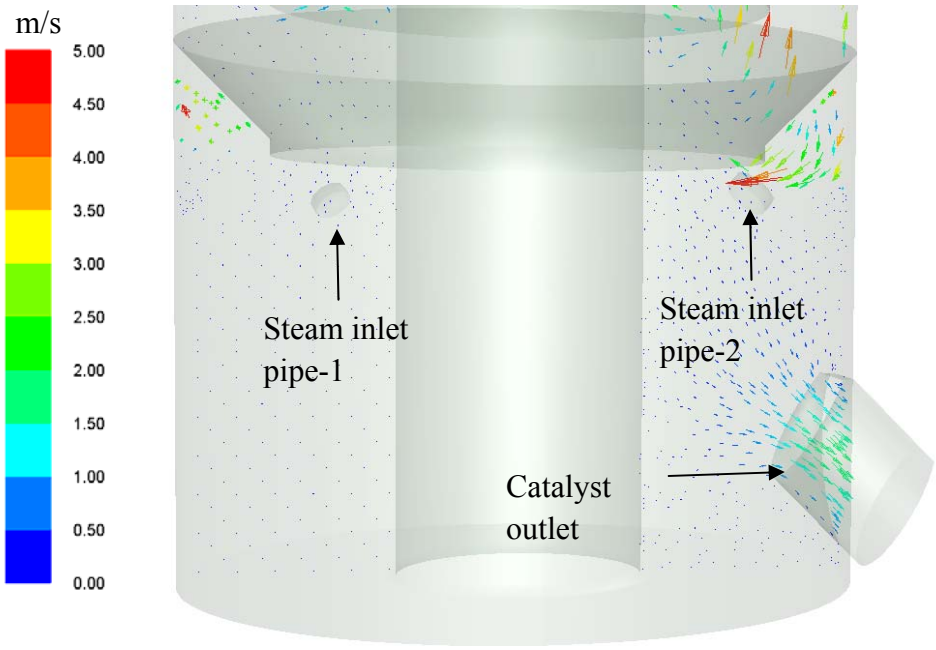

Figure 5.9: Time-averaged (mean) vector plot of steam velocity at 45° plane.

5.2.2. Hydrodynamics of stripper with FRSI Configuration

The contour plots of mean volume fraction of steam for the FRSI configuration are shown in Figure 5.10a. The plots are drawn at the transverse planes at the same locations as for the SPSI configuration (Figure 5.8c). The 3D contours of the mean catalyst holdup across the stripper are shown in Figure 5.10b. Contours are drawn for different iso values ranging from 0.2 to 0.6 of mean catalyst holdup across the stripper with full ring steam inlet.

It can be seen that the steam followed a well defined zigzag shaped path through the baffles, which was due to the shape of baffles in which provides higher contact between the catalyst and stripping steam. Although the steam distribution was uniform at the bottom, some radial non-uniformity was also observed along the height of the stripper. It was clearly visible in the

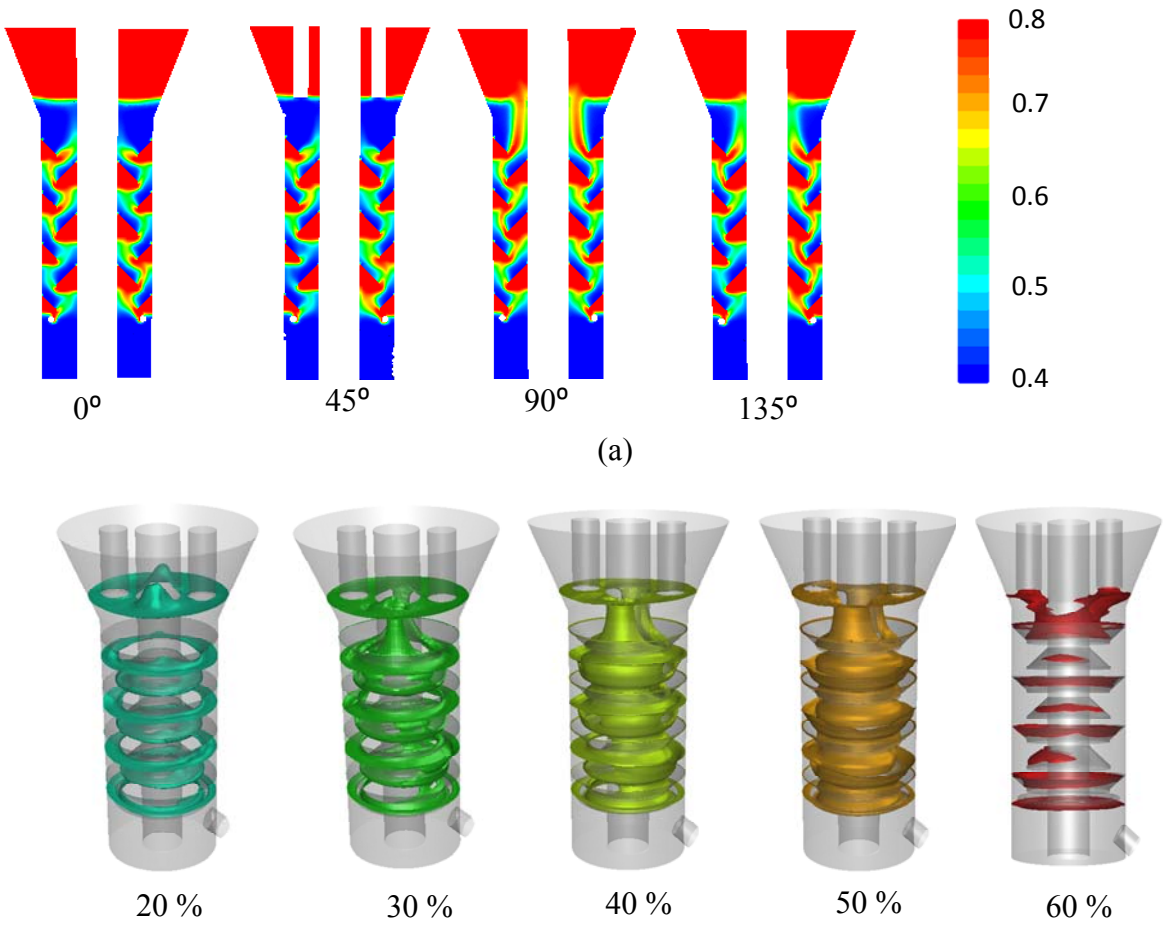

Figure 5.10: Full ring steam inlet stripper: (a) Contours of time averaged (mean) volume fraction of steam, (b) 3D contours of time averaged (mean) volume fraction of catalyst, (c) Top view of stripper.

lower regions of stripper for 45° and 90° cross-sectional planes. Also in the top region of stripper, plumes were noticed in the disengager section for 90° and 135° planes, while this

was absent in planes of 0° and 45°. This indicates the presence of channeling or bypassing. However it was not as severe as noticed in the stripper fitted with SPSI configuration. The catalyst particles flow down in all directions of stripper as seen in Figure 5.10b. The catalyst distribution varied from 20% to 60 % across the stripper. The bulk of the flow was occurring in the central region of the stripper. Maximum holdup was noticed near the baffle walls, while the minimum holdup was seen near the stripper column walls.

Figure 5.11 shows the mean velocity vector plot of steam at 45°cross sectional plane. The path of the steam is clearly seen in the vectors of the high magnitude. The highlighted region in the stripper shows the presence of bypassing in the bottom region of stripper. A fraction of steam coming from steam inlet ring, enters the region between baffle-1 (disc) wall and stripper wall (dead zone). This steam then recirculated to the bulk of steam flow. While in the next baffle (donut), a similar behaviour is observed, as some portion of steam entered the dead zone region between baffle-2 wall and riser wall, only to be recirculated back to the bulk flow. This pattern was observed all along the height of stripper. Eventually this kind of back mixing provides enhanced contact between particle and gas phases.

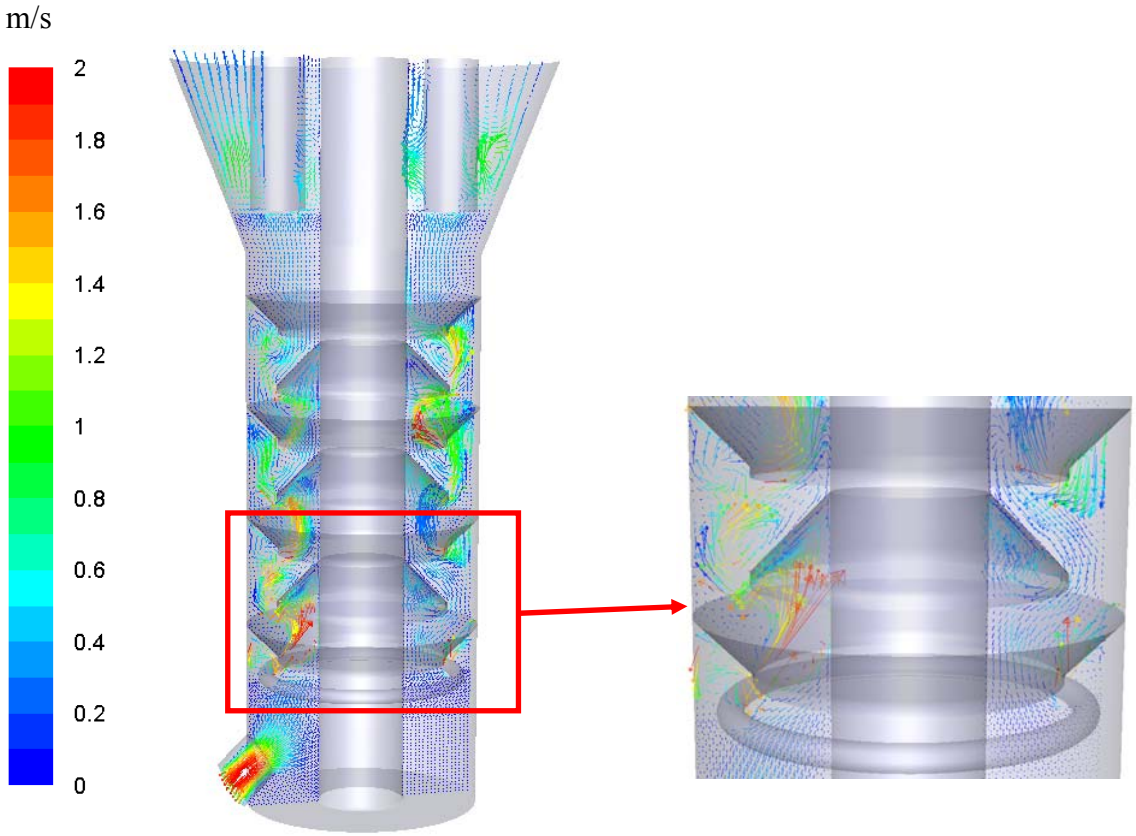

Figure 5.11: Time averaged (mean) vector plot of steam velocity at 45° plane.

5.2.3. Effect of Steam Inlet Configuration on Steam Velocity Field

To study the effect of steam inlet configuration on the steam distribution, the mean radial and axial steam velocities were calculated along the axial height of stripper for the both inlet configurations. The first point was taken immediately above the steam inlet, consequent points were taken at the bottom and top of each baffle till the disengagement section. Figure 5.12a and Figure 5.12b show a comparison of the mean radial and axial steam velocities respectively.

The mean steam radial velocity magnitude (Figure 5.12a) for FRSI stripper oscillated between 0.1 and 0.3 m/s all along the height of stripper. At the disc shaped baffles, a part of steam enters the dead zone between the baffle wall and stripper wall only to be recirculated back. This axial location was dominated by recirculation currents and back mixing and hence we obtained a higher radial velocity magnitude at the start of disc baffles. At the top of the disc baffle, due to a large open area and no restrictions, the radial velocity was comparatively lower. At the entry to the donut baffle, some amount of steam entered into the dead zone region between the baffle wall and riser wall. However, this steam was recirculated back into the main flow. Hence, at these locations higher radial velocities were observed. In general, the radial velocity was higher at the steam entry of a baffle region and was lower when the steam left the baffle region. The variation in the radial velocity at different baffle locations was more pronounced in the initial 5m, clearly indicating the influence of the steam inlet and catalyst outlet. At the bottom section of the stripper, higher local velocities were expected due to the influence of air inlet region, the effect of this local velocity variation was somewhat dampened by the presence and shape of baffles. The decrease in the magnitudes of the oscillations as the steam moved along the height of stripper indicated that baffles helped in achieving even distribution when combined with a proper steam injection pattern. This suggests that the ideal scenario of uniform radial velocity throughout the stripper can be achieved through a more densely packed baffle structure. One can also envisage higher number of small sized baffles or structured packing to improve the contact of catalyst and steam. It also suggests a move towards next generation stripper internals like packing arrangement (Rall and DeMulder, 2000).

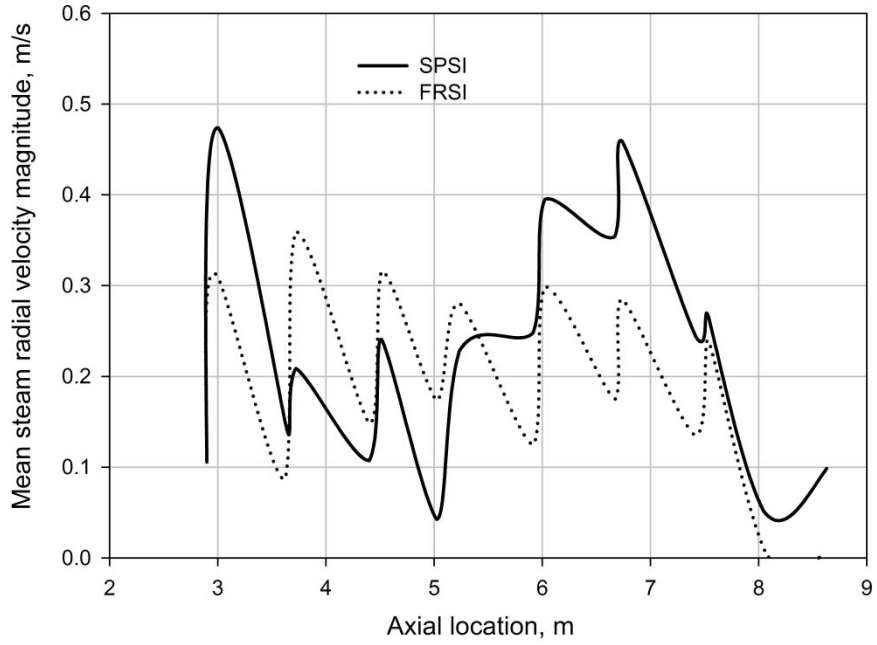

(a)

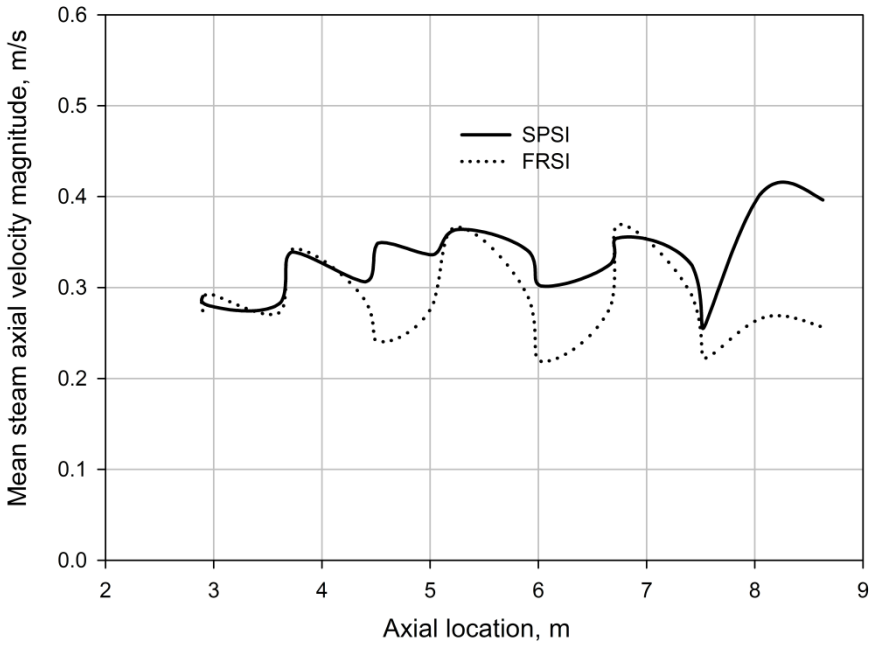

(b)

Figure 5.12: Comparison of time averaged (mean) steam velocities: (a) Radial velocity magnitude, (b) Axial velocity magnitude.

In contrast to the FRSI, the SPSI configuration stripper, which only differed in the steam inlet design configuration, the radial velocity distribution was erratic and a closely defined pattern was not observed. The radial velocity was much higher in the bottom and top sections of stripper, and it was lower in the middle sections of stripper. This was a clear indication of the

presence of bypassing and channeling. Thus it can be clearly seen that for the same internal design, the steam inlet configuration plays a vital role in governing the performance of the stripper. In addition to these two configurations, an alternative multiple single nozzle inlets between the baffles in opposite directions can also be used (Cui et al. 2006a; Rose et al. 2005).

For the FRSI configuration, as with the radial velocity, the axial velocity (Figure 5.12b) followed a cyclical pattern. Higher axial velocities were observed in areas where the annular gap between the baffle and the walls (stripper / riser) were smaller. The axial velocity for the FRSI configuration was maximum in the donut baffle regions compared to the disc baffle regions due to smaller contracting space between the donut baffle and the stripper wall; and minimum in the disc baffle regions due to a relatively larger annular space between baffle and riser walls. In contrast to this observation, the mean axial velocity was much higher in the disc baffle regions for the SPSI configuration. The variation in axial velocity was minimal. This pointed to a short-circuiting behaviour. The overall mean axial velocity for the SPSI configuration was 0.32 m/s, while that for the FRSI configuration is 0.28 m/s which was 14 % lower. This implied that for the same operating conditions, the steam spends less time for SPSI configuration compared to the FRSI configuration. Thus the efficiency was lower for the SPSI configuration as efficiency is a function of residence time of the phases.

In order to understand the radial segregation and mixing, x-mean steam velocity vectors were plotted at the entry of 3rd baffle from bottom (Figure 5.13a, b) and at the entry of 4th from bottom (Figure 5.13c, d). Figure 5.13a and Figure 5.13c correspond to the SPSI configuration, whereas, Figure 5.13b and Figure 5.13d correspond to FRSI configuration. At the entry of a baffle, a fraction of steam is trapped in the region between the baffle and the stripper/riser walls. This steam recirculates back to the main domain of steam flow leading to formation of two different regions. Lack of backmixing of steam from the stagnant zones to the bulk of the flow is responsible for the radial segregation. The backmixing phenomenon is attributed to the shape of baffles. Uniform backmixing ensures a good mixing and eventually helps in achieving better contact between the phases and hence better stripping rates.

For the SPSI configuration, at the entry of disc baffle (Figure 5.13a), back mixing (indicated by higher x mean velocity) was predominant only in two quadrants (I and II). Hence, a highly segregated flow was observed at this location. As the steam moved upwards to the donut

baffle (Figure 5.13c), the radial segregation reduced with increased backmixing observed in three quadrants (I, II and IV). For the FRSI configuration however, better backmixing was predicted in all four quadrants (Figure 5.13b, d). In general the radial segregation of steam was more pronounced in SPSI configuration compared to the FRSI configuration.

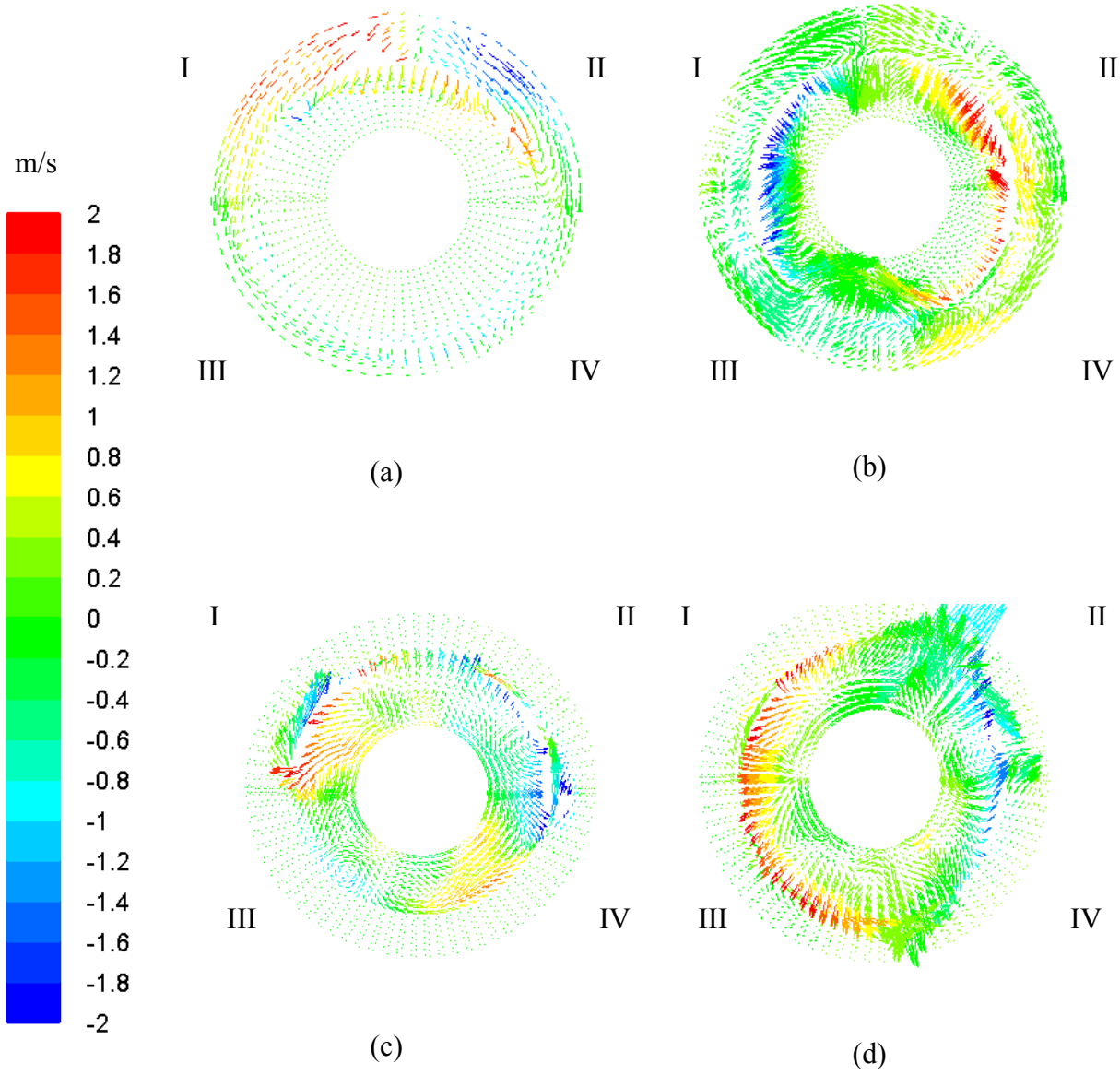

Figure 5.13: Comparison of vector plots for x-mean steam velocity.

5.2.4. Effect of Steam Inlet Configuration on Catalyst Distribution

The radial distribution of catalysts means axial velocity and mean catalyst volume fraction along the height of the stripper are compared in Figure 5.14. The particles descend from the inlet at the top region and reach the topmost disc shaped baffle (at 9 m). As they enter the baffle region, the particles slide along the baffle wall and are forced towards the central riser.

Therefore, maximum axial velocity was observed in this open region between the riser wall and disc baffle. The particles then moved down against the upward motion of air to the donut baffle region (at 8 m). In this region, the particles are forced to enter a narrow cross sectional region between stripper wall and donut baffle. This contraction gives rise to a steep peak in the axial velocity in this region. This pattern continues alternatively until the particles reach the steam inlet region (Figure 5.14a). Higher solid axial velocity was observed at locations where the air velocity was higher. In dead zones below the baffle walls, almost zero or negative axial velocities was observed. The minimum velocities observed in the dead zones reflected the unused area in stripping operation reducing the efficiency of this design.

The radial average mean catalyst volume fraction along the stripper height for SPSI and FRSI configurations is shown in Figure 5.14b. At the topmost baffle, bubbling was observed in case of FRSI configuration, thus leading to higher catalyst volume fractions. In contrast, channelling was observed in SPSI configuration, consequently, very low catalyst volume fraction was observed in the top regions of stripper where there was maximum influence of the catalyst inlet. The catalyst particles mostly slide down along the baffle walls, hence higher volume fraction was noticed near the baffle walls and lowest holdup was observed near the walls (riser/stripper). At the same time some catalyst particles are entrained with the steam in to dead zone regions. This behaviour slowly changes as the catalyst particles descend down and enter the region where the influence of steam inlet region was predominant. In the bottom most regions higher holdup was seen near the wall surfaces (riser/stripper). From the baffle located at 8 m to the baffle at 5 m, similar catalyst volume fractions are observed for both the configurations. In the bottom sections (from height 3 m to 4 m), the SPSI configuration exhibited higher holdup compared to the FRSI inlet clearly indicating the pronounced influence of steam injection zone. The average holdup for the SPSI configuration also increased significantly (from 28% to 44%) between first two baffles. This jump in the holdup within a single baffle zone for SPSI inlet indicated the presence of bypassing and mal-distribution. For the SPSI and FRSI configuration, the overall average solids holdup across the stripper was 26% and 30 % respectively. Thus, the catalyst residence time was higher for the FRSI configuration allowing better stripping.

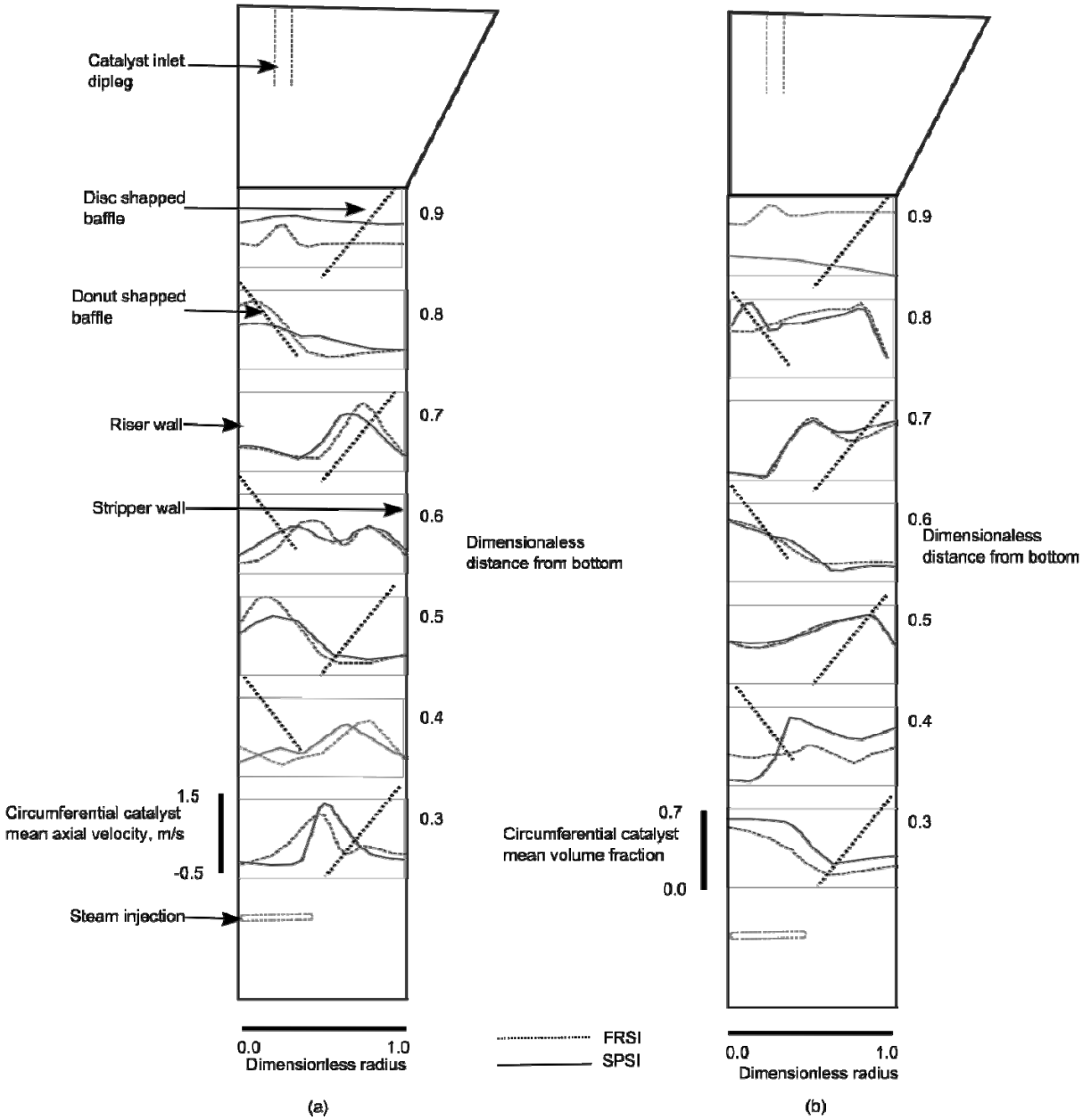

Figure 5.14: Comparison of time averaged (mean) radial profiles along the height of stripper: (a) Catalyst axial velocity, (b) Catalyst volume fraction.

5.3. Conclusion

In this chapter, the hydrodynamic characteristics of a industrial scale FCC steam stripper fitted with different steam inlet configurations was investigated using 3D CFD studies. The modified Wen-Yu drag model was used to account for the cohesive nature of Geldart A particles, which showed reasonable agreement with industrial data on solids holdup distribution. It was observed that the steam inlet configuration plays a critical role in governing the hydrodynamics of the stripper. For the same internal configuration (disc and donut), drastically different flow patterns were observed for different steam inlets.

The effect of asymmetric nature of catalyst outlet on the hydrodynamics was also investigated. The lack of symmetry in catalyst outlet has a significant effect on the flow characteristics of the stripper fitted with SPSI inlet configuration. Severe maldistribution and channelling was noticed in the stripper fitted with SPSI inlet configuration. In this arrangement, nearly 17 % of the steam entering from steam inlet near to the solids outlet was carried along with the catalyst to the regenerator section due to asymmetric nature of catalyst outlet. A large variation in steam radial velocity was also observed all along the height of stripper which indicated the presence of segregation. In addition, higher steam and catalyst axial velocities were noticed in all sections of stripper. This indicated lower residence time and lower stripping efficiencies. Low catalyst holdup in stripper fitted with SPSI inlet was also noticed when compared with stripper fitted with FRSI inlet configuration. These shortcomings can be overcome by using multiple steam injection portals all along the height of stripper or a symmetric catalyst outlet design.

The stripper fitted with FRSI inlet configuration exhibited some segregation and channelling at the bottom section of stripper which was caused by the asymmetric catalyst outlet design. However, the segregation was not as severe as SPSI stripper case. Recirculation and back mixing was noticed in the baffle regions, leading to the mixing of phases. Due to uniform steam inlet design maldistribution and channelling was minimal. Radial velocities were maximum near the entry region of baffles, indicating the presence of recirculation zones. Two different zones of velocity were noticed in the baffle entry and outlet regions, which were dominated by recirculation zones. Lower steam axial velocity was noticed for stripper fitted with FRSI configuration. This will have a positive effect of residence time and efficiency. The performance of stripper can be further enhanced by reducing the distance between the baffles or more number of small sized baffles can be used to improve the contact of catalyst and steam. The study provides a better understanding of the inlet configuration on the stripper performance and describes the possible avenues to improve the performance through design alternatives.

6. CFD MODELLING APPLIED TO ADVANCED FCC STRIPPER TECHNOLOGY

Performance of the FCC catalyst stripper is affected by a variety of design and operating parameters. The key for achieving optimal performance in a stripper lies in the selection of stripper internals. The older commercial stripper units have been pushed beyond design limits for handling more catalyst circulation rate in an attempt for de-bottlenecking the process. In the long run, this leads to deterioration of stripping efficiency and affecting operability. Stripper designs have been mostly limited to disc and donut baffles and the shed deck type trays. The main limitation of trays, baffles type internals are high restricted area, catalyst flux, associated back mixing and reduced catalyst residence time and zones of catalyst stagnation (Rall and Demudler, 2000). Taking into account these limitations associated with internal trays or baffles, a new type of structured packing internals for stripper in considered in this study. An industrial scale FCC stripper unit fitted with structured packing internals has been studied using 3D CFD model. The schematic of the stripper is shown in Figure 6.1.The full ring steam inlet (FRSI) inlet configuration was used for the stripper fitted with packing (Ref-Chapter 5). Figure 6.1 shows the stripper fitted with a stack of structured mixing elements. Total eleven stack elements were arranged continuously on top of one another such that each stack element was perpendicular to the next element.

6.1. CFD Model

The two fluid models with KTGF closures as used in chapter 4 were used in these simulations. The governing equations can be summarized as follows:

Gas-phase continuity

$$\frac{\partial}{\partial t}(\varepsilon_g \rho_g) + \nabla \cdot (\varepsilon_g \rho \vec{v}_g) = 0 \tag{6.1}$$

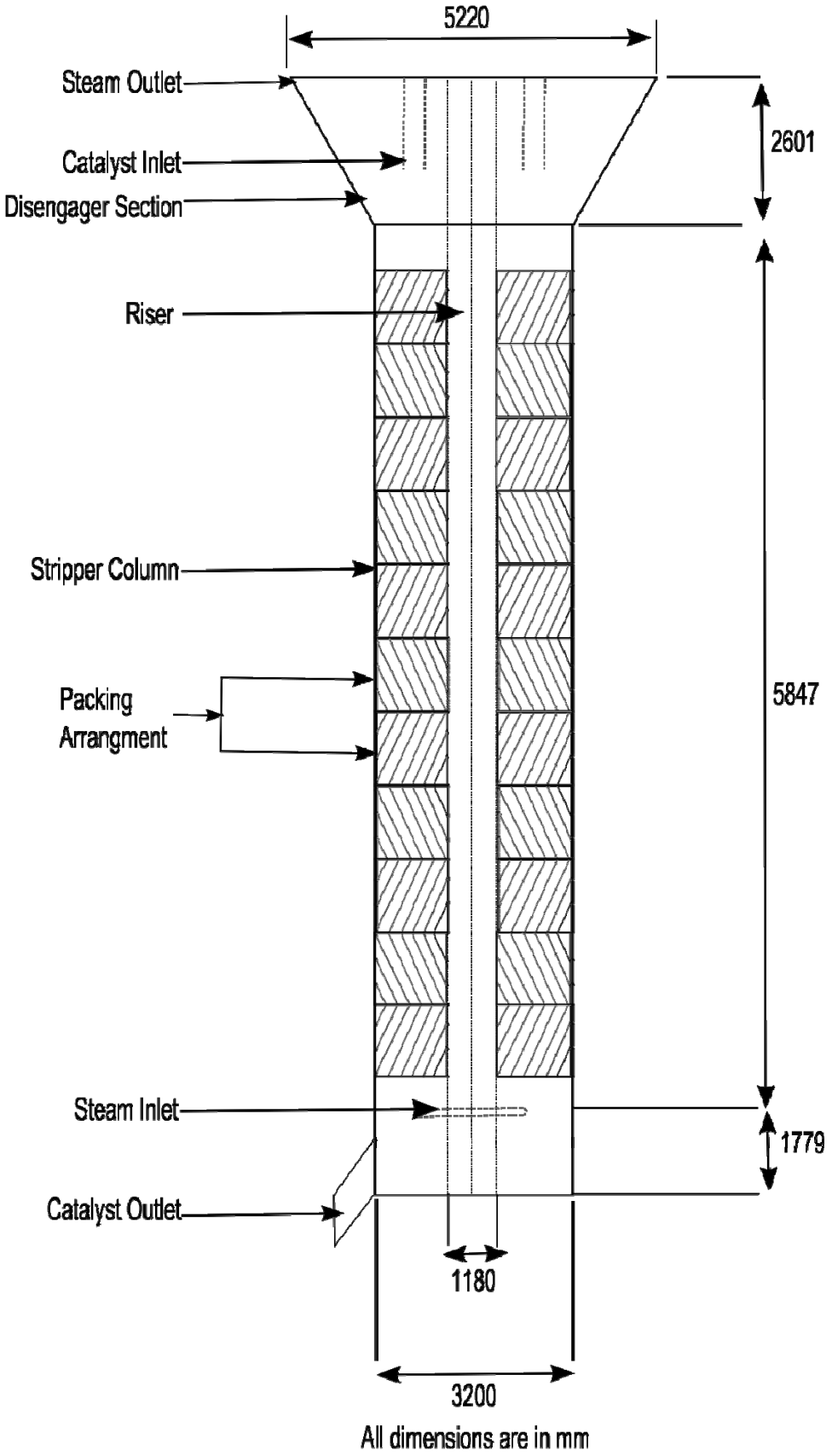

Figure 6.1: Schematic of stripper fitted with packing internals.

Solid-phase continuity

$$\frac{\partial}{\partial t}(\varepsilon_s \rho_s) + \nabla \cdot (\varepsilon_s \rho \vec{v}_s) = 0 \tag{6.2}$$

Gas-phase momentum

$$\frac{\partial}{\partial t}(\varepsilon_g \rho_g \vec{v}_g) + \nabla \cdot (\varepsilon_g \rho_g \vec{v}_g \vec{v}_g) = -\varepsilon_g \nabla P_g - \nabla \cdot \tau_g + K_{gs}(\vec{v}_g - \vec{v}_s) + \varepsilon_g \rho_g \vec{g} \tag{6.3}$$

Solids-phase momentum

$$\frac{\partial}{\partial t}(\varepsilon_s \rho_s \vec{v}_s) + \nabla \cdot (\varepsilon_s \rho_s \vec{v}_s \vec{v}_s) = -\varepsilon_s \nabla P_g - \nabla \cdot S_s - K_{gs}(\vec{v}_g - \vec{v}_s) + \varepsilon_s \rho_s \vec{g} \tag{6.4}$$

The thermal energy equations have not been included over here due to the anticipated negligible heat effects in cold-flow fluidized beds. The modified Wen-Yu drag law and the same closures equations as used in previous Chapter 5 were used in this work.

6.1.1. Simulation Method and Boundary Conditions

Simulations were conducted using commercial CFD software Fluent 6.3.16 (of Ansys Inc). The geometry and mesh were created in Gambit 2.3.16 (of Ansys Inc). The geometry of the stripper with packing internals is shown in Figure 6.2. The packing blades are edge-to-edge with no overlap. The packing element layers are rotated 90 degrees from adjacent layers. An unstructured meshing scheme had to be followed due to high skewness factor near the edges in the packing layers. A finer meshing was used in the packing layer and the free board region and a coarser mesh was used in the bottom section stripper. The average cell size was 37 mm as shown in Figure 6.3.

QUICK discretization scheme was used for the momentum and volume-fraction differencing scheme, and time discretization was first order. The solution of the pressure from the momentum equations used a pressure correction equation that corrects the pressure and the velocities after every iteration according to the SIMPLE algorithm. Simulations were carried out for a solid flux of 45 kg/m^{2}s, and a superficial steam velocity of 0.25 m/s was used. Velocity inlets boundary conditions were used for both solid and gas inlets. The catalyst phase was allowed to enter elluitrated along with air at catalyst inlet, where the catalyst inlet velocity was 1.4 m/s with a phase hold up of 0.165. A pressure outlet boundary condition was specified at the top of the stripper. Solids were free to leave if entrained and were not

returned to the computational domain. The simulations were carried out in a transient manner. The volume fraction and velocity of the both phases were monitored across the domain. The simulations were deemed "fully-developed" once these quantities reached a dynamic steady state, which took approximately 60 seconds of real time. Time averaged data for the phase velocities and volume fraction were then collected for the next 110 seconds.

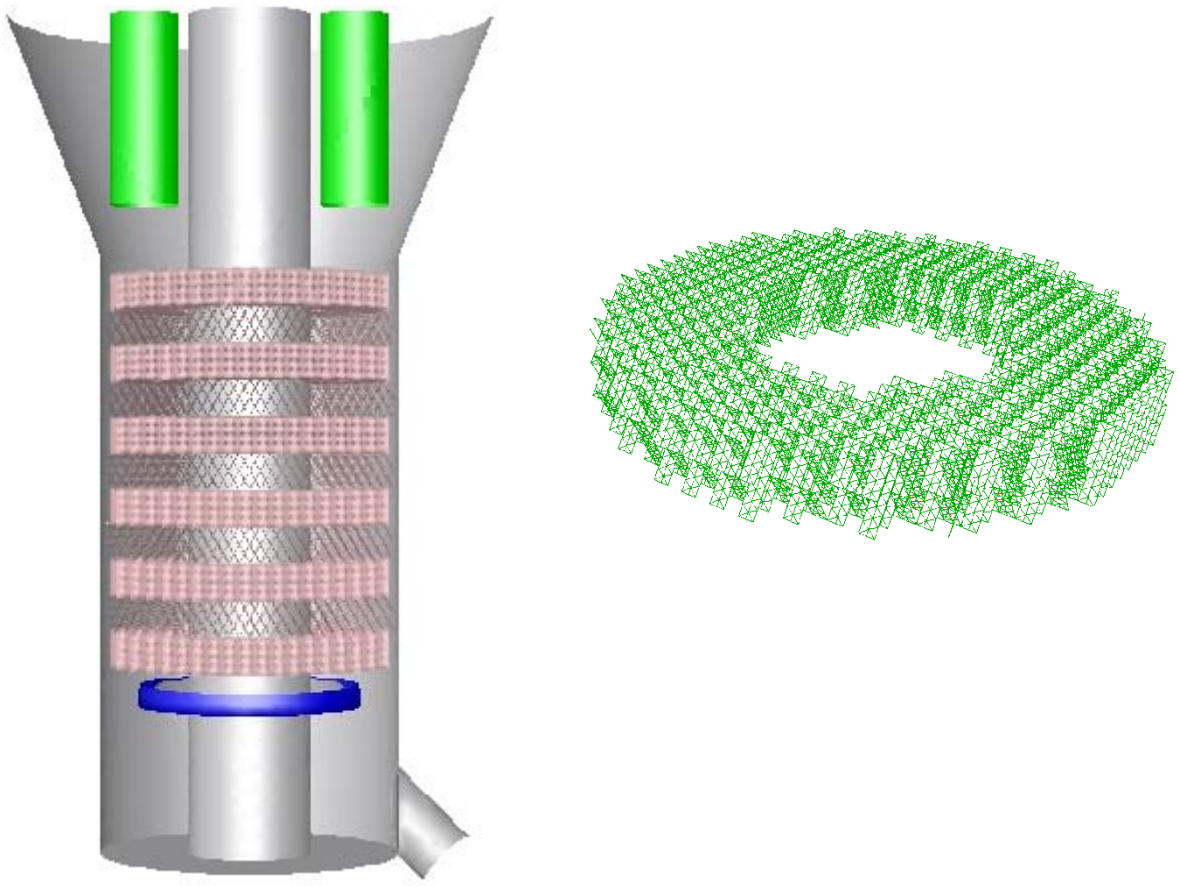

(a) (b)

Figure 6.2: (a) 3D geometry of stripper with packing internals, (b) A packing element.

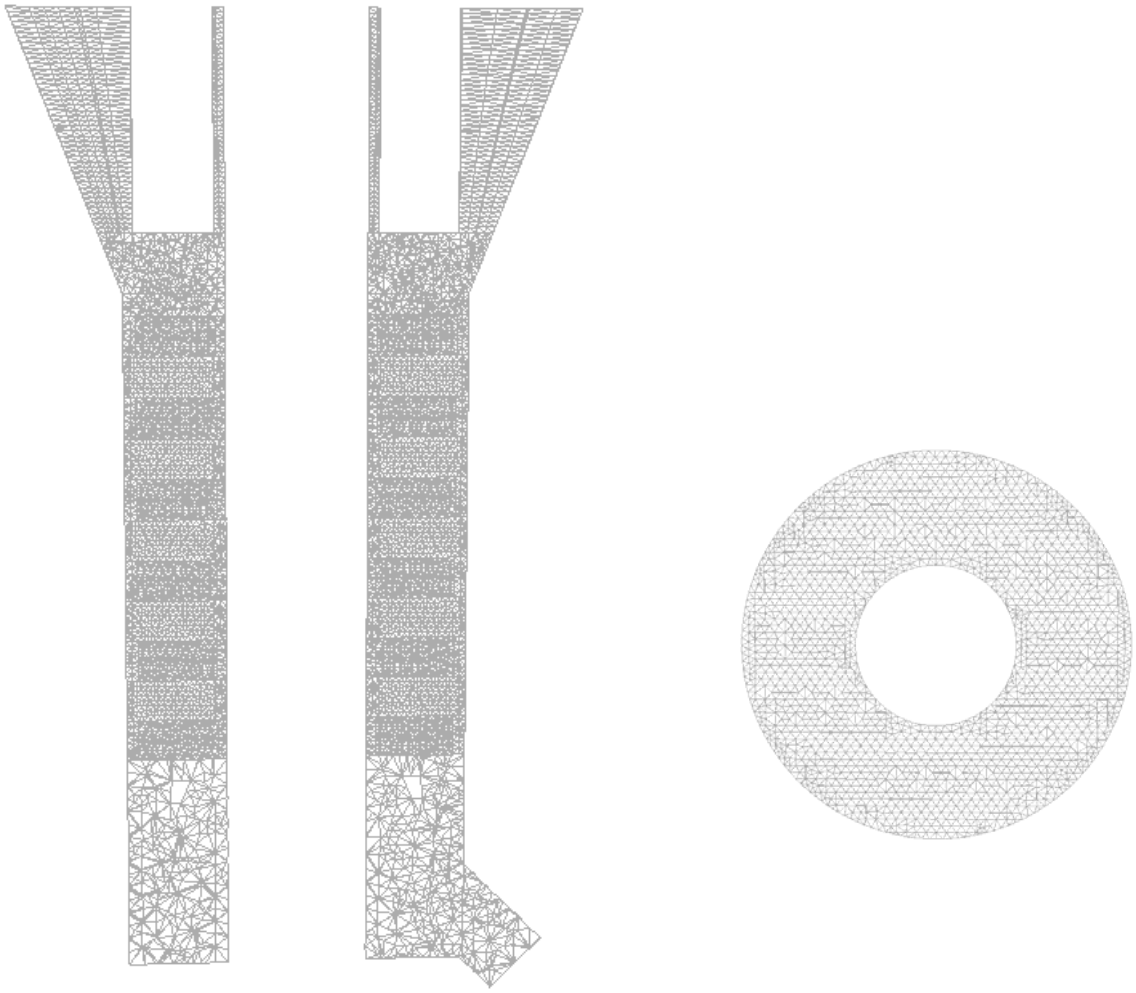

Figure 6.3: Stripper mesh: (a) Vertical cross sectional view, (b) Horizontal cross sectional view.

6.2. Results and Discussion

The following sections discuss the hydrodynamic characteristics of a stripper fitted with packing internals. This is followed by a qualitative and quantitative comparative study of the phase velocity and holdup distribution from baffle type stripper (Chapter 5). All simulations were conducted for a steam superficial velocity of 0.25 m/s and catalyst mass flux of 45 kg/m^2s.

6.2.1. Hydrodynamics of Stripper Fitted with Packings

The contour plots of the time-averaged volume fraction of steam are shown in Figure 6.4a. The contour plots were drawn at the transverse planes at the same locations as in Chapter 5

(section 5.2.2). Figure 6.4b shows the 3D contour plots of the time-averaged catalyst hold up across the stripper with full ring steam inlet.

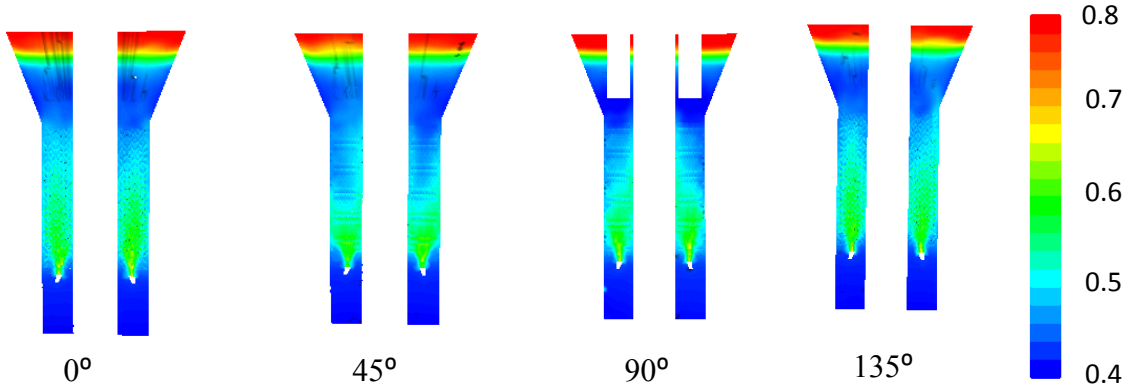

(a)

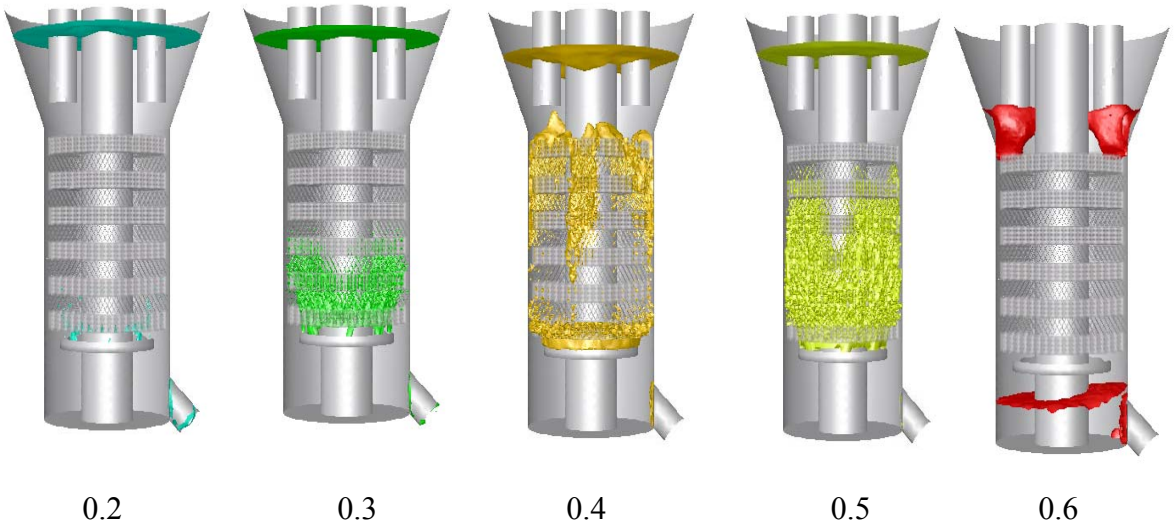

(b)

Figure 6.4: Stripper fitted with packing internals: (a) Contours of mean volume fraction of steam at different angles, (b) 3D contours of mean volume fraction of catalyst.

It can be observed in Figure 6.4a that there was a uniform steam volume fraction of ~ 50% to ~60% in most part of the stripper with no indication of any presence of steam pockets and channelling (which dominated the baffle type stripper in Chapter 5). This arrangement also ensured that upto ~95% of the vessel area was used for stripping operation by eliminating dead zones and channelling. This observation was in contrast to the observations made in the previous chapter 5, for stripper fitted with disc and donut baffles, which exhibited dead zones

and channelling behaviour. Figure 6.4b shows the change in solid holdup with the height of stripper. It was noticed that the solid holdup in the stripper predominantly ranged between 40% to 50 %. This was a clear indication of absence of maldistribution, which was noticed in the stripper fitted with baffle internals.

shows the time-averaged velocity vector plot of steam at 45° cross-sectional plane. As the steam enters the stripper from the bottom section, it enters the first layer of packing, where the structure packing alignment ensures that the steam is distributed equally both in the axial and radial directions. Then the steam enters the next layer of packing which is fitted at 90° right of the preceding packing layer. Here again the same mechanism forces the steam the move upward equally in the axial and radial directions. This alternative arrangement of stacks one on another fitted at 90°, helps in achieving a uniform distribution of steam in all sections of the stripper, as seen in the highlighted region. In the coming sections the comparison of radial and axial mixing of the phases are compared and discussed.

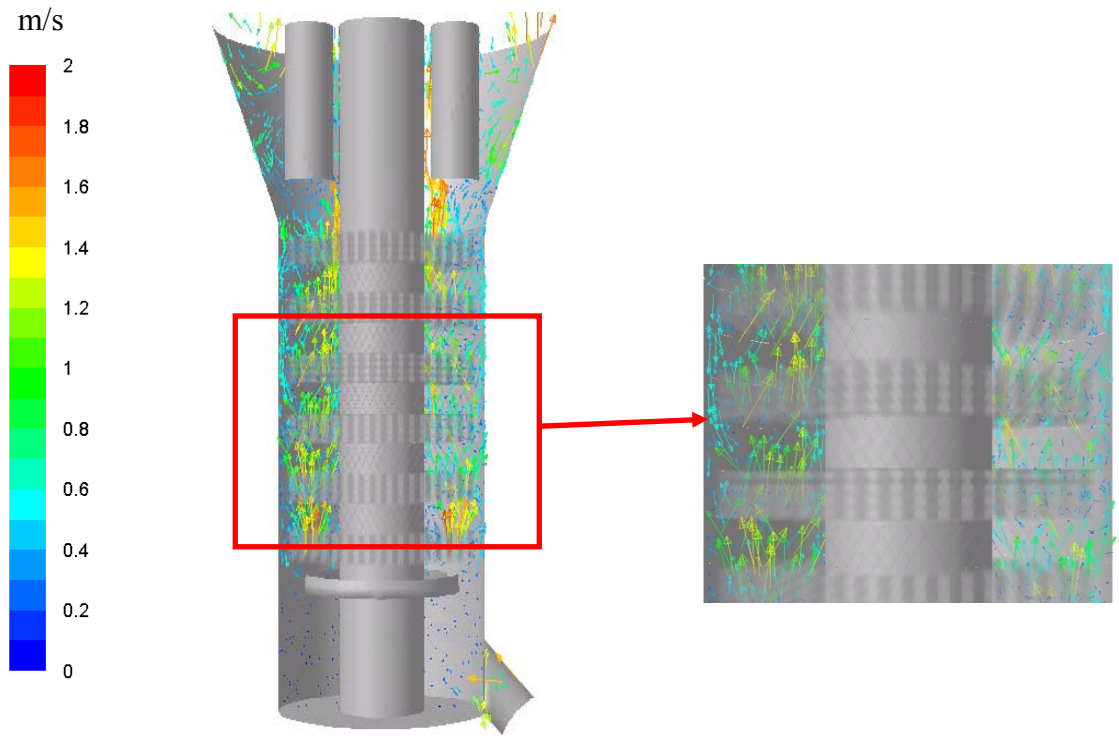

Figure 6.5: Steam mean velocity vector plot at 45°cross sectional plane.

6.2.2. Effect of Internal Configuration on Steam Velocity Field

To understand the effect of internal configuration on steam distribution, mean steam axial velocity was obtained at different axial locations along the height of the stripper for the both internal types (packing and baffles), and were plotted in Figure 6.6. In the stripper fitted with baffles, as the steam flows upward in a zigzag manner, it was observed that the mean steam axial velocity was fluctuating between 0.22 m/s to 0.36 m/s (Figure 6.6). The axial velocity for the stripper with baffles configuration was maximum in the donut baffle regions due to smaller contracting space between the donut baffle and the stripper wall, and minimum in the disc baffle regions due to a relatively larger annular space between baffle and riser walls. The fluctuating axial velocity decreased the residence time of steam in the stripper and adversely affected the stripping rates. However, for the same operating conditions, the stripper fitted with packing showed much improved performance. Initially, lower axial velocity was observed near the sparger, where the solid volume fraction was low. As the solid volume fraction increased, the axial velocity also increased. The axial velocity was almost constant in the rest of the stripper section as the solid volume fraction was nearly uniform. At the top of the stripper, the steam velocity again decreased as very low solid volume fraction was observed in this region. The overall mean steam axial velocity for stripper fitted with packing was higher when compared to the stripper fitted with baffles.

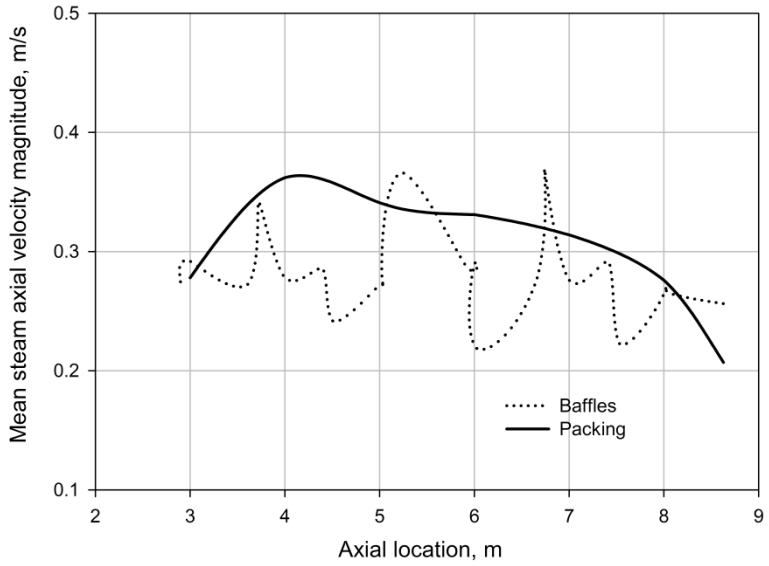

Figure 6.6: Mean steam axial velocity distribution along the height of stripper.

In order to understand the effect of internal configuration on back mixing, the mean steam x velocity vectors were plotted at the entry of 3rd baffle/packing from bottom (Figure 6.7a, b) and at the entry of 4th baffle/packing from bottom (Figure 6.7c, d). Figure 6.7a, Figure 6.7c correspond to the stripper fitted with baffle, while Figure 6.7b, Figure 6.7d correspond to the stripper fitted with packings. As discussed in the previous chapter, at the entry of a baffle, a fraction of steam is trapped in the region between the baffle and the stripper/riser walls. This steam recirculates back to the main domain of steam flow leading to formation of two different regions. This backmixing phenomenon is attributed to the shape of baffles. Figure 6.7a and Figure 6.7c shows that there is uniform backmixing in the stripper fitted with baffles in all the four quadrants. Depending upon the shape of baffles, the steam is either moved in or out (dotted arrows). For the stripper system, where catalyst has to be stripped off of the entrained/adsorbed hydrocarbons using steam, it is better if the catalyst particle always comes in contact with fresh steam. Therefore, the back mixing of steam phase in a stripper, will lead to low stripping efficiency and hence will affect the overall performance of the FCC unit. For the same axial planes for the packing arrangement, which is made of interlocked plates, minimum back mixing behaviour is observed (Figure 6.7b and Figure 6.7d). The interlocked plates in the packing structure help in attaining even steam distribution and ensure plug flow behaviour of steam phase by avoiding recirculation and back mixing.

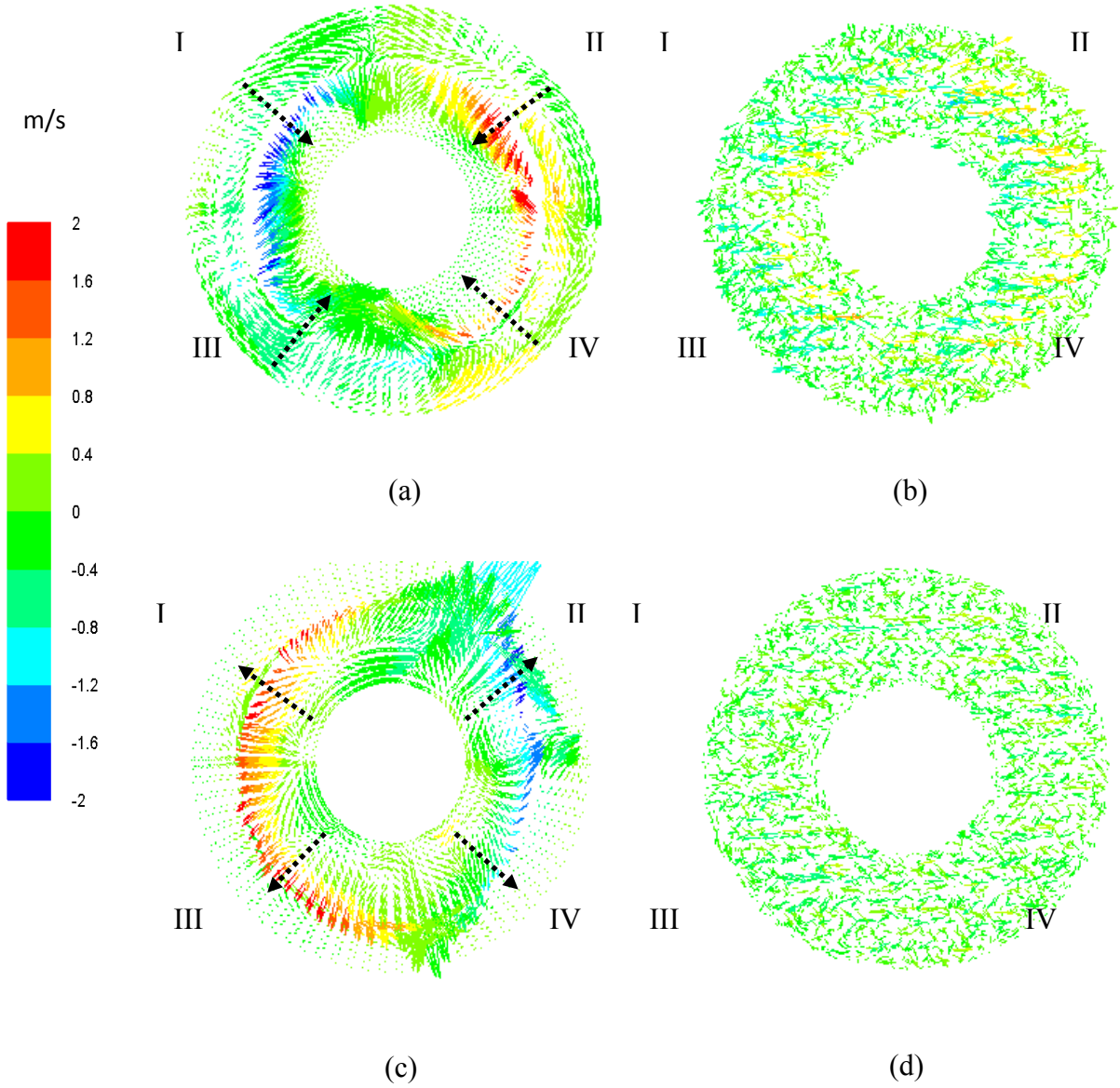

Figure 6.7: Comparison of vector plots for x mean steam velocity.

6.2.3. Effect of Internal Configuration on Catalyst Distribution

The radial distributions of mean axial velocity of catalyst and mean catalyst volume fraction along the height of the stripper are shown in Figure 6.8. The particles descend from the inlet at the top region and reach the topmost disc shaped baffle (at 9 m) for the stripper fitted with baffles. As they enter the baffle region, the particles slide along the baffle wall and are forced towards the central riser. Thus a maximum axial velocity was observed in this open region between the riser wall and disc baffle. The particles proceed down against the upward motion of air and enter the donut baffle region (at 8 m). In this region, the particles are forced to enter a narrow cross sectional region between stripper wall and donut baffle. This contraction

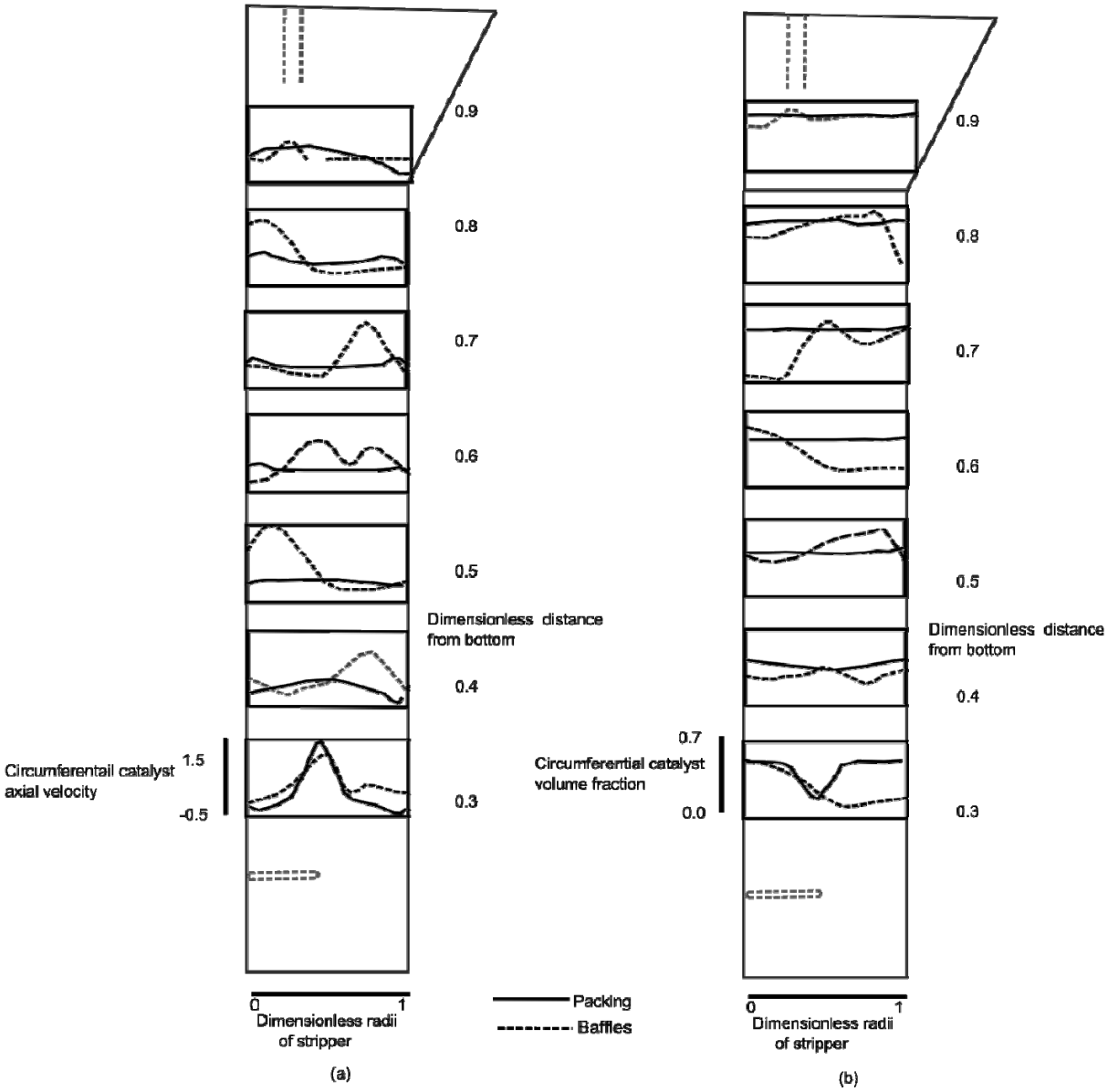

Figure 6.8: Comparison of circumferential mean axial velocity and mean catalyst volume fraction.

gives rise to a steep peak in the axial velocity in this region. This pattern continued alternatively till the particles reached the steam inlet region (Figure 6.8a). Higher solid axial velocity was observed at locations where the air velocity was higher. In dead zones below the baffle walls, almost zero or negative axial velocities were observed. The minimum velocities were observed in the dead zones which then reduced the efficiency. In contrast to this observation, for stripper fitted with packings, the catalyst axial velocity was uniform in all sections, except at the bottom section near the steam inlet. Over all the catalyst axial velocity was higher for the stripper fitted with baffles when compared to stripper fitted with packing internals, indicating lower residence time of catalyst particles.

The radial average mean catalyst volume fraction along the stripper height for stripper fitted with baffle and packing internal configurations are shown in Figure 6.8b. Higher catalyst volume fraction was noticed near the baffle walls and lower catalyst volume fraction was observed near the riser or stripper wall. The higher catalyst volume fraction below the baffle was due to the entrainment in the dead zone region. An opposite behaviour was noticed in the lower sections of the stripper. In this region, the influence of steam inlet was predominant. In contrast to the top region, a higher catalyst volume fraction was observed near the walls. The presence of non uniform radial variation of solid holdup along the height of stripper indicated maldistribution of the catalyst phase. On the other hand, for the same operating conditions, stripper fitted with packing exhibited uniform solid holdup in all sections of the stripper except at the bottom. Unlike the stripper fitted with baffles, the radial variation of solid holdup was minimum and overall higher solid holdup was observed at all locations.

6.3. Conclusions

Simulations of a cold flow industrial scale FCC stripper fitted structured packing were performed. The effect of internal configuration on steam and catalyst distribution in both axial and radial directions was examined. The CFD model predicted that the stripper fitted with internal packings exhibit uniform distribution of catalyst and steams phases and showed absence of dead zones and reduced back mixing. By elimination of the dead zones, stripper fitted with packing offered more area for stripping operation, conversely less steam will be needed when comparing for the same stripping operation in a stripper fitted with baffles. Lesser steam means lower energy consumption, which is vital. By reducing the back mixing and providing uniform distribution, the stripper fitted with packing also provided a better

contact between the phases. A better contacting between the phases will always lead to higher mass transfer rates between the catalyst and steam; therefore more hydrocarbons are expected to be stripped off from the catalyst. Thus, using structured packings as internals for steam stripper can be a viable alternative to conventional internals that offers substantial optimization and cost reduction opportunities.

7. SUMMARY AND CONCLUSIONS

The work accomplished in thesis provides a better understanding of the hydrodynamics of industrial scale FCC strippers. It sheds new insights on the effect of different internals and inlet configurations on the stripper hydrodynamics. Experimental studies were successfully carried out to measure the solid holdup and time of flight for particles. Computational models were developed and validated by comparing the predicted results with the experimental results. A detailed parametric study was conducted to analyse the effect of steam inlet configuration and internals for an industrial scale stripper. The following is an itemized summary of the major conclusions drawn from this study:

7.1. Summary

1) Experimental scale stripper was designed and commissioned using the residence time and solid holdup data from an industrial-scale FCC stripper. γ-ray densitometry and time of flight experiments were carried out for different operating conditions for the stripper fitted with disc and donut baffles.

2) 3D CFD simulations for the experimental scale FCC stripper were carried out using the two fluid Eulerian approach and were validated with the experimental data.

3) 3D CFD simulations of industrial scale FCC Stripper were conducted for two different steam inlet configurations and compared against each other. These were a simple pipe steam inlet (SPSI) and a full ring steam inlet (FRSI).

4) The effect of the asymmetric nature of the catalyst outlet on the hydrodynamics was also investigated.

5) As an alternative to baffles internals, a structured packing internals was also studied using 3D computational model for an industrial scale stripper.

7.2. Major Conclusions from Experiments

1) The design and shape of disc and donut baffles led to a zigzag flow through the stripper baffles.

2) The observed holdup profiles in γ-ray densitometry experiments were asymmetric in nature, thus emphasizing the need for 3D modelling studies.

3) Radial segregation was observed at lower superficial gas velocities, and an increase in the superficial gas velocity led to a decrease in the solid holdup. Several dead zones were also noticed in the regions under the baffles.

4) The particle mean time of flight of the particle increased with the air flow rate, but at the same time it decreased with the solid flow rates. The long tails observed in the E-curves confirmed the presence of dead zones in the stripper fitted with baffles.

7.3. Major Conclusions from CFD Simulations

1) The CFD simulations predicted asymmetric radial profiles elucidating the need for 3D simulating of these equipments.

2) The CFD simulations compared well with the experimental solid holdup observations. CFD simulations also clearly predicted a number of recirculation zones and dead zones as observed in the experimental analysis. Local defluidization zones were also identified in the donut baffle regions.

3) The model predicted that the solid holdup profiles along the height of stripper were greatly influenced by the shape and position of baffles.

4) The solid axial velocities and the volume fractions were observed to be influenced by the gas velocity. The particle axial velocities were low near the wall region indicating that the particles slide down on the baffle walls.

5) The experimental scale CFD simulations and the industrial scale CFD simulations both qualitatively predicted the presence of dead zones and back mixing.

6) The stripper fitted with SPSI inlet configuration showed segregation and maldistribution of the catalyst across the whole stripper. The lack of symmetry in catalyst outlet pipe and uneven distribution of steam were considered to be the causes of these irregularities.

7) The large variations in steam radial velocity and high steam axial velocity were found to be associated with the stripper with SPSI inlet configuration. This can lead to segregation and lower steam residence time inside the stripper, eventually affecting the stripper operational performance.

8) The Stripper fitted with FRSI inlet configuration exhibited minimal segregation. The uniform steam injection design helped in achieving better radial distribution of the both phases and lower axial velocities.

9) It was also understood that the baffles play a vital role in creating recirculation or back mixing zones enabling the phases to come in contact with each other.

10) Stripper fitted with internal packings exhibited uniform distribution of catalyst and steams phases and exhibited the absence of dead zones and reduced back mixing.

11) By reducing the back mixing and providing uniform distribution, the stripper fitted with the packings provided better contact between the phases.

12) Higher mass transfer rate are expected with packings due to the better contacting between the phases and therefore more hydrocarbons are expected to be stripped from catalyst surface.

13) By elimination of dead zones, stripper fitted with packing offers nearly 95% of the vessel area for stripping operation, conversely less steam will be utilized when comparing for the same stripping operation in the stripper fitted with baffles. Lesser steam means lower energy consumption, which is vital.

14) Uniform steam and catalyst velocities were observed all along the height of the stripper, fitted with structured packing internals. Higher solid holdup was noticed in the stripper fitted with packing compared to stripper fitted with baffles indicating higher stripping efficiency.

7.4. Recommendations for Future Work

1) Complete RPT experiments should be carried out to analyse particle local velocities. Knowledge of particle velocities will be useful in studying particle residence time in each baffle unit. Particle local velocity experiments can then be extended to the

stripper fitted with packing internals. It is also recommended to do solid holdup studies for stripper fitted with packing internals.

2) New techniques should be developed to accommodate the use of very small FCC catalyst particles in the RPT experiments.

3) New methods should be developed to improve the densitometry technique, particularly near the wall regions where the accuracy is low. As an alternative other experimental techniques like electrical capacitance tomography (ECT) should be also be used.

4) Numerical experiments should be carried out for flooding conditions to understand the effect of operating condition on the onset of flooding behaviour.

5) The short comings in the stripper fitted with SPSI configurations can be overcome by using multiple steam injection portals all along the height of stripper, or using a symmetric catalyst outlet.

6) CFD simulations should be carried out for different type of catalyst inlet distributors along with different steam inlets. These simulations will provide FCCs greater flexibility in operation.

7) The distance between the baffles can be reduced or more number of small sized baffles can be used to improve the contact of catalyst and steam. Full scale CFD studies should be carried out on this type of internals arrangement.

8) Mass Transfer studies should be carried out to determine the efficiency of stripper fitted with packing internals. This will provide further understanding on the effect of packing arrangements.

REFERENCES

Arandes, J., Azkoiti, M., Bilbao, J., de Lasa, H., 2000. Modelling FCC units under steady and unsteady state conditions. The Canadian Journal of Chemical Engineering 78, 111-123.

Arbel, A., Huang, Z., Rinard, I., Shinnar, R., Sapre, A., 1995. Dynamic and control of fluidized catalytic crackers. 1. Modeling of the current generation of FCC's. Industrial & Engineering Chemistry Research 34, 1228-1243.

Avidan, A.A., 1992. FCC is far from Being a Major Technology. Oil and Gas Journal 90, 59-67.

Avidan, A.A., Edwards, M., Owen, H., 1990. Innovative improvements highlight FCC's past and future. Oil and Gas Journal 88, 33-54.

Bhusarapu, S., Fongarland, P., Al-Dahhan, M., Dudukovic, M., 2004a. Measurement of overall solids mass flux in a gas-solid circulating fluidized bed. Powder Technology 148, 158-171.

Bhusarapu, S., Al-Dahhan, M., Dudukovic, M., 2004b. Quantification of solids flow in a gas-solid riser: single radioactive particle tracking. Chemical Engineering Science 59, 5381-5386.

Bhusarapu, S., Al-Dahhan, M., Dudukovic, M., 2006. Solids flow mapping in a gas-solid riser: Mean holdup and velocity fields. Powder Technology 163, 98-123.

Bi, H., Cui, H., Grace, J., Kern, A., Lim, C., Rusnell, D., Song, X., McKnights, C., 2004. Flooding of Gas- Solids Countercurrent Flow in Fluidized Beds. Industrial Engineering and . Chemistry. Research 43, 5611-5619.

Bi, H., Grace, J., Lim, C., Rusnell, D., Bulbuc, D., McKnight, C., 2005. Hydrodynamics of the stripper section of fluid cokers. The Canadian Journal of Chemical Engineering 83, 161-168.

Boemer, A., Qi, H., Renz, U., 1997. Eulerian simulation of bubble formation at a jet in a two-dimensional fluidized bed. International Journal of Multiphase Flow 23, 927-944.

Boyer, C., Duquenne, A.-M., Wild, G., 2002. Measuring techniques in gas-liquid and gas-liquid-solid reactors. Chemical Engineering Science 57, 3185-3215.

Cheng, W., Kim, G., Peters, A., Zhao, X., Rajagopalan, K., Ziebarth, M., Pereira, C., 1998. Environmental fluid catalytic cracking technology. Catalysis Reviews 40, 39-79.

Cui, H., Grace, J., McKnight, C., Zhang, T., Rose, I., Bi, X., Lim, J., Burgardt, D., 2006a. Jet configuration for improved fluidized bed stripping. Chemical Engineering Journal 125, 1-8.

Cui, H., Strabel, M., Rusnell, D., Bi, H., Mansaray, K., Grace, J., Lim, C., McKnight, C., Bulbuc, D., 2006b. Gas and solids mixing in a dynamically scaled fluid coker stripper. Chemical Engineering Science 61, 388-396.

Ding, J., Gidaspow, D., 1990. A bubbling fluidization model using kinetic theory of granular flow. AIChE Journal 36, 523-538.

Dudukovic, M.P., 2002. Opaque multiphase flows: experiments and modeling. Experimental Thermal and Fluid Science 26, 747-761.

Enwald, H., Peirano, E., Almstedt, A.E., 1996. Eulerian two-phase flow theory applied to fluidization. International Journal of Multiphase Flow 22, 21-66.

Ergun, S., 1952. Fluid flow through packed columns. Chemical. Engineering. Progress 48, 89-94.

Gao, J., Chang, J., Xu, C., Lan, X., Yang, Y., 2008a. CFD simulation of gas solid flow in FCC strippers. Chemical Engineering Science 63, 1827-1841.

Gao, J., Chang, J., Lan, X., Yang, Y., Lu, C., Xu, C., 2008b. CFD modeling of mass transfer and stripping efficiency in FCCU strippers. AIChE Journal 54, 1164-1177.

Gera, D., Gautam, M., Tsujib, Y., Kawaguchib, T., Tanakab, T., 1998. Computer simulation of bubbles in large-particle fluidized beds. Powder Technology 98, 38-47.

Gibilaro, L., Di Felice, R., Waldram, P., 1985. Generalized friction factor and drag coefficient correlations for fluid-particle interactions. Chemical Engineering Science 40, 1817-1823.

Gidaspow, D., 1994. Multiphase flow and fluidization: continuum and kinetic theory descriptions. Academic Pr.

Godfroy, L., Chaouki, J., Larachi, F., 1999. Position and velocity of a large particle in a gas/solid riser using the radioactive particle tracking technique. The Canadian Journal of Chemical Engineering 77, 253-261.

Goldschmidt, M., Beetstra, R., Kuipers, J., 2002. Hydrodynamic modelling of dense gas-fluidised beds: comparison of the kinetic theory of granular flow with 3D hard-sphere discrete particle simulations. Chemical Engineering Science 57, 2059-2075.

Goldschmidt, M., Kuipers, J., van Swaaij, W., 2001. Hydrodynamic modeling of dense gas-fluidized beds using the kinetic theory of granular flow: effect of restitution coefficient on bed dynamics. Chemical Engineering Science 56, 571–578.

Grace, J.R., 1990. High-velocity fluidized bed reactors. Chemical Engineering Science 45, 1953-1966.

Gustavsson, M., Almstedt, A., 2000. Two-fluid modelling of cooling-tube erosion in a fluidized bed. Chemical Engineering Science 55, 867-879.

Harrison, D., Grace, J.R., 1971. Fluidized beds with internal baffles. J.F. Davidson and D. Harrison, Editors, Fluidization, Academic Press, UK (Chapter 13).

Hong, R., Guo, Q., Luo, G., Zhang, J., Ding, J., 2003. On the jet penetration height in fluidized beds with two vertical jets. Powder Technology 133, 216-227.

Hoomans, B., Kuipers, J., Briels, W., Van Swaaij, W., 1996. Discrete particle simulation of bubble and slug formation in a two-dimensional gas-fluidised bed: a hard-sphere approach. Chemical Engineering Science 51, 99-118.

Huilin, L., Gidaspow, D., Bouillard, J., Wentie, L., 2003a. Hydrodynamic simulation of gas-solid flow in a riser using kinetic theory of granular flow. Chemical Engineering Journal 95, 1-13.

Huilin, L., Yurong, H., Gidaspow, D., 2003b. Hydrodynamic modelling of binary mixture in a gas bubbling fluidized bed using the kinetic theory of granular flow. Chemical Engineering Science 58.

Hulme, I., Clavelle, E., van der Lee, L., Kantzas, A., 2005. CFD modeling and validation of bubble properties for a bubbling fluidized bed. Industrial Engineering Chemistry Research 44, 4254-4266.

Jenkins, J., Savage, S., 2006. A theory for the rapid flow of identical, smooth, nearly elastic, spherical particles. Journal of Fluid Mechanics 130, 187-202.

Jin, Y., Wei, F., Wang, Y., 2003. Effect of Internal Tubes and Baffles. Handbook of fluidization and fluid-particle systems, 171.

Jin, Y., Yu, Z., Zhang, L., Shen, J., Wang, Z., 1982. Pagoda-shaped internal baffles for fluidized bed reactors. International Chemical Engineering 22, 269-279.

Johnson, P., Jackson, R., 2006. Frictional–collisional constitutive relations for granular materials, with application to plane shearing. Journal of Fluid Mechanics 176, 67-93.

Kaneko, Y., Shiojima, T., Horio, M., 1999. DEM simulation of fluidized beds for gas-phase olefin polymerization. Chemical Engineering Science 54, 5809-5821.

King, D., 1992. Fluidized catalytic crackers: an engineering review. Fluidization VII O.P. Potter, D.J. Nicklin Eds., Engineering Foundation. 15-26.

Kunii, D., Levenspiel, O., 1991. Fluidization engineering. Butterworth-Heinemann.

Kwauk, M., Shi, J., Wang, J., 1996. Chemical Engineering Handbook (2nd ed). Chemical Industry Press, Beijing China , (Chapter 21), 94–95

Larachi, F., Kennedy, G., Chaouki, J., 1994. A [gamma]-ray detection system for 3-D particle tracking in multiphase reactors. Nuclear Instruments and Methods in Physics Research Section A: Accelerators, Spectrometers, Detectors and Associated Equipment 338, 568-576.

Lathouwers, D., Bellan, J., 2001. Modeling of dense gas-solid reactive mixtures applied to biomass pyrolysis in a fluidized bed. International Journal of Multiphase Flow 27, 2155-2187.

Lettieri, P., Newton, D., Yates, J., 2002. Homogeneous bed expansion of FCC catalysts, influence of temperature on the parameters of the Richardson-Zaki equation. Powder Technology 123, 221-231.

Lun, C.K.K., S. B. Savage, D. J. Jeffrey and N. Chepurniy, 1984, "Kinetic theories for granular flow: inelastic particles in Couette flow and slightly inelastic particles in a general flow field.", Journal of Fluid Mechanics 140, 223–256.

Mathiesen, V., Solberg, T., Hjertager, B., 2001. Predictions of gas/particle flow with an Eulerian model including a realistic particle size distribution. Powder Technology 112, 34-45.

Matsen, J.M., 1985. Fluidized beds. Bisio, A., Kabel, R.L. (Eds.), Scaleup of Chemical Processes. Wiley Interscience, New York.

McCarthy, S.J., Raterman, M.F., Smalley, C.G., Sodomin, J.F., Miller, R.B., 1997. Refinery improves FCC yields using latest process technologies. Oil and Gas Journal 95, 56-69.

McKeen, T., Pugsley, T., 2002. Simulation of cold flow FCC stripper hydrodynamics at small scale using computational fluid dynamics. International Journal of Chemical Reactor Engineering 1, 1034.

Mckeen, T., Pugsley, T., 2003. Simulation and experimental validation of a freely bubbling bed of FCC catalyst. Powder Technology 129, 139-152.

Miller, R., Yang, Y., Gbordzoe, E., Johnson, D., Mallo, T., 2000. New Developments in FCC Feed Injection and Stripping Technologies, pp. 00-08.

Moseley, J., O'brien, T., 1993. A model for agglomeration in a fluidized bed. Chemical Engineering Science 48, 3043-3050.

Pandit, K., 2007. A DEM study of bubble formation in Group B fluidized beds with and without cohesive inter-particle forces. Chemical Engineering Science 62, 159-166.

Patil, D., Annaland, M., Kuipers, J., 2003. Gas dispersion and bubble-to-emulsion phase mass exchange in a gas-solid bubbling fluidized bed: a computational and experimental study. International journal of chemical reactor engineering (electronic) 1, 1-22.

Peirano, E., Delloume, V., Johnsson, F., Leckner, B., Simonin, O., 2002. Numerical simulation of the fluid dynamics of a freely bubbling fluidized bed: influence of the air supply system. Powder Technology 122, 69-82.

Peirano, E., Delloume, V., Leckner, B., 2001. Two-or three-dimensional simulations of turbulent gas-solid flows applied to fluidization. Chemical Engineering Science 56, 4787-4799.

Rall, R.R., DeMulder, B., 2000. New internal for maximizing performance of FCC catalyst strippers. Twelth Refining Seminar San Francisco.

Ranade, V., 2002. Computational flow modeling for chemical reactor engineering. Academic Pr.

Rivault, P., Nguyen, C., Laguerie, C., Bernard, J.R., Aquitaine, E., 1995. Countercurrent stripping dense circulating beds effect of the baffles. Fluidization VIII J.F. Large, C. Laguerie Eds., Engineering Foundation, 725-732.

Rose, I., Cui, H., Zhang, T., McKnight, C., Grace, J., Bi, X., Lim, J., 2005. Towards an ultimate fluidized bed stripper. Powder Technology 158, 124-132.

Roy, S., 2000. Quantification of Two-Phase Flows in Liquid-Solid Risers. D. Sc. Thesis, Washington University in St. Louis, MO, USA.

Roy, S., Larachi, F., Al-Dahhan, M., Dudukovic, M., 2001. Resolution and sensitivity in computer-automated radioactive particle tracking (CARPT), p. 122.

Roy, S., Kemoun, A., Al-Dahhan, M., Dudukovic, M., 2002. A method for estimating the solids circulation rate in a closed-loop circulating fluidized bed. Powder Technology 121, 213-222.

Roy, S., Kemoun, A., Al-Dahhan, M., Dudukovic, M., 2005. Experimental investigation of the hydrodynamics in a liquid-solid riser. AIChE Journal 51, 802-835.

Schmidt, A., Renz, U., 1999. Eulerian computation of heat transfer in fluidized beds. Chemical Engineering Science 54, 5515-5522.

Schmidt, A., Renz, U., 2000. Numerical prediction of heat transfer in fluidized beds by a kinetic theory of granular flows. International Journal of Thermal Sciences 39, 871-885.

Schaffer D., 1987 “Instability in the evolution equations describing incompressible granularflow”, J. Diff. Eq., 66, 19-50.

Senior, R.C., Smalley, C.G., Gbordzoe, E., 1998. Hardware modifications to overcome common operating problems in FCC catalyst strippers. In: Fan, L.S., Knowlton, T.M. (Eds), Fluidization IX, Engineering Foundation New York, 725–732.

Sinclair, J., Jackson, R., 2004. Gas-particle flow in a vertical pipe with particle-particle interactions. AIChE Journal 35, 1473-1486.

Srivastava, A., Sundaresan, S., 2003. Analysis of a frictional-kinetic model for gas-particle flow. Powder Technology 129, 72-85.

Stellema, C., Kolar, Z., De Goeij, J., Schouten, J., Van den Bleek, C., 1997. Solids Residence Time Distribution in Interconnected Fluidized Beds. New York, NY: American Institute of Chemical Engineers, 1971-c2002., pp. 40-45.

Syamlal, M., O'Brien, T., 1989. Computer simulation of bubbles in a fluidized bed, pp. 22-31.

Taghipour, F., Ellis, N., Wong, C., 2005. Experimental and computational study of gas-solid fluidized bed hydrodynamics. Chemical Engineering Science 60, 6857-6867.

Tsuji, Y., Kawaguchi, T., Tanaka, T., 1993. Discrete particle simulation of two-dimensional fluidized bed. Powder Technology 77, 79-87.

Upadhyay, R., Roy, S., 2010. Investigation of hydrodynamics of binary fluidized beds via radioactive particle tracking and dual source densitometry. The Canadian Journal of Chemical Engineering 88, 601-610.

Utikar, R., Ranade, V., 2007. Single jet fluidized beds: Experiments and CFD simulations with glass and polypropylene particles. Chemical Engineering Science 62, 167-183.

Van Wachem, B., Schouten, J., Krishna, R., Van den Bleek, C., 1998. Eulerian simulations of bubbling behaviour in gas-solid fluidised beds. Computers & Chemical Engineering 22, S299-S306.

Wang, G., S., G.J., M., X.C., 2004. Evolutionary Design on FCC Reactors Driven by the High Temperature and Short Contact Time Demands. Petroleum Science and Technology 22, 1581-1594.

Wen, C.-Y. and Y. H. Yu, 1966. "Mechanics of fluidization", Chemical Engineering Progress Symposium. Ser.,62, 100–111.

Wilson, J., 1997. Fluid catalytic cracking technology and operations. Pennwell Corp.

Wrench, R., Glasgow, P., 1992. FCC hardware options for the modern cat cracker, pp. 1-8.

Zhang, Y., Grace, J., Bi, X., Lu, C., Shi, M., 2009. Effect of louver baffles on hydrodynamics and gas mixing in a fluidized bed of FCC particles. Chemical Engineering Science 64, 3270-3281.

Zhang, Y.M., 2003. Study on the gas–solid flow in FCCU stripper. M.S.Thesis, China University of Petroleum, Beijing

Zhang, Y.M., Lu, C.X., Shi, M.X., 2004. Study on the gas–solid mass transfer performance in catalyst stripper. Journal of Chemical Engineering of Chinese Universities 18, 409-413.

APPENDIX-I

$$I = I_0 e^{-\mu_{eff}\rho_{eff}l_{eff}} \tag{3.1}$$

$$-\ln\left(\frac{I_{g,m,s}}{I_{g,m}}\right) = \overline{\varepsilon_{s,l}}\left(\mu_s\rho_s - \mu_g\rho_g - \mu_m\rho_m\right)l_{eff} \tag{3.2}$$

Operating Condition : Air flow rate = 0.74 m/s

: Solid Flow rate = 0.33 kg/s

L/R = 0.85

I0= 48536

I = 38625

Length of metal part (riser and internals) = 0.4

Length of empty medium = 6.8

μ_{solid} = 0.1569

μ_m = 0.585

Solid holdup = ln (48536/ 38625)/ ((0.585*0.4) + (0.1569*6.8))

Solid holdup = 0.313